OPEN ACCESS

University of BRISTOL

This electronic thesis or dissertation has been downloaded from Explore Bristol Research, http://research-information.bristol.ac.uk

Author:
Mcilwraith, Alex J

Title:
Roles for Polarity in Shape Determination in the Liverwort Marchantia polymorpha

General rights
Access to the thesis is subject to the Creative Commons Attribution - NonCommercial-No Derivatives 4.0 International Public License. A copy of this may be found at https://creativecommons.org/licenses/by-nc-nd/4.0/legalcode This license sets out your rights and the restrictions that apply to your access to the thesis so it is important you read this before proceeding.

Take down policy
Some pages of this thesis may have been removed for copyright restrictions prior to having it been deposited in Explore Bristol Research. However, if you have discovered material within the thesis that you consider to be unlawful e.g. breaches of copyright (either yours or that of a third party) or any other law, including but not limited to those relating to patent, trademark, confidentiality, data protection, obscenity, defamation, libel, then please contact collections-metadata@bristol.ac.uk and include the following information in your message:

• Your contact details
• Bibliographic details for the item, including a URL
• An outline nature of the complaint

Your claim will be investigated and, where appropriate, the item in question will be removed from public view as soon as possible.

Roles for Polarity in Shape Determination in the Liverwort *Marchantia polymorpha*

Alexander James McIlwraith

A dissertation submitted to the University of Bristol in accordance with the requirements for award of the degree of Master's by Research in the Faculty of Life Sciences.

Word count = 23,266

Abstract

Plant shape is determined by developmental programmes which result in distinct plant morphologies across land plants, which are thought to have diverged from the Charophycean algae around 500 million years ago. Polarised growth axes help regulate growth in early plant development and can be defined through the differential distribution of signalling molecules both locally and globally across plant tissues. Growth as a flattened mat of indeterminately growing tissue called the thallus characterises growth in the early diverging land plant group called liverworts. This ancient plant architecture makes liverworts suitably positioned in the phylogeny of land plants to answer questions on fundamental plant biology.

Prior work has shown that thallus shape in a liverwort model system, *Marchantia polymorpha*, can be explained using a modelling approach. However, such computational approach could not describe some naturally observed elongated thalli shapes in other liverwort species. Here, results from a previously conducted but updated modelling approach incorporating polarity are included to set hypotheses for *M. polymorpha* growth.

Using pharmacological treatments and previously generated *M. polymorpha* lines which have been genetically engineered, I test modelling hypotheses and show through quantification and analysis of thalli phenotypes that phytohormones auxin and cytokinin are involved in polarity specification via PINs in *M. polymorpha*. In addition to growth experiments, I used a confocal approach to screen and explore PIN-GFP lines to identify the localisations of PIN proteins across the *M. polymorpha* thallus.

When both experimental approaches are taken together, my results identify the roles for polarity on thallus growth involving feedback between phytohormones auxin and cytokinin and explore which polarity modelling hypotheses generated by modelling best explain the growth observed in *M. polymorpha* thalli. I also suggest future work towards a more complete understanding of shape determination during *M. polymorpha* development.

Author Declaration

I declare that the work in this dissertation was carried out in accordance with the requirements of the University's Regulations and Code of Practice for Research Degree Programmes and that it has not been submitted for any other academic award. Except where indicated by specific reference in the text, the work is the candidate's own work. Work done in collaboration with, or with the assistance of, others, is indicated as such. Any views expressed in the dissertation are those of the author.

Alexander McIlwraith, July 2021

Acknowledgments

Throughout the writing of this thesis many people and given me their time and support, and I would like to use this opportunity to thank some of the people who have helped me along this formative journey. Firstly, I would like to thank my supervisor, Dr. Jill Harrison, whose direction and feedback has been invaluable to me not only as a student, but also as a human. I would also like to thank Dr. Jeremy Solly for starting the *Marchantia* shape project and helping create the models which laid the foundations for this thesis.

I would like to thank the Dr. Harrison's lab group members: Dr. Vicky Spencer, Dr. Zoe Nemec Venza, Wei Liu, Katie Jeal, and Sophie Carpenter for always being there to help and adjusting so well to the tribulations of the past year. I would like to extend my thanks to the members of Professor Claire Grierson's lab who provided so much feedback in lab group meetings.

Thank you to all those in Lab 324 for the company in the lab and any help along the way, and especially to Dr. Lucia Primavesi and Helen Martin for keeping the everything in the lab in order, notably amongst the chaos of the past year. I am very grateful to the Wolfson Bioimaging Facility, especially Dr. Alan Leard, who so patiently helped me find my feet using the confocal microscope.

I would like to thank the Lady Downe Trust for presenting me with the Lady Downe Award to complete this Master's by Research degree.

Last but not least, I would like to thank my parents, Neil and Sally, and siblings, Mel, Ben and Niall for showing me there is no place like home. And to all my friends - in Bristol and beyond - thank you for all the memories along the way.

Table of Contents

Chapter 1. Introduction

Across the tree of life, plants have evolved to optimize the display of photosynthetic tissues (Niklas & Kerchner, 1984). This has resulted in elaborate plant shape variations between plant groups, most notably in the flowering plants which have determinate planar lateral organs such as leaves arranged around an upright stem (Harrison, 2017). More ancient plant forms include the indeterminate, flattened mat of tissue called the thallus which characterises growth in liverworts. Much less is known about shape determination in liverworts in comparison to other groups such as the flowering plants. Studies in these early diverging land plants, combined with the literature on other plant groups allows the developmental mechanisms to be identified as broadly applicable to land plant development or more specific at the group level.

Plant shape

The diverse nature of land plants is staggering. The particular shape achieved by a plant is the result of control of growth at both the local and global level, with distinct morphologies making use of divergent developmental programmes (Pires & Dolan, 2012). Plant shape is restricted by the presence of the cell wall, hence shape changes during development occur through differential growth rates and rotation, which are often in preference to particular orientations. It has therefore been noted that the influence of genes on growth rate, growth anisotropy (growth that is not equal in all directions), and the direction of growth collectively explain the growth and shape change in plants throughout development (Coen et al., 2004). However, plant shape is also restricted by tissue connectiveness so growth of one particular region can lead to mechanical constraint of another region, complicating the ability the understand how genes control plant shape (Bassel et al., 2014; Kennaway et al., 2011). Therefore, to understand resultant growth and overall plant shape throughout development, both cellular geometry and growth must be considered.

Marchantia polymorpha as a model system for shape determination

Liverworts belong to the bryophyte sister lineage of vascular plants, which are estimated to have diverged from the last common ancestor of land plants around 470 million years ago (Morris et al., 2018). This makes *Marchantia* polymorpha suitably positioned in the land plant phylogeny to ask key questions about land plant evolution. Despite phylogenetic advances of the modern era setting the context for the model to be used to answer questions of evolution, *M. polymorpha* has been used as a model system for plant physiology and morphology for nearly 200 years (Shimamura, 2016). *M. polymorpha* has a haploid gametophyte-dominant life cycle and is increasingly becoming a model system of choice in evo-devo plant biology with a fully sequenced genome and transformation protocols available (Bowman et al., 2017; Ishizaki et al., 2016).

As *M. polymorpha* thalli grow they undergo a series of formulaic shape transitions as the thalli grow from regions of stem cells which are located in the apical notch (Solly et al., 2017; see **Figure 1**). Thalli develop from vegetative propagules known as gemmae which offer a uniform starting point to better understand developmental processes. Work combining computational modelling and growth analyses has started to

dissect the determination of thallus shape in *M. polymorpha*, with anisotropic growth shown to be sufficient to explain thallus shape in *M. polymorpha* when patterned relative to apical notches (Solly et al., 2017). The *M. polymorpha* model system therefore offers the opportunity to identify fundamental requirements of plant shape determination and this thesis works to build upon that knowledge and develop a more complete understanding of shape determination in liverworts.

Polarity in development

Polarity refers to the asymmetric distribution of components. In biological systems this can be at multiple levels, including locally at the cellular level or globally across a tissue. The polar orientation of cells within tissues was historically only well researched in animal cells, but a greater understanding of polarity in plants was garnered around the beginning of the current century. By still mostly elusive processes but in a similar fashion to animal development, the generation of polarised axes during early development orchestrates cell differentiation patterns and tissue growth. It is largely believed that polarity mechanisms in plants and animals are distinct, with known regulators for polarity in animal systems missing the genomes of plants (see Kania et al., 2014 for review). Growth can be oriented with respect to the symmetry (or axiality) of polarity components specified by signals such as differential concentrations of signalling molecules across tissues which define the overall polarities.

There is a host of evidence that polarity modulates growth in biological systems, with auxin transport in *Arabidopsis thaliana* forming the basis for an understanding of polarity field in plant development such as the auxin maximum achieved in the *A. thaliana* root tip (Coen et al., 2004; Sabatini et al., 1999). More recently, it has been demonstrated that *A. thaliana* leaves have a persistent polarity field across the tissue, with the stomatal protein BASL revealing a polarity field in mutant plants which lack stomatal lineages (Mansfield et al., 2018). Furthermore, ectopic BASL mirrors polarity patterns observed in other proteins which suggests a commonality of polarity-generating mechanisms, which may prove crucial in regulating growth and therefore determining plant shape. The link between tissue-level and cellular-level polarity has also recently been elucidated in *A. thaliana* with the finding that SOSEKI proteins localise to cellular axes and locally interpret global polarity cues, resulting in influence over cell division orientations and therefore plant architecture (Yoshida et al., 2019). This work also highlighted the fundamental importance of cell polarity to multicellular organisms with both plant and animal cell systems both converging on a similar protein domain.

The use of computational models in developmental plant biology

A computer modelling approach allows conceptual ideas to become engineered into workable computer simulations which can generate quantitative and testable hypotheses. In plant evo devo the combined use of live imaging, image analysis, and computational modelling to test hypotheses has already provided insight into plant development (see Roeder et al., 2011 for review). The use of models allows the tissue connectiveness, in addition to just the activity of genetic regulators alone to be incorporated into complete frameworks predicting the effect of growth on development, and this can then be used to better understand the genetic regulation of development. Models which incorporate polarity across tissues, such as the Growing Polarised Tissue (GPT) framework builds on the orientations of particular growth axes specified independently of stresses to the tissue by morphogens in the tissue (Kennaway et al., 2011). This modelling approach is built upon regulatory networks of polarity, gene expression and growth rate with the growth rate regulatory network collectively determining plant morphogenesis. The framework establishes growth axes by the diffusion gradients of a specific chemical or protein. Tissue polarity is generated by growth which is in parallel (Kpar) or perpendicular (Kper), to local polarity cellular signals which are genetically determined (Kennaway et al., 2011). Growth then determines the overall plant shape. Typically, two axes of polarity are sufficient to generate flat shapes, although a third axis is required for the complexity of folded shapes such as the diverse leaf shapes generated in carnivorous flowering plants (Whitewoods et al., 2019).

The application of computational models to growth in real plants

The combination of computer models alongside plant growth experiments can give a real understanding of the plant growth observed and studies have been conducted to unravel polarity and shape determination by linking modelling work to live imaging and analysis in real plants. Until recently the persistent polarity field across plant organs was theoretical and lacking evidence from studies in real plants. However, advances in studies in *A. thaliana* have provided evidence for such persistent model. For example, the GPT framework has been experimentally validated in a study that showed varying model parameters allowed for different predicted *A. thaliana* leaf shapes generated by anisotropic growth with reference to the established axis which could then linked to gene regulation (Kuchen et al., 2012). Furthermore, *A. thaliana* petal shape has also been modelled showing that in contrast to leaf development, growth orientations in petals diverge from the leaf tip yet follow the same basic framework involving growth rates occurring either parallel or perpendicular to the axis across the organ (Sauret-Güeto et al., 2013). The authors were also able to link the growth pattern to a zinc finger transcription factor, JAGGED, which promotes growth whilst modulating tissue polarity, again linking plant shape to genetic regulation.

These studies make it clear that modelling polarity in plants at the level of the tissue with an experimental framework integrating real plant growth can be used to describe genetic regulation of plant growth. This thesis aims to build on the knowledge generated in angiosperm model systems into more early diverging land plants and identify what genetic regulators may be responsible for determining the polarity across liverwort thallus tissue.

Plant hormones and PIN proteins

Morphogens are chemical signals that can diffuse through tissues and regulate growth. Plant hormones such as auxin, cytokinin, brassinosteroids, gibberellic acid and ethylene are small molecules derived from various essential metabolic pathways which regulate plant growth and can act as morphogens (Santner et al., 2009). Two types of morphogens have been defined with reference to describing plant growth and shape changes; regionalising, which emphasize differences between growth regions, and polarising, which orient cell axes (Coen et al., 2004). Along with tissue regional identities, morphogens can be modelled to describe the development of plant shape. This thesis focuses on two plant hormones in particular: auxin and cytokinin.

Auxin signalling has a rich literature which defines auxin as a versatile coordinator of growth and development across both long and short distances within plants (see Leyser, 2018 for review). It has become apparent that the specificity achieved by the auxin-centric signalling pathway is not by the signal itself but by the cellular perception of it. Changes to gene expression in the auxin response involves degradation of AUX/IAA transcriptional repressors (Gray et al., 2001). Despite a less rich literature, another key hormone in plant development is the cytokinin phytohormone family. These are derivatives of adenine which are also known to influence many aspects of plant development such as cell division and proliferation via a phosphorelay signalling pathway (Kieber & Schaller, 2014).

The movement of auxin around plant tissues is significant in determining the developmental pattern. Polar auxin transport is the directional movement of auxin between cells, with auxin efflux proteins to be localised to just one side of the cell and thus directing auxin movement. Modulation of such directional flow is significant in controlling development. Members of the PIN-FORMED (PIN) protein family were the first identified in *A. thaliana* through a mutant screen which reported a mutant, *pin1*, significantly lacking in plant organs (Okada et al., 1991). The PIN1 protein was then identified as a transmembrane auxin efflux carrier component, identifying the PIN protein family as key components in the patterning of the plant body plan (Gälweiler et al., 1998). Subsequent work has elucidated the role PIN-dependent auxin transport in plant development (see Adamowski & Friml, 2015 for review). In *A. thaliana*, PIN proteins have been shown to have a polarised distribution in the plasma membrane (Gälweiler et al., 1998; Heisler et al., 2005). More recent work has implicated both auxin and cytokinin in the regulation of the polarity of *A. thaliana* PIN proteins at specific domains in the plasma membrane (Marhavý et al., 2014). This thesis seeks to understand if such interplay is responsible for changes to plant shape in a liverwort, *M. polymorpha*.

Auxin, cytokinin, and PINs in the *M. polymorpha* model system

Work on the regulation of plant shape in *M. polymorpha* has sought to understand how growth patterns observed throughout development are regulated by endogenous signals. Auxin responses are spatially distributed across the thallus tissue and change during development of the thallus (Ishizaki et al., 2012) . In *M. polymorpha*, the auxin biosynthetic pathway is significant to proper development, with mutants exhibiting a phenotype that lacks proper tissue patterning (Eklund et al., 2015). *M. polymorpha* has a two-component cytokinin signalling pathway which is conserved with *A. thaliana* and it has also been shown that cytokinin is necessary for proper organ formation in *M. polymorpha* (Aki et al., 2019). In *A. thaliana*, the cross-talk of auxin and cytokinin biology has been noted at many levels of development (Schaller et al., 2015; Su et al., 2011). This thesis seeks to understand if there is a level of cross-talk between auxin and cytokinin in establishing polarity across the thallus in *M. polymorpha* shape determination.

M. polymorpha is known to have 4 PIN proteins, three non-canonical (MpPINW, MpPINX, MpPINY) and one canonical (MpPINZ; Bennett et al., 2014a). Recent work has shown that the canonical PIN in *M. polymorpha*, MpPINZ, is able to rescue the severe defects of *pin1/3/4/7* mutant in *A. thaliana* shoot and root development (Zhang et al., 2020). This implicates the canonical PIN structure as playing a significant role in the establishment of the complex architecture during shoot and root development observed in land plants.

The ‘Notch Pre-patterns Growth’ Model

Integration of both a modelling approach and some studies in real plants has started to elucidate the mechanisms behind shape determination in *M. polymorpha*, and this thesis sought to build upon this work (Solly, 2015; Solly et al., 2017). The comparison of computational models built upon the GPT framework concerning *M. polymorpha* shape to real plant growth in previous work suggests that a ‘Notch-pre-patterns-growth’ model was sufficient to capture all shape transitions in early *M. polymorpha* development (Solly et al., 2017). The authors determined by comparing computer models to real plant growth that isotropic growth with growth rate heterogeneity is sufficient to account for proper thallus development had no requirement for polarity. The model is defined by the following parameters, outlined in **Figure 1.1**: a gemma-shaped starting canvas was detailed with specific regional identity factors, APEX and TRANSITION (**Figure 1.1A**).

The fixed place identity factor APEX defined the production of APEXPROX, a mobile growth promoting morphogen. A boundary between APEX and the rest of the canvas was defined as TRANSITION, with each having characteristic regional growth rules. The two distinct tissue regions, DIFFERENTIATED and UNDIFFERENTIATED, determined the action of the morphogen APEXPROX. In UNDIFFERENTIATED tissue, APEXPROX diffused freely throughout the tissue and decayed proportionally with distance from the APEX. In DIFFERENTIATED tissue APEXPROX specified the production of DIFTISSUE, another morphogen which was not free to move, hence representing the decay. The overall growth of the thallus could be explained by the differential growth responses in DIFFERENTIATED and UNDIFFERENTIATED fixed tissue regions (**Figure 1.1B**). The authors used surgical and pharmacological experiments to suggest auxin as the diffusible morphogen APEXPROX to regulate plant growth (Solly et al., 2017). The action of auxin as a candidate for APEXPROX is also supported by the presence of auxin biosynthesis gene activity in the apical notch (Eklund et al., 2015).

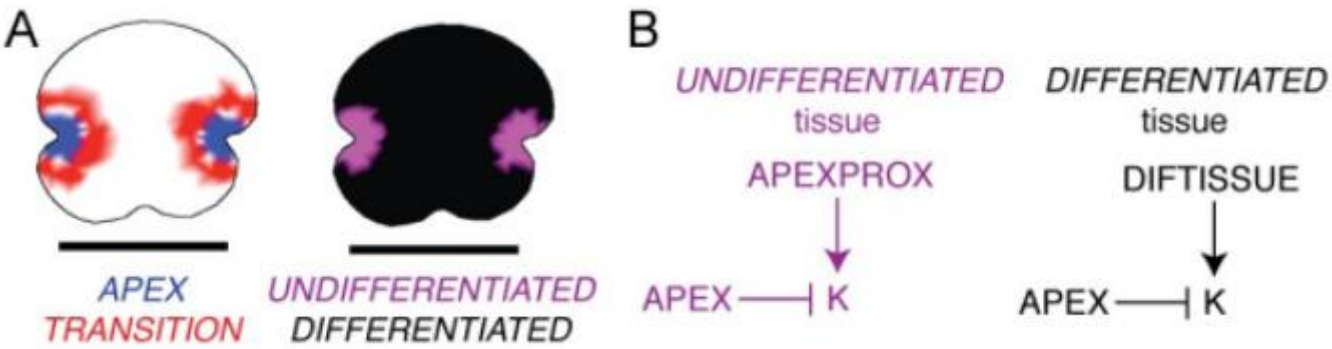

Figure 1.1: Growth rules underlying the Notch Pre-patterns growth model. Figure reproduced from Solly et al., 2017. (**A**) Tissue identities at the starting point of the 'Notch pre-patterns growth' model simulation including APEX, TRANSITION, UNDIFFERENTIATED and DIFFERENTIATED. (**B**) The defining growth (K) rules of the model which specify growth across the canvas.

Aims of this project

The aims of this project were to develop a greater understanding of the role for polarity in the development of *M. polymorpha*. My findings are outlined in two results chapters. A first chapter explores roles for polarity in thallus shape determination by comparing the growth of real plants under different experimental conditions to variant outputs of a model incorporating polarity into thallus development in *M. polymorpha*. A second uses confocal analysis of *M. polymorpha* lines with GFP-tagged MpPINZ proteins to understand where MpPINZ proteins localise across the thallus. A model of the role for polarity in *M. polymorpha* combining results from modelling, growth experiment and confocal work will be discussed.

Chapter 2. Materials and Methods

Tissue culture and growth experiments

Growth experiments

M. polymorpha gemmae were plated onto 9cm petri dish, using a sterile pipette tip to remove gemmae from the gemma cups of stock lines. A small droplet of water enabled the precise translocation of the gemmae onto the media. The basal growth medium of choice for all experiments was Gamborg's B5 medium, adjusted to pH 5.8 and with 0.8% agar. Several plates were grown for each treatment. Both experimental and stock lines were maintained in a REF-TECH growth chamber under white light in long-day conditions (16-hour light, 8-hour dark cycles). The wild-type line used in all experiments was Takaragaike-1 (Ishizaki et al., 2008).

Pharmacological treatments

All treatments involving exogenous hormones were prepared by diluting stock hormone solutions into growth media as media was cooling. The negative control for each treatment group were of equal volume solvent for each treatment. The use of 1-naphthaleneacetic acid (NAA), L-Kynurenine (L-Kyn), and 1-n-naphthylphthalamic acid (NPA) were all from stock hormone solutions that were stored at -20°C between experiments. NAA hormone solution was stored as a 100µM stock dissolved in 70% EtOH. L-Kyn stock solution was stored as a 100mM solution in dimethyl sulfoxide (DMSO). NPA hormone solution was stored as a 1mM stock dissolved in 70% EtOH and 2% DMSO.

For cytokinin mutants, which had curved tissues, plants were dissected from the growth media using a dissecting microscope and flattened between a microscope slide and glass coverslip.

Mppinz mutant generation

The *Mppinz* mutant lines used in this thesis were generated by Dr. Satoshi Naramoto (Hokkaido University, Japan) using a CRISPR/Cas9 genome editing approach. The following refers to the knockout *Mppinz* (Tak-1 43 1-b) mutants referred to in this thesis. Mutants were generated using a targeted sequence of gctgtacgtggccatgatcctgg. The double strand primer is as shown:

Forward: GCACCCAGCCTCTCGGCTGTACGTGGCCATGATCCGTTTTAGAGCTAGAA

Reverse: TTCTAGCTCTAAAACGGATCATGGCCACGTACAGCCGAGAGGCTGGGTGC

TaKaRa In-Fusion HD Cloning Kit was used to clone the target into the pMpGE_En01 plasmid which was then integrated into pMpGE010 plasmid by a Gateway LR reaction. Following successful generation of the plasmid, the plasmid including the Guide RNA (gRNA) and Cas9 was transformed into the wild-type (Tak-1), resulting in *Mppinz* mutants. Details of *Mppinz* sequencing can be found in **Figure 3.6**.

Cytokinin mutant generation

The overexpression cytokinin mutants were generated by Dr. Jeremy Solly, the constructs and full details of each line generation is found in his PhD thesis (Solly, 2015).

Stock line maintenance

Mature thallus stocks for each line were maintained on deeper petri plates, using the same media but with 1% sucrose to encourage gemmae formation. Gram-negative contaminated stock lines were treated with cefotaxime to restore sterility of stock lines.

Data collection and analyses

Images were taken using Keyence VHX-1000 digital light microscope (Keyence Corporation, Osaka, Japan). Images were loaded into image processing program ImageJ (Schneider et al., 2012) where measures of area, width and length were recorded (**Figure 2.1**). The total area was recorded using the 'Freehand selections' tool, tracing around the perimeter of the thallus. The ratio between width and length was then calculated. The same approach for measures of area and shape were taken during the analysis of plants at the later developmental stages, across a larger overall thallus shape. Counts of gemmae cups were conducted manually at the point of image processing. Only certain thalli, which did not have gross developmental defects were chosen for quantification. For these, please refer to appendices.

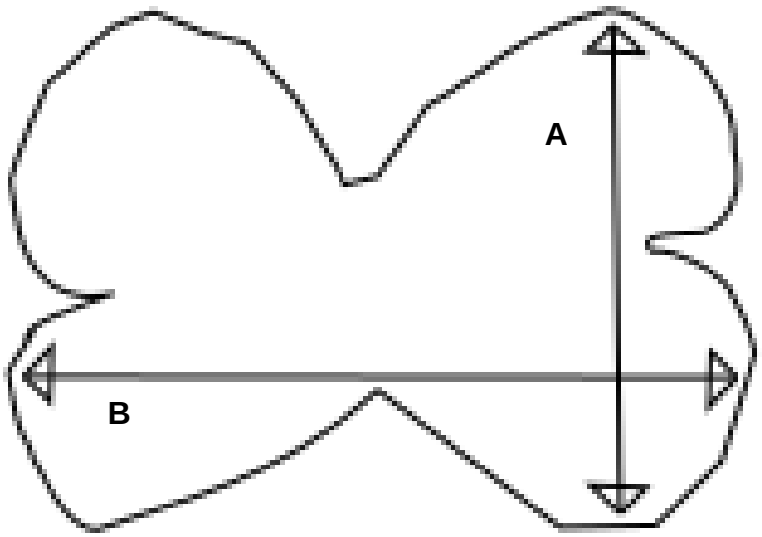

Figure 2.1: Outline of typical *M. polymorpha* thallus, showing how width and length measurements were taken in ImageJ. Images of 6-day old gemmae. The black thallus outline represents the area measure that was taken. (A) The vertical line represents the width measure.(B) The horizontal line represents the length measure. For both width and length measures, the greatest distance was measured on each thallus.

After the generation of data files from ImageJ data was handled using Microsoft Excel. All data visualisations and statistical analyses were conducted using RStudio (RStudio Team, 2020), using the *tidyverse* (Wickham et al., 2019) collection of packages. Statistical tests are stated when used and all sample sizes are shown in figures. Figures were edited using the open-source vector graphics editor Inkscape (Available at: https://inkscape.org).

PCR and sequencing of *Mppinz* mutants

DNA extraction from approximately 60mg of young thallus tissue was achieved using a CTAB extraction buffer (comprising of: 2 M Tris-HCL (pH8); 5 M NaCl; CTAB; 0.5 M EDTA; PVP-40; β-mercaptoethanol; ascorbic acid; dH_20), and following RNaseA treatment, samples were extracted with 24:1 chloroform-isoamyl alcohol prior to precipitation with 0.7 x volume isopropanol. Pellets were washed with 70% ethanol and dissolved in TE.

The DNA concentrations were measured for each sample using a NanoDrop (ThermoFisher Scientific, Massachusetts, United States) and PCR was then performed using a Q5® High-Fidelity DNA Polymerase kit (M0491) available from New England BioLabs (Massachusetts, United States). Each 10µL PCR reaction was run for 35 cycles with a denaturing temperature of 98°C for 10 seconds, an annealing temperature of 66°C for 25 seconds, and an extension period at 72°C for 30 seconds. A negative control of MilliQ water was included. Sequencing was outsourced to Eurofins Scientific (TubeSeq service; Luxembourg) after a clean-up of the PCR product using the PCR purification kit (QIAquick PCR purification kit) from Qiagen (Hilden, Germany). Details of sequencing data analysis are provided in the text accompanying **Figure 3.6**.

Details and generation of MpPINZGFP lines

MpPINZGFP lines were acquired to identify PIN protein localisations across the body of the thallus during development. The MpPINZGFP lines were generated by the lab of Dr. Satoshi Naramoto (Hokkaido University, Japan), who also provided details of line generation. The lines were made in the *Mppinz* mutant background. To construct the proMpPIN1:MpPIN1eGFP plasmid a MpPIN1 genomic fragment with a 5 kilobase (kb) upstream region and 0.8 kb downstream region was PCR-amplified, using a Tak-1 genomic DNA template and subcloned into pENTR/D-Topo vector (ThermoFisher Scientific, Massachusetts, United States).

The pENTR/D-topo plasmid including the proMpPIN1:MpPIN1 complement fragment was then modified to establish proMpPIN1:MpPIN1:eGFP plasmids. A PCR-amplified eGFP coding sequence was inserted in frame with the coding sequence of MpPIN1 at the hydrophilic loop of MpPIN1 (at 654b from the start codon) by the In-Fusion cloning reaction (TaKaRa, Shiga, Japan) to generate a proMpPIN1:MpIN1:eGFP plasmid, which was subsequently integrated into pMpGWB401 by a Gateway LR reaction. The functionality of proMpPIN1:MpPIN1:eGFP plasmids was confirmed by transforming into *Mppinz* mutants, resulting in generation of MpPINZGFP lines.

Confocal Microscopy

Tissue preparation for confocal microscopy involved removing gemmae from the gemma cups of stock lines two hours ahead of imaging and placing them between a microscope slide and glass coverslip in water. Confocal microscopy was carried out using a multi-laser confocal laser scanning microscope (Leica SP5) with help from the Wolfson Bioimaging Facility at the University of Bristol. Excitation was with an argon laser at 488nm with 20% laser power. Emission from GFP was collected at 500-550nm for the GFP lines (using a Leica HyD detector; Leica, Wetzlar, Germany) and autofluorescence was collected at 620-680nm (using a Leica PMT2 detector; Leica, Wetzlar, Germany) for the autofluorescence detection to generate composite images. A 512x512 format was used with a 400Hz bidirectional scan. Z-stacks with a z-step size of 2µM were used to visualise localisations through the depth of the gemma. A previously published positive SNARE line (MpSYP13B) was included as a positive control in confocal experiments (Kanazawa et al., 2020). For experiments involving mannitol, a 1 M stock solution was prepared fresh and diluted when appropriate.

Analysis of confocal images

ImageJ was used for analysis of confocal images (Schneider et al., 2012). Data were imported into ImageJ in .lif format and stacks were viewed using the hyperstack tool. The colour options were ‘colorized’, meaning each channel was opened separately allowing colour channels to be selected manually. From these separate channels composite images could be made. Z projections from stacks were produced from the raw data, using max intensity at each layer to produce single images of the *M. polymorpha* gemma. Where appropriate the composite scans were produced from max intensity Z projects from both channels. Scale bars were saved at the point of image acquisition. In order to better understand the localisation of proteins across the gemmae, orthogonal view was used in both XZ and YZ (**Figures 4.5 – 4.12)**.

Chapter 3. Growth Experiments to Understand Polarity-Dependent Shape Variation in *Marchantia Polymorpha*

Introduction

A number of different growth patterns throughout the development of a tissue could theoretically result in the same final tissue shape, so in order to distinguish the exact growth patterns that cause a specific tissue morphology an experimental approach is necessary (Coen et al., 2004). This chapter shows growth experiments designed to test predictions of a new computational model and interrogate polarity-dependent growth in *M. polymorpha.*

A newer model accounting for polarity across the thallus

The following modelling work was conducted by Jeremy Solly (unpublished). The conclusions of the prior 'Notch pre-patterns growth' model published by Solly et al. (2017) had no requirement for growth anisotropy or polarity in shape determination. However, the model is insufficient to explain the natural shape diversity seen in liverwort species. For instance, *Riccia fluitans* has a more elongated thallus shape than *Marchantia polymorpha*. This shape variation between the liverwort species can be seen in images taken by Dr. Jeremy Solly shown in **Figure 3.1**.

Figure 3.1: Natural variation in liverwort thalli shape shows the extent to which the thallus can be elongated beyond the 'Notch-pre-patterns growth' model. Images reproduced from Dr. Jeremy Solly's PhD thesis (Solly, 2015). Arrows represent the apical notches and both scale bars represent 1mm. (**A**) Three time points of growth in *Marchantia polymorpha* development. (**B**) Three time points in *Riccia fluitans* development, showing a much more elongated development thallus shape.

To further explore shape variation, tissue polarity was integrated into the 'Notch pre-patterns growth' model by incorporation of further fixed identity factors named EDGE and MIDLINE which specify the production or decay of POLARISER (POL), a third morphogen (**Figure 3.2A**, **B, overleaf**). POL determined the regional polarities in a polarity field across the gemma-shaped canvas depending on the source to sink relationship of the morphogen. Three different variant polarity fields were modelled to interrogate the differences between different source and sink relationships. APEX was the source of the morphogen in all the different iterations, but the sink of POL was specified as absent, in a region across the middle (MIDLINE) of the thallus, or around the perimeter of the thallus (EDGE). The model also determined the effect of the above polarities on overall plant shape by growth rules which orientated growth (K) in relation to polarity (**Figure 3.2B**). The most noticeable differences between the polarity orientations in each variant were along the top and in the centre of the thallus as follows (**Figure 3.2B**):

- APEX source, no sink: polarity ran towards the edge and centre of respective canvas regions.
- APEX source, MIDLINE sink: polarities were approximately parallel to the edge and notch to notch axis in respective canvas regions.
- APEX source, EDGE sink: polarities were perpendicular pointing to the edge and divergent in respective canvas regions.

The ratio of growth occurring parallel (Kpar) to perpendicular (Kper) was modelled as the action of polarity on the thallus with an end-point which was equivalent to real plants at an early stage of development, the end point of plastochron 1 (**Figure 3.2D**; Solly et al., 2017). When the ratio of Kpar to Kper was set to 1, the outcome resembled the aforementioned 'Notch-pre-patterns growth' model, describing the characteristic development of *M. polymorpha* effectively. Alteration to the ratio of Kpar to Kper in the model allowed thallus shape to be manipulated.

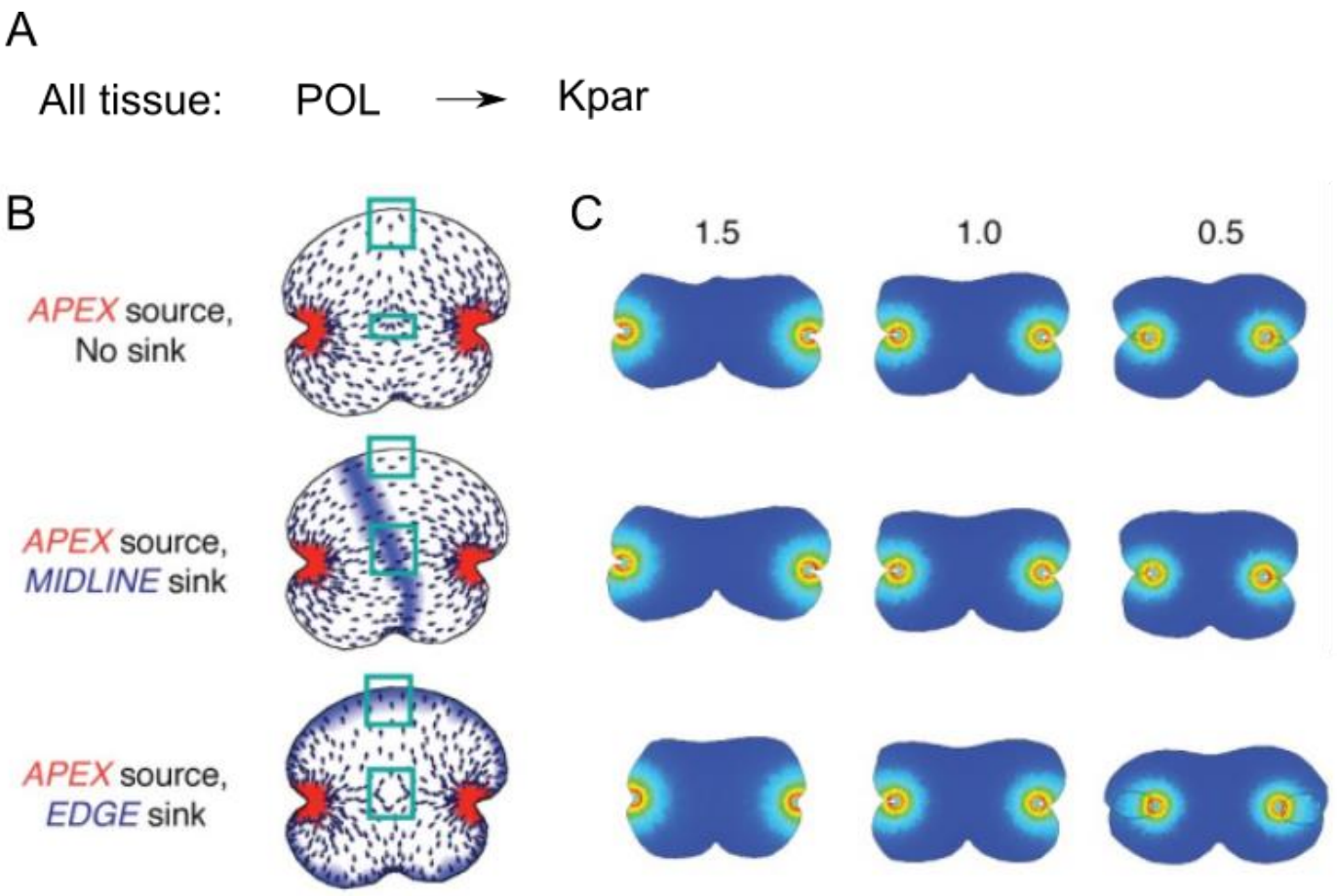

Figure 3.2: The effect of varying polarity fields on thallus shape in a model. Figure produced by Jeremy Solly and Dr. Jill Harrison (unpublished). (**A**) Additional growth (K) rule for the model to incorporate the effect of the morphogen POLARISER (POL) across all tissue in the model. (**B**) Variations of the POLSOURCE and POLSINK distributions which specify polarity fields across the canvases in the model simulations. Green boxes highlight regions of particular interest that differ between the models. (**C**) The resulting growth of the thallus with the differing polarity variations. The variants are shown when Kpar/Kper = 1.5, Kpar/Kper = 1, and Kpar/Kper = 0.5.

Model simulations with the source of POL at APEX and no described sink for POL showed elongated thallus shapes when Kpar/Kper = 1.5 and broadened shapes when Kpar/Kper = 0.5 relative to the simulated baseline shape where Kpar/Kper =1. Similarly, model simulations showing the sink for POL to be at the MIDLINE of the thallus showed elongation when Kpar/Kper =1.5 and a broadening when Kpar/Kper = 0.5. In contrast, model simulations with APEX as the source of POL and the sink described as EDGE showed a much greater elongation of the thallus shape when Kpar/Kper = 0.5.

In addition to the elongation or broadening of the thallus shape against the baseline model simulation, growth around the notch varied between the models. Most notably, where the source of POL is at APEX with the sink at EDGE, and Kpar/Kper = 0.5 the outgrowth of tissue of the thallus lobes engulfs the notch and the same model with Kpar/Kper = 1.5 showed greatly reduced growth around the notches. The model simulations are similar when APEX describes the source for POL and there is no SINK, despite showing opposite effects describing the overall shape of the thallus. It is worth noting that when APEX acts as the source for POL and MIDLINE the sink, there is less growth around the notch showing an observable difference.

The outcome of this unpublished modelling the effect of polarity was elongation or broadening of the thallus. To test the plausibility of the model in identifying roles for polarity in thallus shape determination, I conducted a series of growth experiments using real plants. Quantitative measures of real plants were compared to predictions generated by the model. Both wild-type and mutant thalli were grown from the uniform starting point of gemmae. Experiments to perturb the baseline levels of the plant hormones auxin and cytokinin were also conducted.

Results

Growth following development during the first plastochron

The first growth experiments were conducted in for a period equal to the endpoint of the first plastochron, period of around 6 days and equivalent to the end point of computational modelling for the model variants included in this thesis (Solly et al., 2017).

Application of synthetic auxin below a toxicity threshold results in longer and thinner gemmae

To identify the roles for auxin in polarity-dependent thallus shape variation, gemmae were grown for six days on media containing exogenously applied 1-naphthaleneacetic acid (NAA), a synthetic auxin. Initial experiments built on preliminary lab work by previous group members of Dr. Harrison's lab had indicated a toxic effect at higher concentrations of NAA on thallus growth, and higher concentrations of NAA also induced developmental defects, a finding supported by previous reports (Flores-Sandoval et al., 2015; Ishizaki et al., 2012). Therefore, the concentrations of NAA that were chosen here to reveal polarity-dependent variation of thallus shape were 0nM, 200nM, 400nM, 500nM. Data from the 200nM NAA treatment were excluded to better highlight shape changes at higher concentrations of exogenous NAA concentration.

Tak-1 plants were grown from gemmae for six days and plants were photographed using a Keyence VHX-1000 digital light microscope at 50 X magnification. Images were processed using ImageJ, and area, width, and length measurements were made as described in the methods section. Three independently grown experimental replicates were performed, with at least 30 plants grown for each treatment. **Figure 3.3A** shows the observed change in thallus shape, with exogenous auxin perturbing normal thallus development and showing progressively smaller, more elongated thalli shapes with increasing NAA concentrations.

In two out of three experimental replicates, thallus area decreased in a dose dependent manner with application of NAA (**Figure 3.3B, D, F**). In all three replicates, as concentration of NAA increased, the width: length ratio of the thalli decreased, explaining the shift to longer and thinner thallus shapes from the mock-treated controls (**Figure 3.3C, E, G**). Developmental perturbations comprising a more wrinkled phenotype at higher NAA concentrations were also observed (**Figure 3.3A**) and increased concentrations of NAA resulted in longer rhizoid formations.

The shape changes observed matched predictions from the polarity-dependent model in which plants at the same developmental stage had the same elongated thallus shape. These model variants showed more growth in parallel to the notch-to-notch axis, reflecting the movement of the POLARISER morphogen across the canvas. This was most similar to model variants where APEX acted as the source of POLARISER, and MIDLINE the sink (**Figure 3.2**).

Figure 3.3: Wild-type plants grown on media containing the synthetic auxin NAA are smaller and have a more elongated shape with increasing NAA concentration. (**A**) Light micrographs of a representative sample of each treatment after six days of growth following gemmae transfer. Scale bar represents 1 mm. (**B-G**) Thalli without gross developmental defects were selected and used in shape quantification. Measurements of width, length and area were taken and width: length ratios were calculated. Sample sizes for each treatment are indicated in the figure. (**B**,**D**,**F**) Boxplots showing the dose-dependent decline in area (mm^2) with NAA application. (**C**,**E**,**G**) Boxplots showing the relative decrease in width: length ratios with increased NAA concentration, resulting in longer and thinner thallus shapes at the highest concentration of NAA.

* significant at $p < 0.05$; ** significant at $p < 0.01$; *** significant at $p < 0.001$; **** significant at $p < 0.0001$.

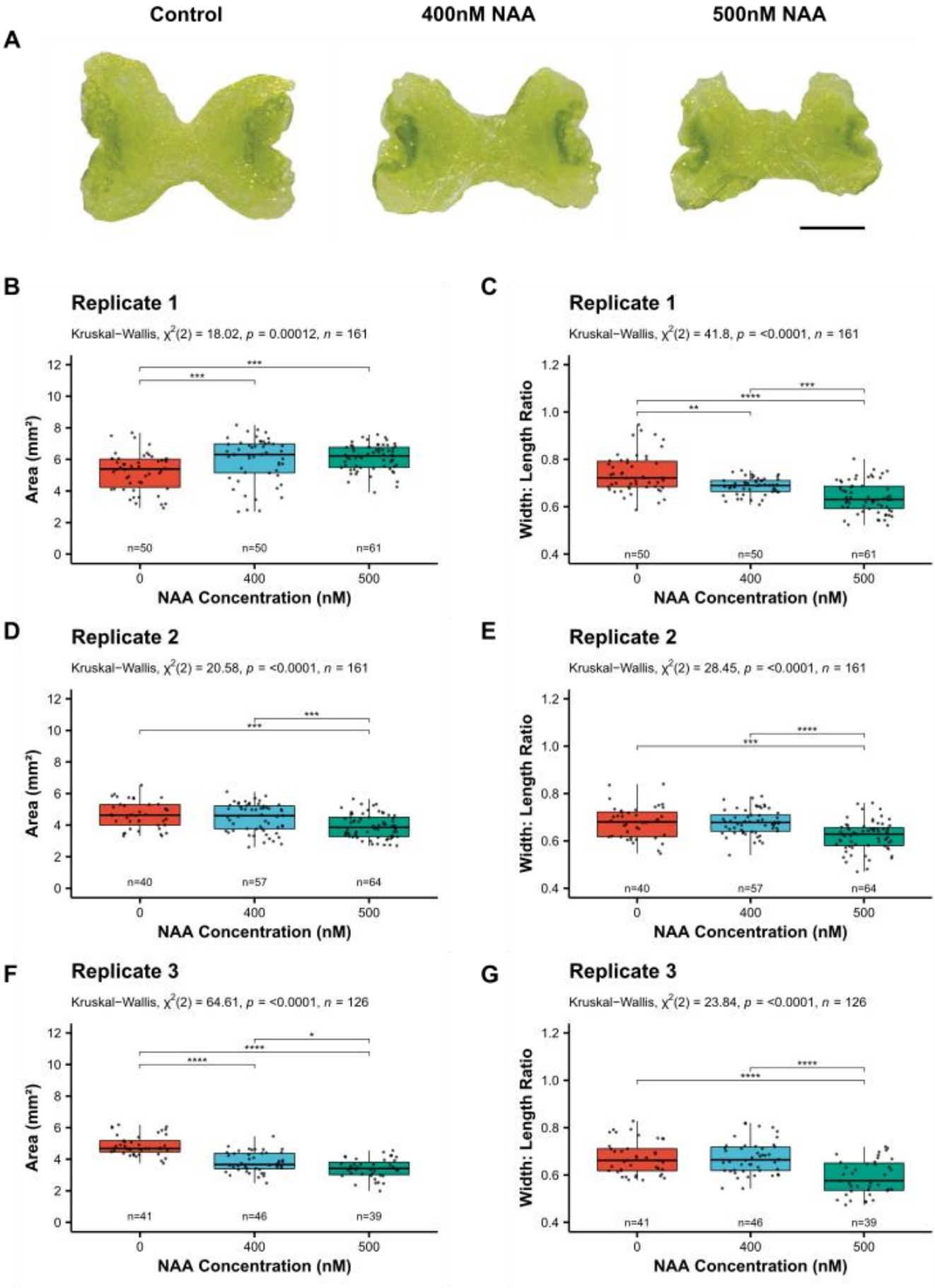
A
Control
400nM NAA
500nM NAA
B
Replicate 1
Kruskal–Wallis, $\chi^2(2) = 18.02$, $p = 0.00012$, $n = 161$
Area (mm²)
n=50
n=50
n=61
NAA Concentration (nM)
C
Replicate 1
Kruskal–Wallis, $\chi^2(2) = 41.8$, $p = <0.0001$, $n = 161$
Width: Length Ratio
n=50
n=50
n=61
NAA Concentration (nM)
D
Replicate 2
Kruskal–Wallis, $\chi^2(2) = 20.58$, $p = <0.0001$, $n = 161$
Area (mm²)
n=40
n=57
n=64
NAA Concentration (nM)
E
Replicate 2
Kruskal–Wallis, $\chi^2(2) = 28.45$, $p = <0.0001$, $n = 161$
Width: Length Ratio
n=40
n=57
n=64
NAA Concentration (nM)
F
Replicate 3
Kruskal–Wallis, $\chi^2(2) = 64.61$, $p = <0.0001$, $n = 126$
Area (mm²)
n=41
n=46
n=39
NAA Concentration (nM)
G
Replicate 3
Kruskal–Wallis, $\chi^2(2) = 23.84$, $p = <0.0001$, $n = 126$
Width: Length Ratio
n=41
n=46
n=39
NAA Concentration (nM)

Application of an auxin biosynthesis inhibitor results in smaller thalli with a shorter and wider shape

Previous studies have shown L-Kynurenine (L-Kyn), a known auxin biosynthesis inhibitor, to regulate thallus size by inhibition of thallus size at APEX (Solly et al., 2017). To further explore roles for auxin levels on *M. polymorpha* growth and shape determination, wild-type (Tak-1) gemmae were grown on 0, 30, or 60 µM of L-Kyn. After six days of growth plants were photographed using a Keyence VHX-1000 digital light microscope at 50 X magnification. Treatment with L-Kyn led to a higher number of developmental defects compared to untreated controls (Appendices). Images of thalli that did not show developmental defects were processed further using ImageJ. Measurements of area, width, and length were taken, and width: length ratios were calculated to quantify the overall shape of the thallus. Across three independently grown experimental replicates, thallus area declined with increasing L-Kyn concentration in a dose-dependent manner (**Figure 3.4A, B, D, F**), in line with the notion that auxin may equate to the growth promoting morphogen APEXPROX (Solly et al., 2017). Thalli treated with L-Kyn also exhibited a shorter and broader thallus shape relative to the control treatment thalli, and these were characterised by higher width: length ratios (**Figure 3.4C, E, G**). Plants' shape transition to a shorter and broader thallus shape may be explained by the patterning of auxin transport across the thallus by a polarity field, with reduced auxin biosynthesis limiting outwards elongation growth.

In relation to the polarity model, real plants treated with L-Kyn most closely resemble the computer model of plants grown to a similar developmental stage which have a bias of growth in the perpendicular axis. These model variants are produced when APEX acts as the source of the polarity morphogen POLARISER, and the EDGE of the thallus acts as the sink when the Kpar/Kper ratio is above 1 (**Figure 3.2**). However, these model variants were also observed when the Kpar/Kper ratio was below 1 but the MIDLINE tissue region of the canvas was the sink for POLARISER. It is therefore possible that application of L-Kyn results in the wider shape observed by inhibiting auxin production in the cells of the notch and as a result more perpendicular growth in the thallus occurs as elongation is inhibited. As L-Kyn works by inhibiting the biosynthesis of auxin, this supports the model insofar as auxin acting to pattern more parallel growth in *M. polymorpha* development through disruption to the polarity across the canvas.

Figure 3.4: Wild-type plants grown on media containing L-KYN are smaller and have a higher width: length ratio than untreated controls.

(**A**) Light micrographs of a typical phenotype of each treatment after six days of growth from gemmae. Scale bar represents 1mm. (**B-G**) Thalli without gross developmental defects were selected and used in shape quantification. Measurements of width, length and area were taken, from which width: length ratios were calculated. Sample sizes for each line are indicated in figure. (**B**,**D**,**F**) Boxplots showing the dose-dependent decline in area (mm^2) with L-KYN application. (**C**,**E**,**G**) Boxplots showing the relative increase in width: length ratios with L-KYN application. * significant at $p < 0.05$; ** significant at $p < 0.01$; *** significant at $p < 0.001$; **** significant at $p < 0.0001$.

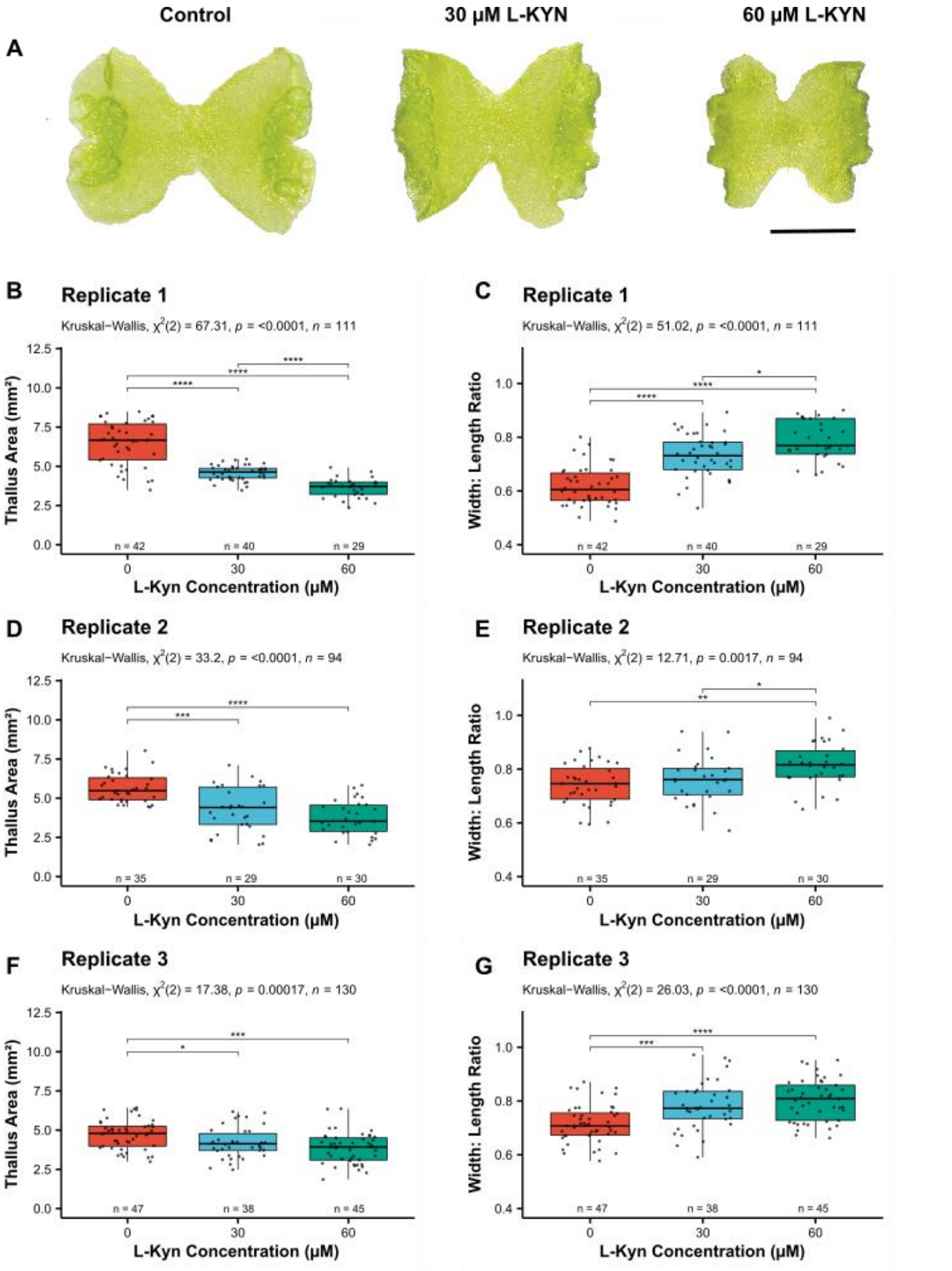
Control
30 µM L-KYN
60 µM L-KYN
A
B
Replicate 1
Kruskal–Wallis, $\chi^2(2) = 67.31$, $p = <0.0001$, $n = 111$
Thallus Area (mm²)
n = 42
n = 40
n = 29
L-Kyn Concentration (µM)
C
Replicate 1
Kruskal–Wallis, $\chi^2(2) = 51.02$, $p = <0.0001$, $n = 111$
Width: Length Ratio
D
Replicate 2
Kruskal–Wallis, $\chi^2(2) = 33.2$, $p = <0.0001$, $n = 94$
n = 35
n = 29
n = 30
E
Replicate 2
Kruskal–Wallis, $\chi^2(2) = 12.71$, $p = 0.0017$, $n = 94$
F
Replicate 3
Kruskal–Wallis, $\chi^2(2) = 17.38$, $p = 0.00017$, $n = 130$
n = 47
n = 38
n = 45
G
Replicate 3
Kruskal–Wallis, $\chi^2(2) = 26.03$, $p = <0.0001$, $n = 130$

Auxin transport inhibition results in smaller thalli with a longer and thinner shape

These data were collected by a technician in Dr Harrison's lab, Laura Weldon. I conducted all analyses following data collection. To test the effect of reduced auxin transport across the thalli, gemmae were first grown on media containing 1-n-naphthylphthalamic acid (NPA), an auxin transport inhibitor. Wild-type thalli (Tak-1) were treated with 0, 5, or 10 µM NPA and then photographed after seven days growth using a Keyence VHX-1000 digital light microscope at 50 X magnification. Images of thalli that did not show gross developmental defects were processed using ImageJ, and measures of length, width and thallus area were taken. The width: length ratio was calculated as a metric of overall plant shape. In some instances, NPA treated thalli were significantly smaller than thalli treated with a solvent control (**Figure 3.5A, B, D, F**). In all experiments, thalli treated with NPA exhibited longer and narrower thallus shapes, characterised by significantly lower width: length ratio than controls, and this effect was particularly notable in the higher concentration NPA treatment (**Figure 3.5C, E, G**). Repeating the experiment with larger sample sizes of at least 30 plants for each treatment could help resolve more clearly the dose-dependent relationship between NPA application and thallus area which was most clearly observed in replicate 1. Pooling data from all replicates removed statistical differences between the replicates.

Reduced auxin transport by MpPINZ inhibition should lead to the accumulation of auxin in cells within the notch and therefore could explain the increased elongation growth at higher concentrations of NPA application. The dose-dependent nature of the effect of NPA application on thallus width: length ratio supports the basis for auxin accumulation in the notch, with the intermediate treatment displaying the transitional effect of reduced auxin transport on the thallus.

As with NAA treatments, NPA treated thalli most closely resembled model variants with more growth occurring in the parallel orientation than perpendicular growth. There is little growth around the notch which was observed in some model variants involving the POLARISER morphogen (**Figure 3.2**). The models which show the elongated thallus and less growth around the notch, namely where APEX acts as the source for POLARISER and the MIDLINE tissue acts as the sink when the Kpar/Kper ratio is above 1 therefore align to the observed phenotype. Such elongation growth implicates a role for a polarity across the canvas in the model in determining such elongated thalli shapes observed in real plants.

Figure 3.5: Wild-type thalli are smaller and have a lower width: length ratio when grown on NPA

(**A**) Light micrographs of typical phenotype of each line after seven days of growth from gemmae. Scale bar represents 1mm. (**B-G**) Thalli without gross developmental defects were selected and quantified. Measurements of width, length and area were taken, from which width: length ratios were calculated. Sample sizes for each line indicated in figure. (**B**,**D**,**F**) Boxplots showing the decrease in thallus area (mm^2) with NPA application. (**C**,**E**,**G**) Boxplots showing the dose-dependent decrease in width: length ratios between treatments, showing the progressive transition to a longer and thinner thallus shape with NPA application.

* significant at $p < 0.05$; ** significant at $p < 0.01$; *** significant at $p < 0.001$; **** significant at $p < 0.0001$.

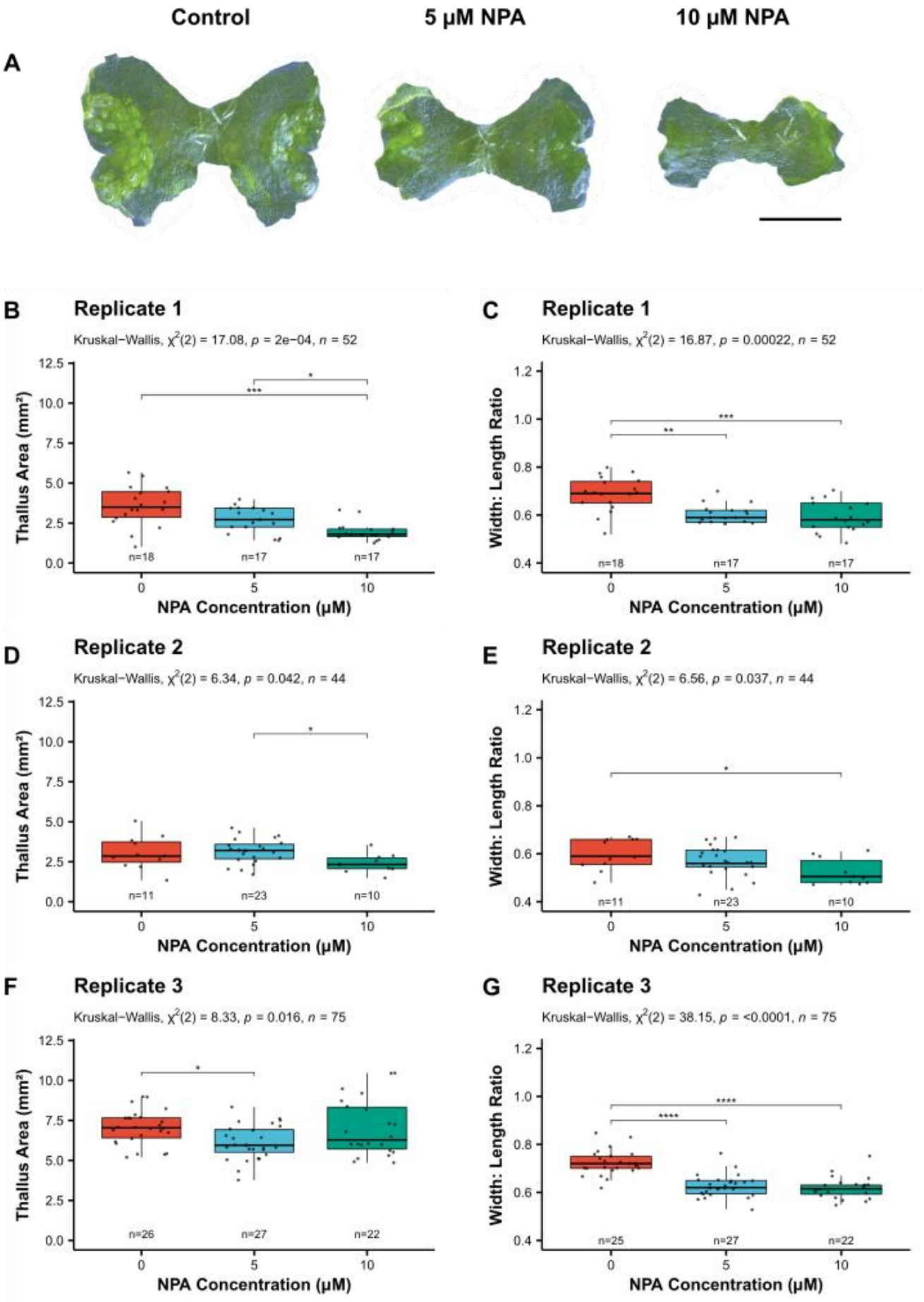
Control
5 µM NPA
10 µM NPA
A
B
Replicate 1
Kruskal–Wallis, $\chi^2(2) = 17.08$, $p = 2e{-}04$, $n = 52$
Thallus Area (mm²)
n=18
n=17
n=17
NPA Concentration (µM)
C
Replicate 1
Kruskal–Wallis, $\chi^2(2) = 16.87$, $p = 0.00022$, $n = 52$
Width: Length Ratio
D
Replicate 2
Kruskal–Wallis, $\chi^2(2) = 6.34$, $p = 0.042$, $n = 44$
n=11
n=23
n=10
E
Replicate 2
Kruskal–Wallis, $\chi^2(2) = 6.56$, $p = 0.037$, $n = 44$
F
Replicate 3
Kruskal–Wallis, $\chi^2(2) = 8.33$, $p = 0.016$, $n = 75$
n=26
n=27
n=22
G
Replicate 3
Kruskal–Wallis, $\chi^2(2) = 38.15$, $p = <0.0001$, $n = 75$
n=25
n=27
n=22

Mppinz mutants

A comprehensive study of PIN protein origin and structure previously revealed that *M. polymorpha* has 4 PIN proteins: MpPINW, MpPINX, MpPINY, and MpPINZ (Bennett et al., 2014a). The study identifies PINZ as the sole canonical protein, with a structure that dates to the last common ancestor of all plants.

To further test the effect of auxin transporter function in polarity-dependent shape determination, *Mppinz* mutant lines were first generated by Dr. Satoshi Naramoto using a CRISPR approach (see Chapter 2) and kindly given for experimental use. Upon receiving the lines, I verified the mutant line sequences by PCR and sequencing.

Sequencing the mutants

MpPINZ from both *Mppinz* mutant lines were sequenced alongside the wild-type, Tak-1, to confirm line identity and to better understand the genomic background. Following DNA extraction, a PCR reaction was undertaken to amplify *MpPINZ* before sending the samples to sequence. For analysis of the sequences received, DNA and protein sequences were aligned using MEGA X (Kumar et al., 2018) using a ClustalW approach.

Figure 3.6B shows a schematic diagram for *PINZ* in *M. polymorpha* (*MpPINZ*). Two primer pairs were tried with one pair targeting the whole MpPINZ coding region and another targeting just the start of the first exon. PCR products were generated using the latter primer pair, and these primers are shown in **Figure 3.6A**. Sequencing revealed a single base pair insertion into the Mp*PINZ* gene (**Figure 3.6C**), resulting in a frameshift in mutant sequences relative to the wild-type (**Figure 3.6D**).

Figure 3.6: Mp*pinz* mutant sequencing confirmed insertion mutation resulting in frameshift in the mutant sequences relative to the wild-type.

(**A**) Primers used for the PCR reaction. The primers flank the start of the first exon of *MpPINZ* gene. (**B**) Schematic illustrating the structure of *MpPINZ*. Locations of the MpEIR1 For and MpEIR1 Rev primer pair are shown as described in (**A**). A second primer pair MpPINZ For and MpPINZ Rev are also shown here but these did not successfully amplify the entire coding region in either wild-type or mutant plant samples. (**C**) Sequence alignment showing *MpPINZ* sequence from Tak-1 and the two Mp*pinz* mutant plants, *Mppinz(1)* and *Mppinz(2)*. The red box highlights the starting codon of the open reading frame, Exon 1 as in (**B**). The yellow highlights represent a deviation from the Tak-1 sequence, with an insertion of a single base pair (Adenine) in both *Mppinz(1)* and *Mppinz(2)* after location A298 relative to the wild-type sequence. (**D**) The open reading frames for each sequence were identified after translation and then aligned to Tak-1 showing the resulting frameshift in mutant lines. The yellow represents deviation for the Tak-1 sequence. The sequence conservation is represented by grey bars, with darker bars representing a stronger level of conservation.

A

MpEIR1For: GCTAATTCAGGGAAGTTCGTGAATG

MpEIR1Rev: GATGGTGATCATCCAGTCGAAGC

B

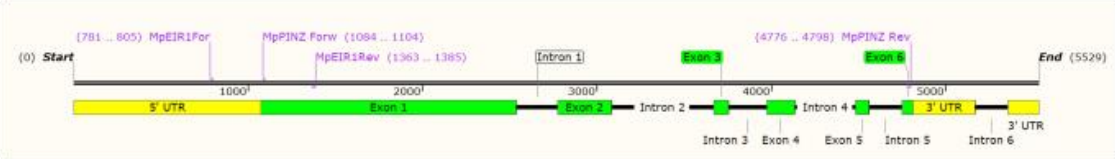

C

```
Tak1_MpEIR1 For      GGTTGGTCGCGGAGA-CTGCTCGAACTCCAGTCGAGGATCGTCACGGCGACTGGCTCGGGGGCGTGTCCA 69
MpPINZ1_MpEIR1 For   -GTTCG-CGCGGAGATCTGCTCGAACTCCAGTCGAGGATCGTCACGGCGACTGGCTCGGGGGCGTGTCCA 68
MpPINZ2_MpEIR1 For   -GGTGGTCTCGGAGATCTGCTCGAACTCCAGTCGAGGATCGTCACGGCGACTGGCTCGGGGGCGTGTCCA 69

Tak1_MpEIR1 For      AATTTTACCTGCTGCAGCTGGGCGAGCGAGCTGCCCTGCTGTGTCTGCCCGGGCGACATTCCGAATAAAT 139
MpPINZ1_MpEIR1 For   AATTTTACCTGCTGCAGCTGGGCGAGCGAGCTGCCCTGCTGTGTCTGCCCGGGCGACATTCCGAATAAAT 138
MpPINZ2_MpEIR1 For   AATTTTACCTGCTGCAGCTGGGCGAGCGAGCTGCCCTGCTGTGTCTGCCCGGGCGACATTCCGAATAAAT 139

Tak1_MpEIR1 For      GCAGGAGACAAGGAGCATAAGGACCTGTTAGCGTGCCGAGCTCGCGCGAGCTCTGTCCGTCGGCTCGGGG 209
MpPINZ1_MpEIR1 For   GCAGGAGACAAGGAGCATAAGGACCTGTTAGCGTGCCGAGCTCGCGCGAGCTCTGTCCGTCGGCTCGGGG
MpPINZ2_MpEIR1 For   GCAGGAGACAAGGAGCATAAGGACCTGTTAGCGTGCCGAGCTCGCGCGAGCTCTGTCCGTCGGCTCGGGG 209

Tak1_MpEIR1 For      CTGCTGCTGCCAGCAAGCGGAACGAGCTCGGGACTCGAAGAACAAAGCAGCGACAATGATCAACGCGCAC 279
MpPINZ1_MpEIR1 For   CTGCTGCTGCCAGCAAGCGGAACGAGCTCGGGACTCGAAGAACAAAGCAGCGACAATGATCAACGCGCAC 278
MpPINZ2_MpEIR1 For   CTGCTGCTGCCAGCAAGCGGAACGAGCTCGGGACTCGAAGAACAAAGCAGCGACAATGATCAACGCGCAC 279

Tak1_MpEIR1 For      GATCTCTACAATGTCCTCA-GCGCGGTGATACCGCTGTACGTGGCCATGATCCTGGCCTACGGGTCGGTG 348
MpPINZ1_MpEIR1 For   GATCTCTACAATGTCCTCAAGCGCGGTGATACCGCTGTACGTGGCCATGATCCTGGCCTACGGGTCGGTG 348
MpPINZ2_MpEIR1 For   GATCTCTACAATGTCCTCAAGCGCGGTGATACCGCTGTACGTGGCCATGATCCTGGCCTACGGGTCGGTG 349

Tak1_MpEIR1 For      AAATGGTGGGGGATTCTGACGCCGGATCAATGCGGGGGCATCAATCGCTTCGTGGCCGTGTTCGCCGTGC 418
MpPINZ1_MpEIR1 For   AAATGGTGGGGGATTCTGACGCCGGATCAATGCGGGGGCATCAATCGCTTCGTGGCCGTGTTCGCCGTGC 418
MpPINZ2_MpEIR1 For   AAATGGTGGGGGATTCTGACGCCGGATCAATGCGGGGGCATCAATCGCTTCGTGGCCGTGTTCGCCGTGC 419

Tak1_MpEIR1 For      CGCTGCTGTCGTTCAAGTTCATCGCGCTCAACGATCCCTACACCATGAACTACCAGTTCATCGCAGCAGA 488
MpPINZ1_MpEIR1 For   CGCTGCTGTCGTTCAAGTTCATCGCGCTCAACGATCCCTACACCATGAACTACCAGTTCATCGCAGCAGA 488
MpPINZ2_MpEIR1 For   CGCTGCTGTCGTTCAAGTTCATCGCGCTCAACGATCCCTACACCATGAACTACCAGTTCATCGCAGCAGA 489

Tak1_MpEIR1 For      CGCCATGTCGAAGATCGCCATCCTGATTCTGCTGGGCCTGTGGGCGCGCTACACCAAGCGCGGCAGCTTC 558
MpPINZ1_MpEIR1 For   CGCCATGTCGAAGATCGCCATCCTGATTCTGCTGGGCCTGTGGGCGCGCTACACCAAGCGCGGCAGCTTC 558
MpPINZ2_MpEIR1 For   CGCCATGTCGAAGATCGCCATCCTGATTCTGCTGGGCCTGTGGGCGCGCTACACCAAGCGCGGCAGCTTC 559

Tak1_MpEIR1 For      GACTGGATGA--TCCACCA--TCAAAA 581
MpPINZ1_MpEIR1 For   GACTGGATAGACCCCACCAATTCAAAA 585
MpPINZ2_MpEIR1 For   GACTGGATGA--TCCACCA--TCAAAA 582
```

D

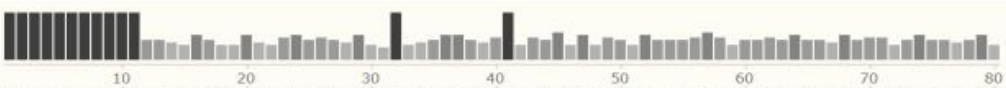


```
Tak1          MINAHDLYNVLSAVIPLYVAMILAYGSVKWWGILTPDQCGGINRFVAVFAVPLLSFKFIALNDPYTMNYQFIAADAMSKI 80
MppinZ(1)     MINAHDLYNVLKRGDTAVRGHDPGLRVGEMVGDSDAGSMRGHQSLRGRVRRAAAVVQVHRAQRSLHHELPVHRSRRHVED 80
MppinZ(2)     MINAHDLYNVLKRGDTAVRGHDPGLRVGEMVGDSDAGSMRGHQSLRGRVRRAAAVVQVHRAQRSLHHELPVHRSRRHVED 80
```


```
Tak1          AILILLGLWARYTKRGSFDWMIHHQ-- 105
MppinZ(1)     RHPDSAGPVGALHQARQLRLDRPHQFK 107
MppinZ(2)     RHPDSAGPVGALHQARQLRLDDPPSK- 106
```

Loss-of-function *Mppinz* mutants are smaller and have a longer and thinner thallus shape after six days of growth

Mppinz mutant development was quantified relative to the wild-type phenotypes (**Figure 3.7A**). Two *Mppinz* lines and a wild-type control were grown from gemmae for 6 days. Plants were photographed using a Keyence VHX-1000 digital light microscope at 50 X magnification. Images were processed using ImageJ, and thallus area, width, and length measurements were made. Three independently grown experimental replicates were performed, with at least 30 plants grown for each line. Mutant thalli were significantly smaller than wild-type thalli in all three replicates (**Figure 3.7A, B, D, F**). Mutant lines exhibited longer and narrower thallus shapes, with significantly lower width: length ratios than wild-type controls (**Figure 3.7C, E, G**).

Beyond differences in thallus shape during development, additional rhizoids on the dorsal surface of the thallus and defective development of gemma cups were observed, but these phenotypes were not quantified.

The defects of *Mppinz* mutant lines further suggest roles for auxin in *M. polymorpha* polarity-dependent shape determination and demonstrate that auxin can fulfill the requirements of the APEXPROX morphogen in model simulations (Solly et al., 2017). Applying these data to the newer model accounting for polarity shows a strong fit to shapes arising through simulation with some polarity variants. The *Mppinz* mutant shows less lobe growth around the notch than wild-type plants, as in models where APEXPROX acts as the source and the EDGE is the sink for the POLARISER morphogen. However, simulations where APEX acts as the source for POLARISER and the MIDLINE tissue acts as the sink, and Kpar/Kper is above 1 are better matched to the *Mppinz* mutant phenotype.

The phenotype observed in the *Mppinz* mutants mirrors that of plants treated with a high concentration of NPA (**Figure 3.6**), supporting the hypothesis that accumulation of auxin in the notch results in more elongation growth, observed by lower width: length ratios in both experiments. Similarly, low levels of growth in the notch were observed in both pharmacological and genetic approaches. The mutant approach suggests that the effects of NPA on *M. polymorpha* shape are not off-target (Teale & Palme, 2018).

Figure 3.7: Mp*pinz* mutant plants are smaller and have a lower width: length than wild-type plants.

(**A**) Light micrographs showing typical phenotype of each line after six days of growth from gemmae. Scale bar represents 1mm. (**B-G**) Suitable thalli lacking developmental defects were selected and quantified and width: length ratios were calculated. Sample sizes for each line are indicated in the figure. (**B**,**D**,**F**) Boxplots showing the smaller thallus area (mm^2) of *Mppinz* mutants relative to the wild-type. (**C**,**E**,**G**) Boxplots quantifying the longer and thinner thallus shape of the loss-of-function mutants, shown as a lower width: length ratio.

* significant at $p < 0.05$; ** significant at $p < 0.01$; *** significant at $p < 0.001$; **** significant at $p < 0.0001$.

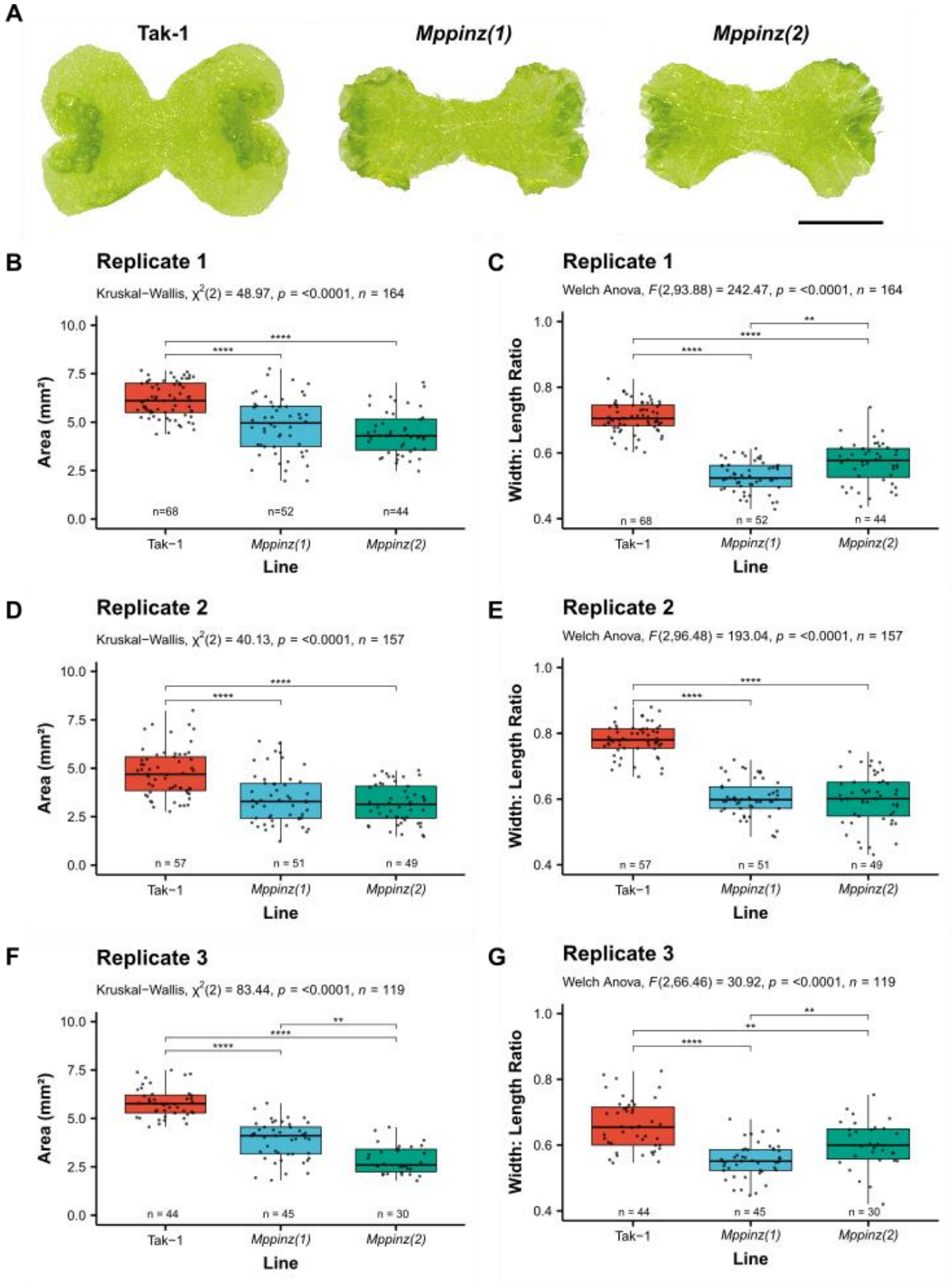
A
Tak-1
Mppinz(1)
Mppinz(2)
B
Replicate 1
Kruskal–Wallis, $\chi^2(2) = 48.97$, $p = <0.0001$, $n = 164$
Area (mm²)
n=68
n=52
n=44
Tak−1
Mppinz(1)
Mppinz(2)
Line
C
Replicate 1
Welch Anova, $F(2,93.88) = 242.47$, $p = <0.0001$, $n = 164$
Width: Length Ratio
n = 68
n = 52
n = 44
Tak−1
Mppinz(1)
Mppinz(2)
Line
D
Replicate 2
Kruskal–Wallis, $\chi^2(2) = 40.13$, $p = <0.0001$, $n = 157$
Area (mm²)
n = 57
n = 51
n = 49
Tak−1
Mppinz(1)
Mppinz(2)
Line
E
Replicate 2
Welch Anova, $F(2,96.48) = 193.04$, $p = <0.0001$, $n = 157$
Width: Length Ratio
n = 57
n = 51
n = 49
Tak−1
Mppinz(1)
Mppinz(2)
Line
F
Replicate 3
Kruskal–Wallis, $\chi^2(2) = 83.44$, $p = <0.0001$, $n = 119$
Area (mm²)
n = 44
n = 45
n = 30
Tak−1
Mppinz(1)
Mppinz(2)
Line
G
Replicate 3
Welch Anova, $F(2,66.46) = 30.92$, $p = <0.0001$, $n = 119$
Width: Length Ratio
n = 44
n = 45
n = 30
Tak−1
Mppinz(1)
Mppinz(2)
Line

Cytokinin mutants

In *A. thaliana*, auxin acts with cytokinin to modulate PIN function, and therefore I wished to test the hypothesis that cytokinin regulates thallus shape in *M. polymorpha*. Roles for cytokinin in *M. polymorpha* are not well characterised but a cytokinin signalling pathway is conserved with the *A. thaliana* signalling pathway (Aki et al., 2019). To understand the effects of cytokinin on plant shape, mutant lines with disrupted cytokinin production were grown for six days. These mutant lines were made in Dr. Harrison's lab by Jeremy Solly (unpublished data). The line JES32#10 is a cytokinin oxidase overexpressor (*CKXoe*) which results in a net lower concentration of cytokinin across the thallus and JES43#18 is an isopentenyltransferase (IPT) overexpressor which has a net higher level of cytokinin. Prior to imaging, thalli were isolated from the growth medium using forceps and placed under a cover slip on a microscope slide to best observe the thallus shape, as the mutant lines grew were curved, growing either away from (JES32#10) or into (JES43#18) the growth medium. Such epinasty and hyponasty has also been observed in other mutant lines with perturbed levels of both cytokinin and auxin across the thallus in *M. polymorpha* (Aki et al., 2019; Flores-Sandoval et al., 2015). Gemmae were photographed using a Keyence VHX-1000 digital light microscope at 50 X magnification. Thalli that did not show developmental defects were processed using ImageJ, where measures of length, width and area were taken (**Figure 9A**). The lines with a net lower level of cytokinin were mostly smaller than wild-type, and the width: length ratio was again calculated to quantify overall plant shape.

Quantitative data showed that thallus area is decreased in JES32#10 thalli relative to the wild-type, Tak-1, but thalli area is similar between wild-type and JES43#18 thalli (**Figure 3.8B,D,F**). This implicates a reduced net level of cytokinin across the thallus with smaller thalli, but thallus area is not sensitive to increased cytokinin beyond that of the baseline in wild-type plants. In two out of three replicates there was no significant difference between the area of wild-type thalli and JES43#18 thalli. This indicates a sensitivity of growth to cytokinin at lower levels but not beyond the wild-type level. However, differences in net cytokinin did affect plant shape as quantified by the width: length ratio. The JES32#10 line was elongated relative to wild-type plants and the JES43#18 line, correlating with low to high net cytokinin concentrations across the tissue (**Figure 3.8C,E,G**). Relating these data to model variants with differing Kpar/Kper growth specification beyond the initial growth canvas suggests a converse role for cytokinin in polarity-based shape determination to auxin.

The observed phenotypes of the mutant lines closely match the model variants when APEX acts as the source of POLARISER and MIDLINE the sink, as thallus lobes show little growth around the notch (**Figure 3.2**). The model variants showed polarities which were approximately parallel to the notch to notch axis. The JES32#10 line more closely resembled the output of simulations where the Kpar/Kper ratio value was above 1 and the JES43#18 line resembled the output of simulations where Kpar/Kper was below 1.

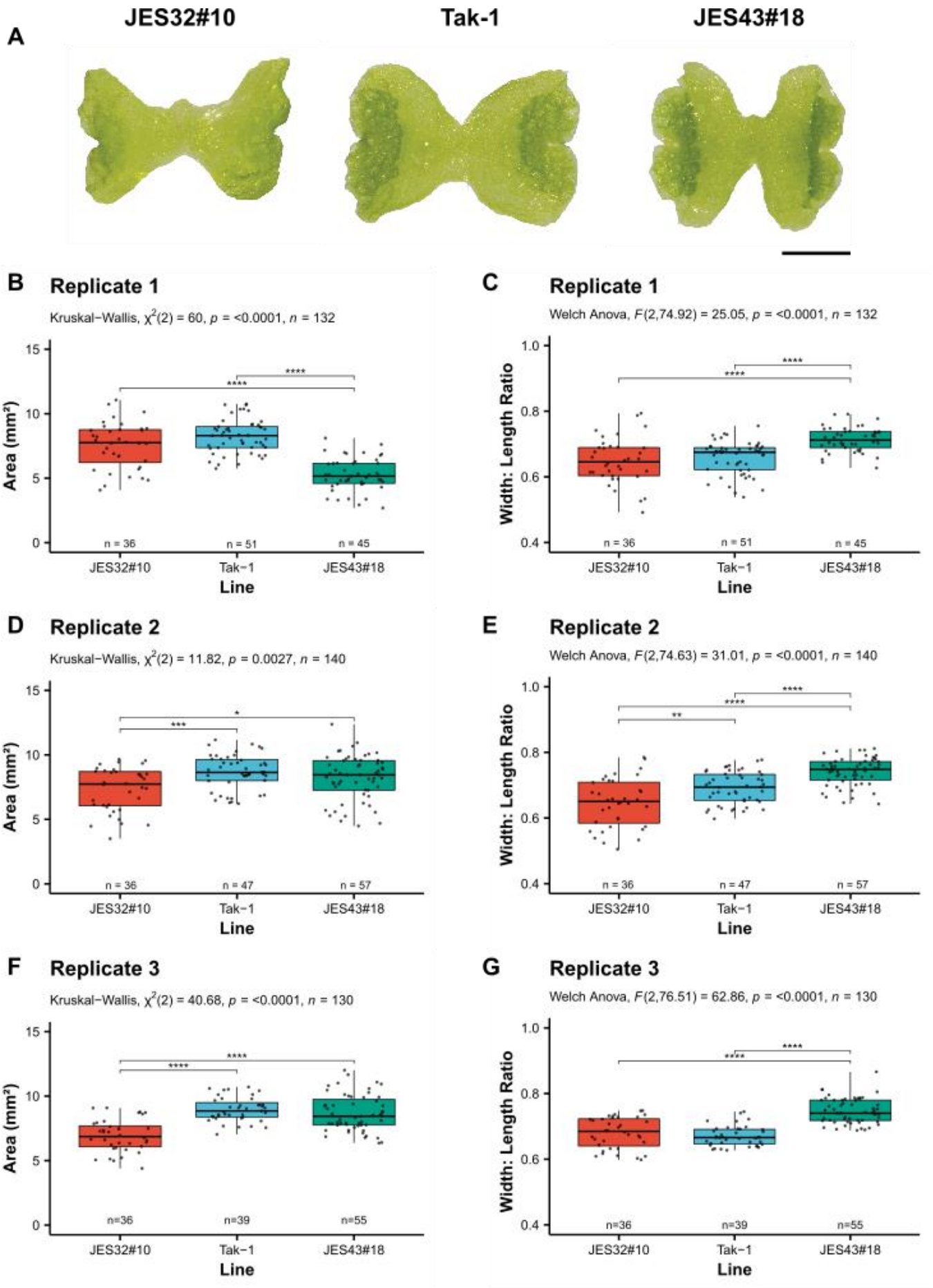
A
JES32#10
Tak-1
JES43#18
B
Replicate 1
Kruskal–Wallis, $\chi^2(2) = 60$, $p = <0.0001$, $n = 132$
Area (mm²)
n = 36
n = 51
n = 45
JES32#10
Tak-1
JES43#18
Line
C
Replicate 1
Welch Anova, $F(2,74.92) = 25.05$, $p = <0.0001$, $n = 132$
Width: Length Ratio
D
Replicate 2
Kruskal–Wallis, $\chi^2(2) = 11.82$, $p = 0.0027$, $n = 140$
n = 47
n = 57
E
Replicate 2
Welch Anova, $F(2,74.63) = 31.01$, $p = <0.0001$, $n = 140$
F
Replicate 3
Kruskal–Wallis, $\chi^2(2) = 40.68$, $p = <0.0001$, $n = 130$
n=36
n=39
n=55
G
Replicate 3
Welch Anova, $F(2,76.51) = 62.86$, $p = <0.0001$, $n = 130$

Figure 3.8: Mutant plants with perturbed cytokinin levels show variation in plant shape along a elongation continuum.

(**A**) Typical light micrographs of phenotype of each cytokinin mutant line and wild-type after six days of growth from gemmae. Scale bar represents 1mm. (**B-G**) Thalli without gross developmental defects were selected and quantified and width: length ratios were calculated. Sample sizes for each line indicated in figure. (**B**,**D**,**F**) Boxplots showing the variations in area (mm^2) between the different plant lines. (**C**,**E**,**G**) Boxplots showing the changes in width: length ratios between the mutant lines relative to wild-type, with JES43#18 resulting in shorter and broader thallus shapes contrasting with the longer and narrower thallus shapes observed in JES32#10 thalli.

* significant at $p < 0.05$; ** significant at $p < 0.01$; *** significant at $p < 0.001$; **** significant at $p < 0.0001$.

Treatment of perturbed cytokinin level mutants with an auxin transport inhibitor

To determine whether the shape changes observed in the cytokinin mutant lines were dependent on the activity of cytokinin on MpPINZ proteins, the cytokinin mutant lines were grown alongside wild-type plants on media containing the auxin transport inhibitor NPA, with the expectation that if shape transitions were dependent on MpPINZ function, they would no longer occur in NPA-treated plants. Plants were photographed after six days of growth from gemmae using a Keyence VHX-1000 digital light microscope at 50 X magnification. Images were processed using ImageJ, and area, width, and length measurements were made. Three independently grown experimental replicates were performed, with at least 30 plants grown for each treatment and for each line. **Figure 3.9A** shows the observed change of thallus phenotype, with NPA perturbing normal thallus development. The shape transitions are evident between both the dose-dependent response of thalli to NPA application (**Figure 3.5**). Shape differences between the wild-type and cytokinin mutant lines were also observed as described from previous data (**Figure 3.8**). Whilst the JES32#10 line appeared to elongate further following NPA treatment, there was little apparent effect of NPA on the JES43#18 line.

The phenotypes of NPA treated plants were quantified, and statistical analyses were first performed within mutant lines treated with three concentrations of NPA and these are shown alongside each other in **Figure 3.9B-G**. Between groups statistical analyses shown in the figure revealed support for significant differences between genetic backgrounds similar to previous data (**Figure 3.8**). In all three genetic backgrounds, NPA application resulted in a transition to smaller thalli, consistent with the notion that auxin transport from the notch is required to promote growth. This transition was most notable and consistent in the JES32#10 line which has a net lower concentration of cytokinin across the thalli. In each genetic background, NPA led to a transition to more elongated thalli shapes. Again, this transition was most notable in the line expressing a lower cytokinin level across the tissue. This shows that the mutant thalli can become even more elongated than with auxin transport inhibition by NPA.

The elongation phenotype in the cytokinin mutants treated with NPA suggests that cytokinin dependent shape transitions are sensitive to auxin transport disruption across the thallus. The effect of NPA therefore may overrule the effect of elevated cytokinin on the thallus, suggesting that shape changes may occur through MpPINZ proteins. An antagonistic role of cytokinin to that of auxin in patterning thallus shape in development is therefore supported. The known interplay of auxin and cytokinin in *A. thaliana* development involves cytokinin regulating auxin distribution by acting as a polarizing cue for the AtPIN1 distribution in plasma membranes (Marhavý et al., 2014). The authors observed that cytokinin increased AtPIN1 depletion and thereby altering the auxin flow through the rearrangement of PIN protein polarities. A similar relationship between auxin and cytokinin could act to pattern auxin transport distribution in *M. polymorpha* and therefore modulate plant shape in development.

In relation to the generation of model polarity variants incorporating the POLARISER morphogen, the application of NPA to the cytokinin mutants combines the shape transitions seen in isolation in experiments already listed in this thesis. As within the experiment looking at just the cytokinin mutants, the JES32#10 line more closely resembled the output of model simulations with a Kpar/Kper ratio value above 1 and the JES43#18 resembling simulations with a value tending below 1 when APEX is the source for POLARISER and MIDLINE acts as the SINK. When NPA application is considered, these model variants could be seen to act as a starting point for the elongation observed in real plants which is seen in the lines, which tends to higher Kpar/Kper ratio and thus a higher level of growth in parallel to the notch-to-notch axis and therefore more elongated thallus shapes.

Figure 3.9: Mutant plants with perturbed cytokinin levels display cytokinin dependent shape transitions which are sensitive to auxin transport inhibition across the thallus.

(**A**) Light micrographs of a typical phenotype of each line grown on media with three different concentrations of NPA for six days from gemmae. Scale bar represents 1mm. (**B-G**) Suitable thalli were selected and quantified. Measurements of width, length and area were taken, from which width: length ratios were calculated. A sample size of at least 30 for each treatment was used. Statistics were carried out within each mutant line. (**B**,**D**,**F**) Boxplots showing the effect of both mutant line and NPA treatment on thallus area (mm^2). Thallus area decreases with NPA application, with differences in sensitivity between the plant lines. (**C**,**E**,**G**) Boxplots showing the variation in width: length ratios with NPA application between the lines. NPA application lowers the width: length ratio of the thalli so more elongated thallus shapes were observed.

* significant at $p < 0.05$; ** significant at $p < 0.01$; *** significant at $p < 0.001$; **** significant at $p < 0.0001$.

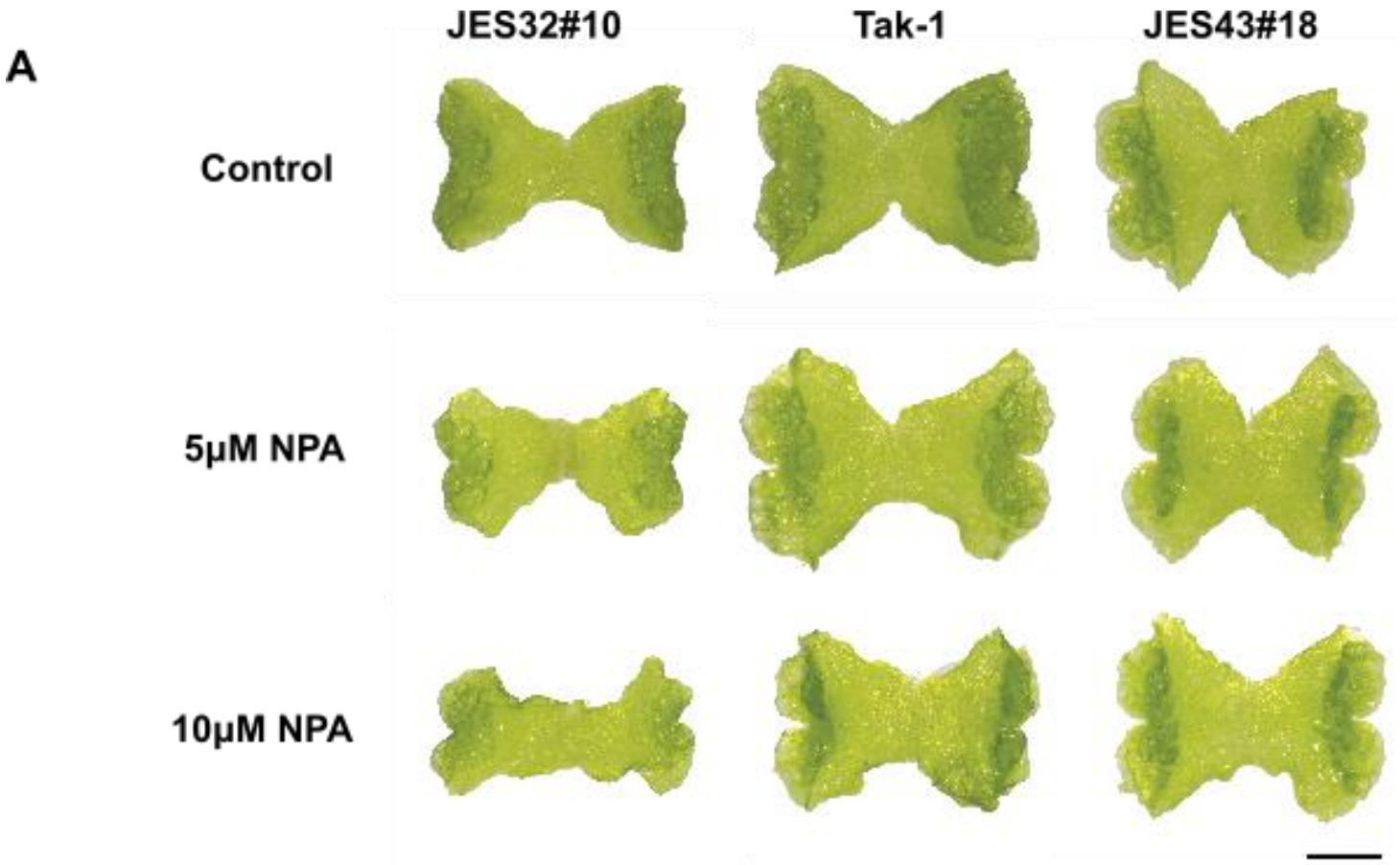

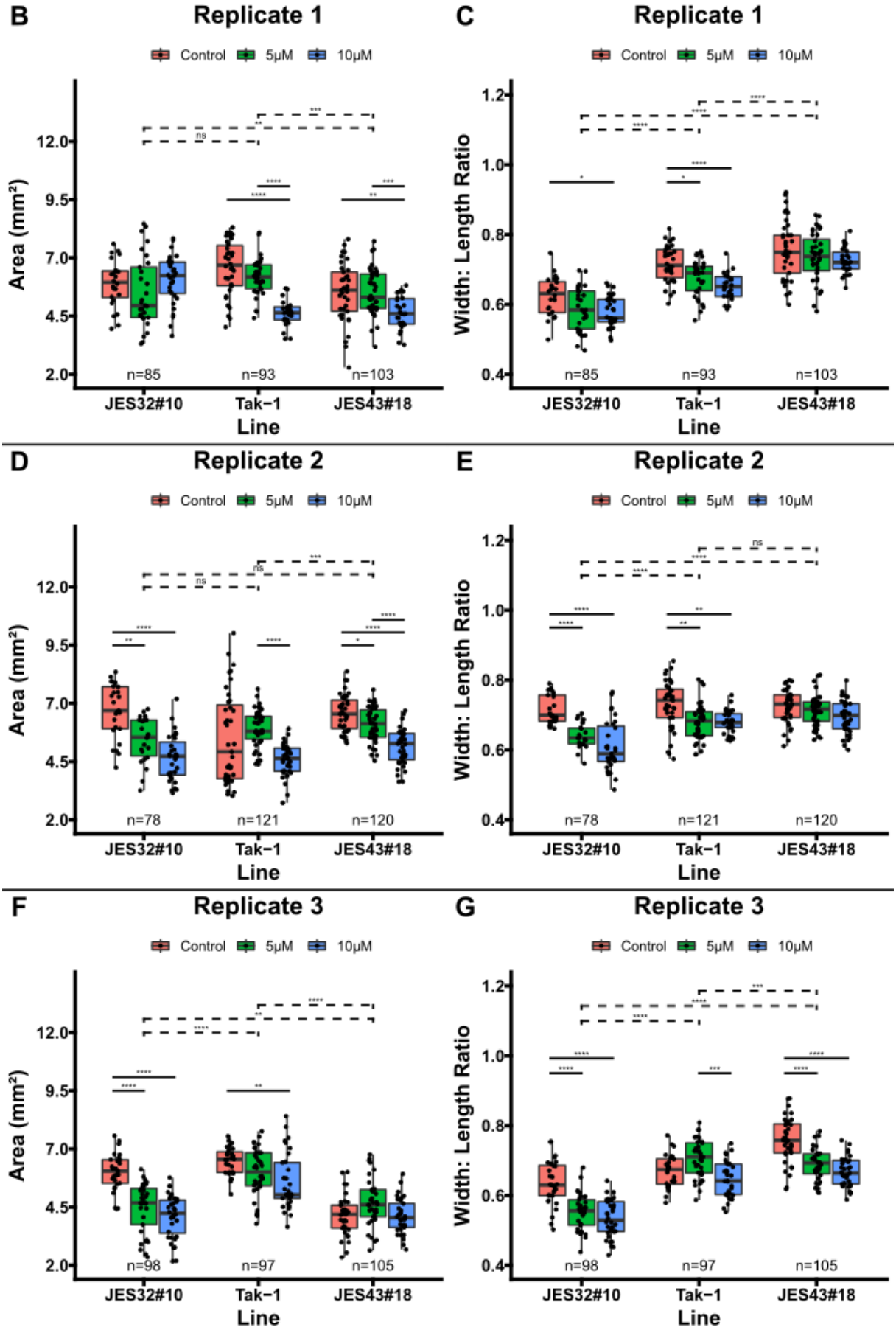
B
Replicate 1
Control
5μM
10μM
Area (mm²)
12.0
9.5
7.0
4.5
2.0
ns
**
***
****
****
***
**
n=85
n=93
n=103
JES32#10
Tak−1
JES43#18
Line
C
Replicate 1
Control
5μM
10μM
Width: Length Ratio
1.2
1.0
0.8
0.6
0.4
****
****
****
*
*
****
n=85
n=93
n=103
JES32#10
Tak−1
JES43#18
Line
D
Replicate 2
Control
5μM
10μM
Area (mm²)
12.0
9.5
7.0
4.5
2.0
ns
ns
***
****
**
****
****
*
n=78
n=121
n=120
JES32#10
Tak−1
JES43#18
Line
E
Replicate 2
Control
5μM
10μM
Width: Length Ratio
1.2
1.0
0.8
0.6
0.4
ns
****
****
****
**
**
n=78
n=121
n=120
JES32#10
Tak−1
JES43#18
Line
F
Replicate 3
Control
5μM
10μM
Area (mm²)
12.0
9.5
7.0
4.5
2.0
****
**
****
****
****
**
n=98
n=97
n=105
JES32#10
Tak−1
JES43#18
Line
G
Replicate 3
Control
5μM
10μM
Width: Length Ratio
1.2
1.0
0.8
0.6
0.4
***
****
****
****
***
****
n=98
n=97
n=105
JES32#10
Tak−1
JES43#18
Line

To further dissect the effect of NPA on the phenotype of the mutant line with a net increased cytokinin level (JES43#18), the results from each of the experimental replicates from the above experiment were further analysed. The wild-type, Tak-1, treatment with no exogenous NPA was compared to the growth of the JES43#18 line at the different concentrations of NPA as above. Two of the three experimental replicates (replicates 1 and 2, shown in **Figure 3.10A-D**) reported no significant differences between in the width: length ratio between treatments, despite showing some support for the JES43#18 line having a smaller thallus area when compared to wild-type. This result contrasts with those of replicate 3 which shows the thallus area of the wild-type was bigger than the JES43#18 line at all concentrations of NPA (**Figure 3.10E**). The shape of JES43#18 thalli without any NPA treatment were significantly broader than wild-type thalli (**Figure 3.10F**), supporting results observed in **Figure 3.8**. At both 5µM and 10µM concentrations of NPA there is no significant difference observed in width: length ratios when compared to the wild-type thalli. This suggests that the inhibition of auxin transport by NPA restores the broader thalli shape of the JES43#18 line to resemble more closely that of wild-type and thus supports the hypothesis that auxin accumulation within cells in the notch influences polarity-dependent shape changes in *M. polymorpha*.

Figure 3.10: Mutant plants with a higher net level of cytokinin across the thallus have shape more closely resembling wild-type with auxin transport inhibition.

Results are from experiment described by **Figure 3.9**. The treatment groups are the wild-type (WT), Tak-1, and three NPA treatments with JES43#18 plants. Boxplots showing the area (**A, C, E**) and width: length ratios (**B, D, F**) of Tak-1 plants compared to JES43#18 plants treated with NPA and a control. Sample sizes are indicated in the figure. Replicate 3 shows wild-type thalli are bigger than JES43#18 plants at all treatments and despite having a broader thallus shape without NPA treatment, width: length ratio more closely resembles wild-type at higher NPA concentrations.

* significant at $p < 0.05$; ** significant at $p < 0.01$; *** significant at $p < 0.001$; **** significant at $p < 0.0001$.

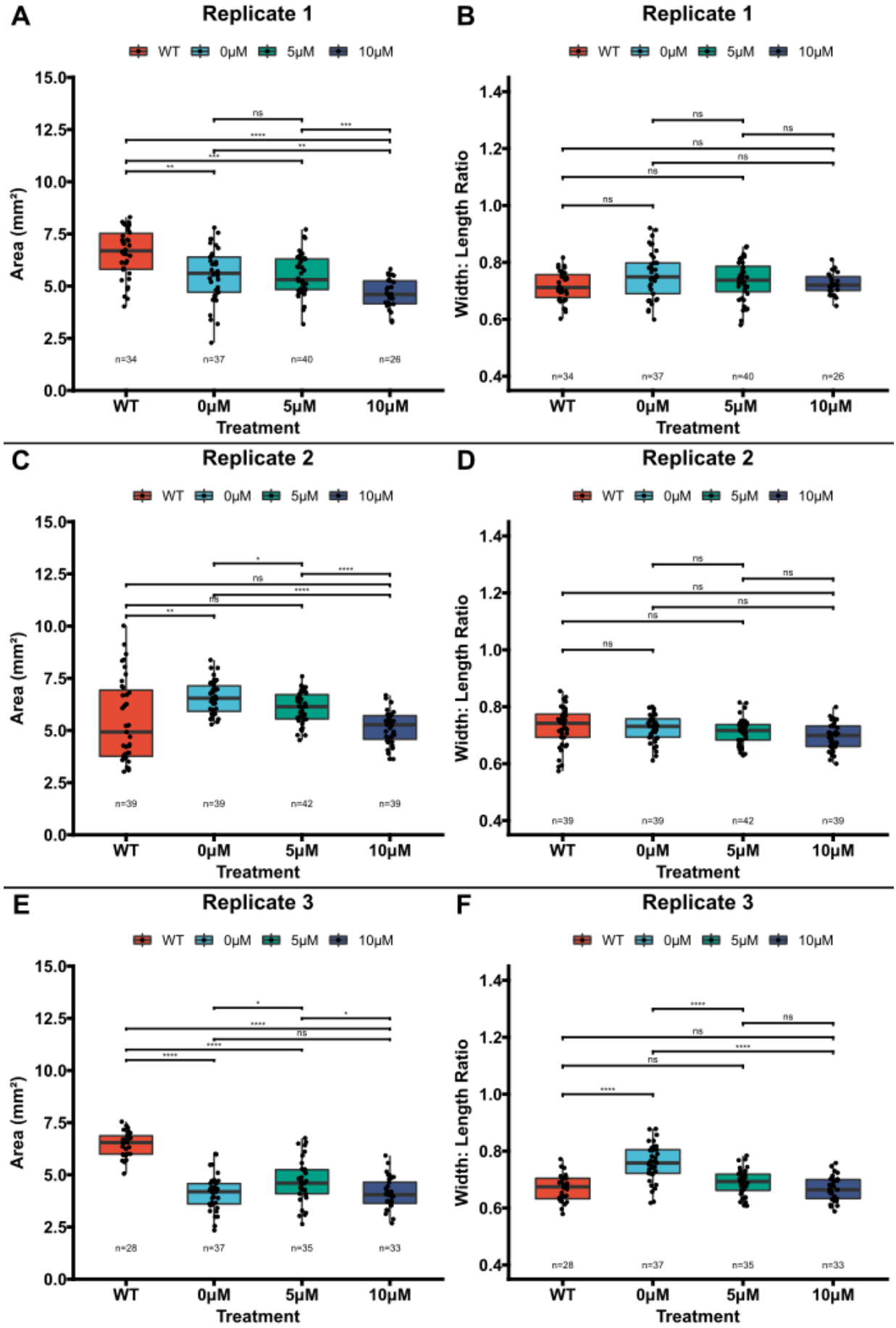
A
Replicate 1
WT 0μM 5μM 10μM
Area (mm²)
15.0
12.5
10.0
7.5
5.0
2.5
0.0
ns
***
****
**
**
***
n=34
n=37
n=40
n=26
WT
0μM
5μM
10μM
Treatment
B
Replicate 1
WT 0μM 5μM 10μM
Width: Length Ratio
1.4
1.2
1.0
0.8
0.6
0.4
ns
ns
ns
ns
ns
ns
n=34
n=37
n=40
n=26
WT
0μM
5μM
10μM
Treatment
C
Replicate 2
WT 0μM 5μM 10μM
Area (mm²)
15.0
12.5
10.0
7.5
5.0
2.5
0.0
*
****
ns
****
ns
**
n=39
n=39
n=42
n=39
WT
0μM
5μM
10μM
Treatment
D
Replicate 2
WT 0μM 5μM 10μM
Width: Length Ratio
1.4
1.2
1.0
0.8
0.6
0.4
ns
ns
ns
ns
ns
ns
n=39
n=39
n=42
n=39
WT
0μM
5μM
10μM
Treatment
E
Replicate 3
WT 0μM 5μM 10μM
Area (mm²)
15.0
12.5
10.0
7.5
5.0
2.5
0.0
*
****
ns
****
****
*
n=28
n=37
n=35
n=33
WT
0μM
5μM
10μM
Treatment
F
Replicate 3
WT 0μM 5μM 10μM
Width: Length Ratio
1.4
1.2
1.0
0.8
0.6
0.4
****
ns
ns
****
ns
****
n=28
n=37
n=35
n=33
WT
0μM
5μM
10μM
Treatment

Later developmental stages

To better understand how *M. polymorpha* development changes along a temporal scale beyond the six days of experiments I have already described, experiments and data are also included at a later developmental stage. This allows for development observations beyond the temporal scope of the model to be contrasted with how shape is achieved in a more developed thallus. *M. polymorpha* growth in the first six days is equivalent to the first plastochron of development, and by two weeks plants have developed through the second plastochron (Solly et al., 2017).

First, a shape analysis approach compared the growth of *Mppinz* mutants with a pharmacological approach using NPA following two weeks of growth. Then, data from experiments involving cytokinin mutants, exogenous NAA and NPA application to wild-type plants, and *Mppinz* mutant development are compared following growth for three weeks.

Shape analysis of thalli following two weeks of growth

Using the same method as for thalli shape analysis following six days of growth, shape analyses by calculation of width: length ratios were conducted after two weeks of growth. Results are shown here for both Tak-1 and *Mppinz* mutants. These can then be compared with pharmacological treatment of thalli with the auxin transport inhibitor NPA at two weeks to give a greater understanding of how shape determination in liverworts is achieved beyond the initial developmental program.

Mppinz mutants at two weeks

Tak-1 and *Mppinz* plants were grown from gemmae for two weeks and photographed using a Keyence VHX-1000 digital light microscope at 10 X magnification. Images were processed using ImageJ, and area, width, and length measurements were made. **Figure 3.11A** shows the observed change of thallus phenotype, with exogenous auxin perturbing normal thallus development. Only one experimental replicate was performed. Area and shape measurements for mutant plants which had developed an additional lobe from the dorsal notch region were measured.

Both mutant line plants had a significantly smaller thallus area compared to the wild-type (**Figure 3.11B**). There was also a significant difference between the mutant lines. Analysis of shape by the width: length ratio was however much less clear. The ratio analysis suggests a significant difference between Tak-1 and both *Mppinz* mutant lines, with the wild-type exhibiting a broader shape (**Figure 3.11C**). This contrasts with results at an earlier developmental stage shown in the first half of this chapter and could be explained by the growth of *Mppinz* mutants growing upwards from the media, opposing the flat, mat-like growth of the wild-type. Such growth lacking outwards elongation is reflected by a broader shape when measured by the ratio. This does not reflect the clear thinner shape observed at the earlier developmental stages. It would not be feasible to attain a measure of width: length ratio by flattening the thalli without damaging tissue and therefore an approach using three-dimensional imaging and quantification for shape analysis could be used (Furuya et al., 2019).

There were also defects of the number of gemma cups of each of the lines in the treatment, however these were not quantified as part of this study. As **Figure 3.11A** shows, despite the wild-type showing gemma cup development, these were only very rarely observed on mutant plants at this stage, similar to the observation of these mutants following three weeks of growth (**Figure 3.15**).

Figure 3.11: *Mppinz* mutants at two weeks of growth from gemma are smaller and have a broader thallus shape relative to wild-type.

(**A**) Light micrographs showing the morphology of *Mppinz* mutants after two weeks growth from gemma. Scale bars represent 1mm. (**B-C**) Thalli without severe developmental defects were selected and quantified. Measurements of width, length and area were taken, from which width: length ratios were calculated. Sample sizes for each line indicated in figure. Boxplots show *Mppinz* mutants are significantly smaller (**B**) than wild-type and have a higher width:length ratio (**C**) indicating a broader thallus shape relative to the wild-type.

* significant at $p < 0.05$; ** significant at $p < 0.01$; *** significant at $p < 0.001$; **** significant at $p < 0.0001$.

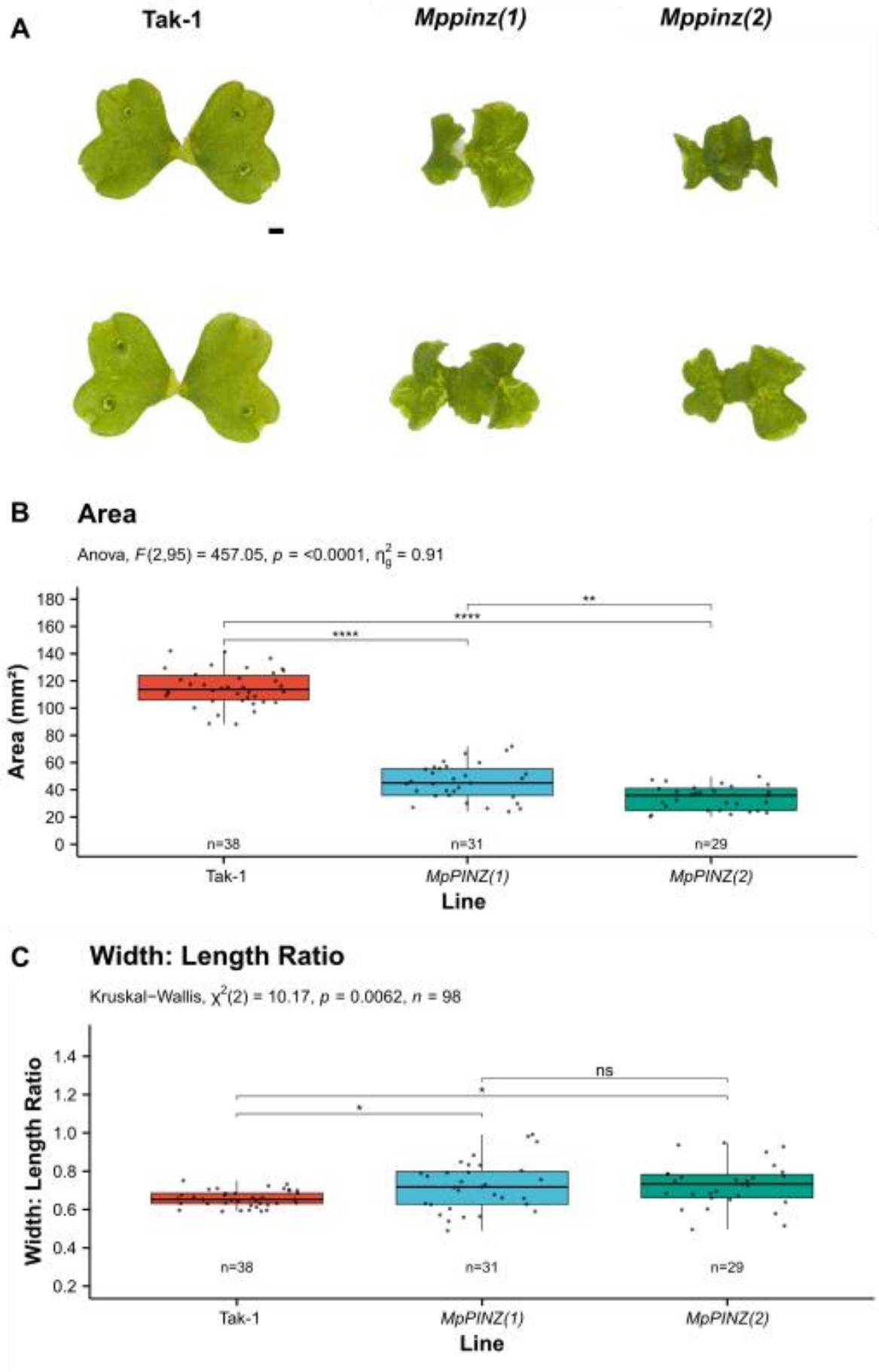
A
Tak-1
Mppinz(1)
Mppinz(2)
B
Area
Anova, F(2,95) = 457.05, p = <0.0001, η²g = 0.91
Area (mm²)
180
160
140
120
100
80
60
40
20
0
**
****
****
n=38
n=31
n=29
Tak-1
MpPINZ(1)
MpPINZ(2)
Line
C
Width: Length Ratio
Kruskal–Wallis, χ²(2) = 10.17, p = 0.0062, n = 98
Width: Length Ratio
1.4
1.2
1.0
0.8
0.6
0.4
0.2
ns
*
n=38
n=31
n=29
Tak-1
MpPINZ(1)
MpPINZ(2)
Line

NPA treatment at 2 weeks

Data were collected by a technician in Dr Harrison's lab, Laura Weldon. I conducted all analyses following data collection. Tak-1 plants were grown from gemmae on media containing the exogenous plant hormone for 3 weeks. Plants were photographed using a Keyence VHX-1000 digital light microscope at 50 X magnification. Images were processed using ImageJ, and area, width, and length measurements were made. Three independently grown experimental replicates were performed, although small samples were available after plants showing developmental defects had been removed.

Figure 3.12A shows the observed change of thallus phenotype, with NPA treatment resulting in smaller thalli with a narrower shape. In replicate three, which has the largest sample sizes, there is a significant linear relationship between the addition of NPA and the effect on both area and width: length ratios. The difference in NPA treated plants having a thinner thallus shape is what would be expected to be observed if *Mppinz* mutants grew with a mat-like thallus phenotype as observed in the NPA-treated plants. These results at a later developmental stage support those from the analysis of plants grown in the same experimental setup but analysed at an earlier stage of development (**Figure 3.5**).

Figure 3.12: *M. polymorpha* thalli treated with NPA have a reduced thallus area and show a transition to longer and thinner thalli shapes after two weeks of growth.

(**A**) Light micrographs showing the typical phenotype of each line after two weeks of growth from gemmae. Scale bar represents 1mm. (**B-G**) Suitable thalli lacking developmental defects were selected and quantified. Measurements of width, length and area (mm^2) were taken, from which width: length ratios were calculated. Sample sizes for each line are indicated for each treatment. (**B, D, F**) Boxplots showing a reduced thallus area (mm^2) in plants treated with NPA after two weeks of growth. (**C, E, G**) Boxplots showing that thalli treated with NPA have a smaller width: length ratio after two weeks of growth.

* significant at $p < 0.05$; ** significant at $p < 0.01$; *** significant at $p < 0.001$; **** significant at $p < 0.0001$.

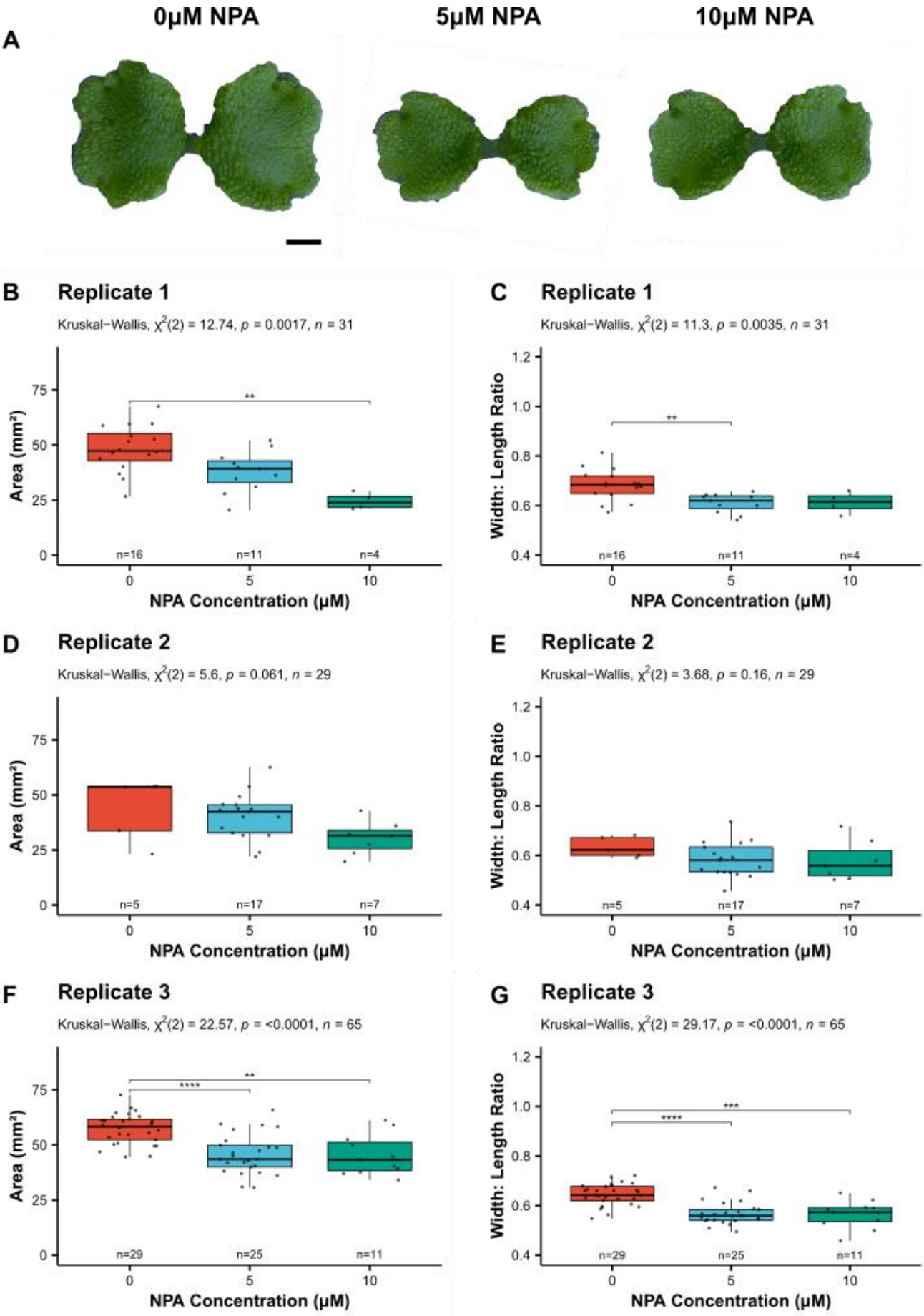
A
0μM NPA
5μM NPA
10μM NPA
B
Replicate 1
Kruskal–Wallis, $\chi^2(2) = 12.74$, $p = 0.0017$, $n = 31$
Area (mm²)
NPA Concentration (μM)
n=16
n=11
n=4
C
Replicate 1
Kruskal–Wallis, $\chi^2(2) = 11.3$, $p = 0.0035$, $n = 31$
Width: Length Ratio
NPA Concentration (μM)
n=16
n=11
n=4
D
Replicate 2
Kruskal–Wallis, $\chi^2(2) = 5.6$, $p = 0.061$, $n = 29$
Area (mm²)
NPA Concentration (μM)
n=5
n=17
n=7
E
Replicate 2
Kruskal–Wallis, $\chi^2(2) = 3.68$, $p = 0.16$, $n = 29$
Width: Length Ratio
NPA Concentration (μM)
n=5
n=17
n=7
F
Replicate 3
Kruskal–Wallis, $\chi^2(2) = 22.57$, $p = <0.0001$, $n = 65$
Area (mm²)
NPA Concentration (μM)
n=29
n=25
n=11
G
Replicate 3
Kruskal–Wallis, $\chi^2(2) = 29.17$, $p = <0.0001$, $n = 65$
Width: Length Ratio
NPA Concentration (μM)
n=29
n=25
n=11

Developmental patterning after three weeks of growth

In addition to the analysis of growth in mutants after two weeks of growth, analysis of *Mppinz* mutants is presented to supplement previous analysis of *M. polymorpha* phenotypes subject to pharmacological treatments after three weeks of growth. Comparison to *Mppinz* mutant lines can enable a greater understanding of the roles of MpPINZ proteins during development.

Cytokinin mutant morphology after three weeks of growth

These data (**Figures 3.13** and **3.14**) are reproduced from the thesis of Jeremy Solly (2015) and are included to highlight mutant phenotypes at a later developmental stage. Tak-1 and cytokinin mutant plants were grown from gemmae on media and plant development was compared following three weeks of growth, using measures of growth, the number of apices and the number of gemma cups formed. **Figure 3.13A** shows the observed change of thallus phenotype, with the shape changes observed in the earlier stages of development described in the first part of this chapter more prominent. Shape analysis was not performed on these plants, but a measure of thallus area showed all mutant lines were smaller compared to the wild-type (**Figure 3.13B**). All mutant lines also showed a lower number of apices and gemma cups in mutant lines.

Figure 3.13: Figure reproduced from Solly (2015). Cytokinin mutant phenotypes observed after three weeks of growth are smaller, have fewer apices and fewer gemma cups compared to wild-type.

(**A)** Light micrographs showing the morphology of cytokinin mutants. (**B-D**) Graphs showing quantitative variables for mutant morphology. Statistical analyses performed was ANOVA. Error bars represent the standard deviation about the mean. Values that do not share a letter within each graph are statistically different ($p \leq 0.05$). Mean thallus area (**B**), Mean number of apices (**C**), and mean number of gemma cups (**D**) were all significantly lower in mutants when compared to the wild-type. (**E**) Side view of the mutant phenotypes. Scale bars across all images is 1cm.

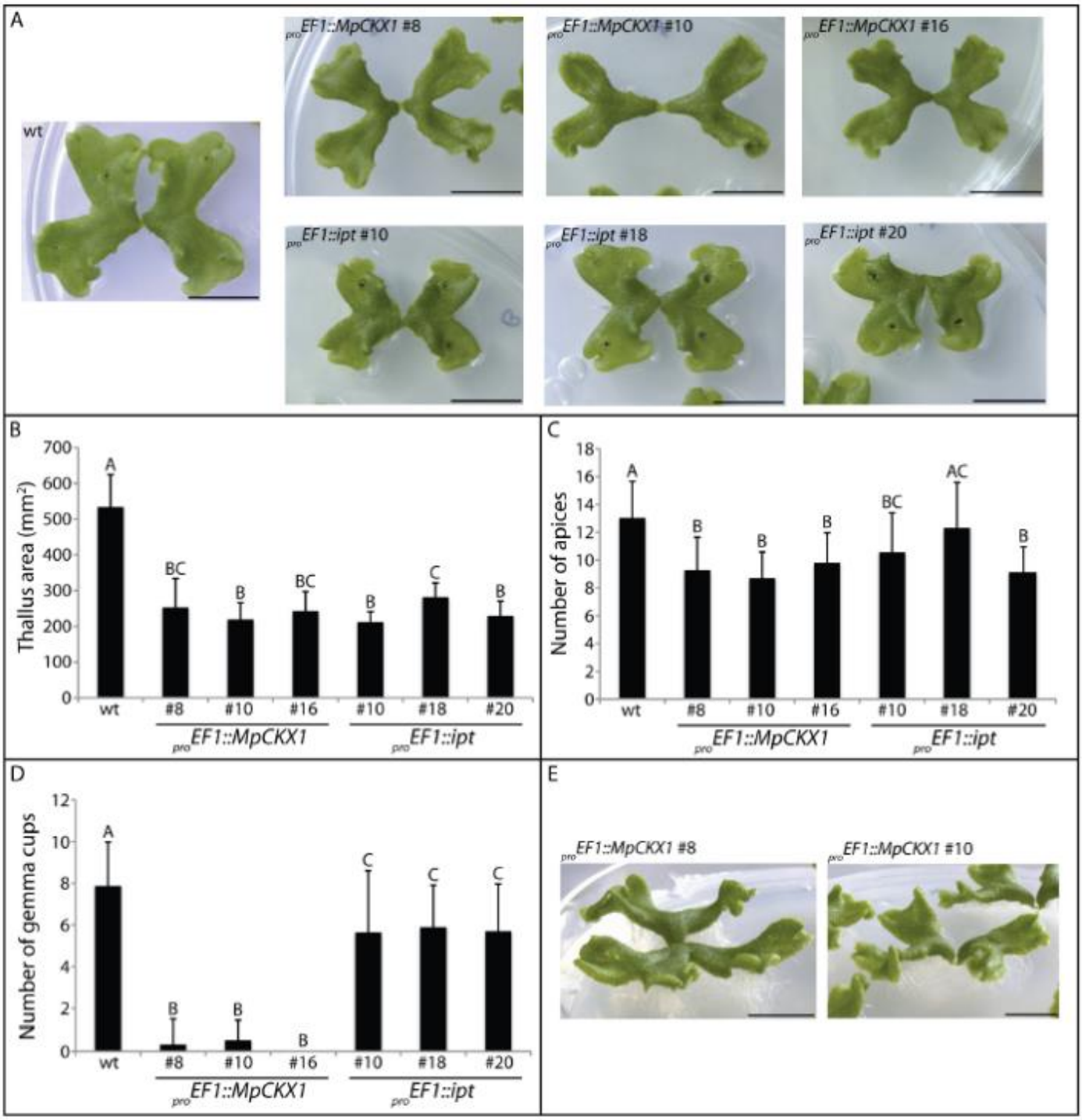
A
wt
proEF1::MpCKX1 #8
proEF1::MpCKX1 #10
proEF1::MpCKX1 #16
proEF1::ipt #10
proEF1::ipt #18
proEF1::ipt #20
B
Thallus area (mm²)
700
600
500
400
300
200
100
0
A
BC
B
BC
B
C
B
wt
#8
#10
#16
#10
#18
#20
proEF1::MpCKX1
proEF1::ipt
C
Number of apices
18
16
14
12
10
8
6
4
2
0
A
B
B
B
BC
AC
B
wt
#8
#10
#16
#10
#18
#20
proEF1::MpCKX1
proEF1::ipt
D
Number of gemma cups
12
10
8
6
4
2
0
A
B
B
B
C
C
C
wt
#8
#10
#16
#10
#18
#20
proEF1::MpCKX1
proEF1::ipt
E
proEF1::MpCKX1 #8
proEF1::MpCKX1 #10

The effect of exogenous NAA and NPA on three-week-old plants

This work was conducted by Jeremy Solly (2015) and is included to show differences in thallus shapes at a later developmental stage to contrast with the earlier developmental stages that I investigated. Tak-1 plants were grown from gemmae on media containing either the exogenous plant hormone NAA or NPA, or a combination of both. Images were taken after three weeks and data was analysed.

NPA and NAA showed similar effect to the morphology of the thallus at three weeks to the growth dynamics observed in experiments over a shorter developmental window. **Figure 3.14A** shows the observed change of thallus phenotype, with exogenous hormone perturbing normal thallus development. The thalli treated with NAA and NPA in isolation are much smaller than the wild-type (**Figure 3.14D-F)** with fewer apices relative to development in the wild-type (**Figure 3.14G-I**). Solly concludes that although reduced thalli size and apical notches were observed in all three replicates, the results were not always significant and as such the effect of NAA on the thallus morphology is clearer. The treatment of both NAA and NPA application led to significantly smaller thalli with fewer apices.

Figure 3.14: Figure reproduced from Solly (2015). The morphology of *M. polymorpha* thalli after three weeks growth on media containing NAA, NPA, or a combination of NAA and NPA.

(**A-C**) Light micrographs showing the effect of NAA and NPA treatments of thalli compared to wild-type control after three weeks growth. Scale bars are 1cm. Black arrows represent apical notches. (**D-L**) Graphs showing quantitative variables for morphological effects of NAA and NPA application on wild-type *M. polymorpha* thallus for three experimental replicates. Statistical analyses performed was ANOVA. Error bars represent the standard deviation about the mean. Values that do not share a letter within each graph are statistically different ($p \leq 0.05$). Sample sizes for the treatments are as follows: (**D, G, J**) $n \geq 15$, (**E, F, H, I, K, L**) $n \geq 28$. Graphs show the mean thallus area (**D-F**), number of apices (**G-I**), and gemma cups (**J-L**).

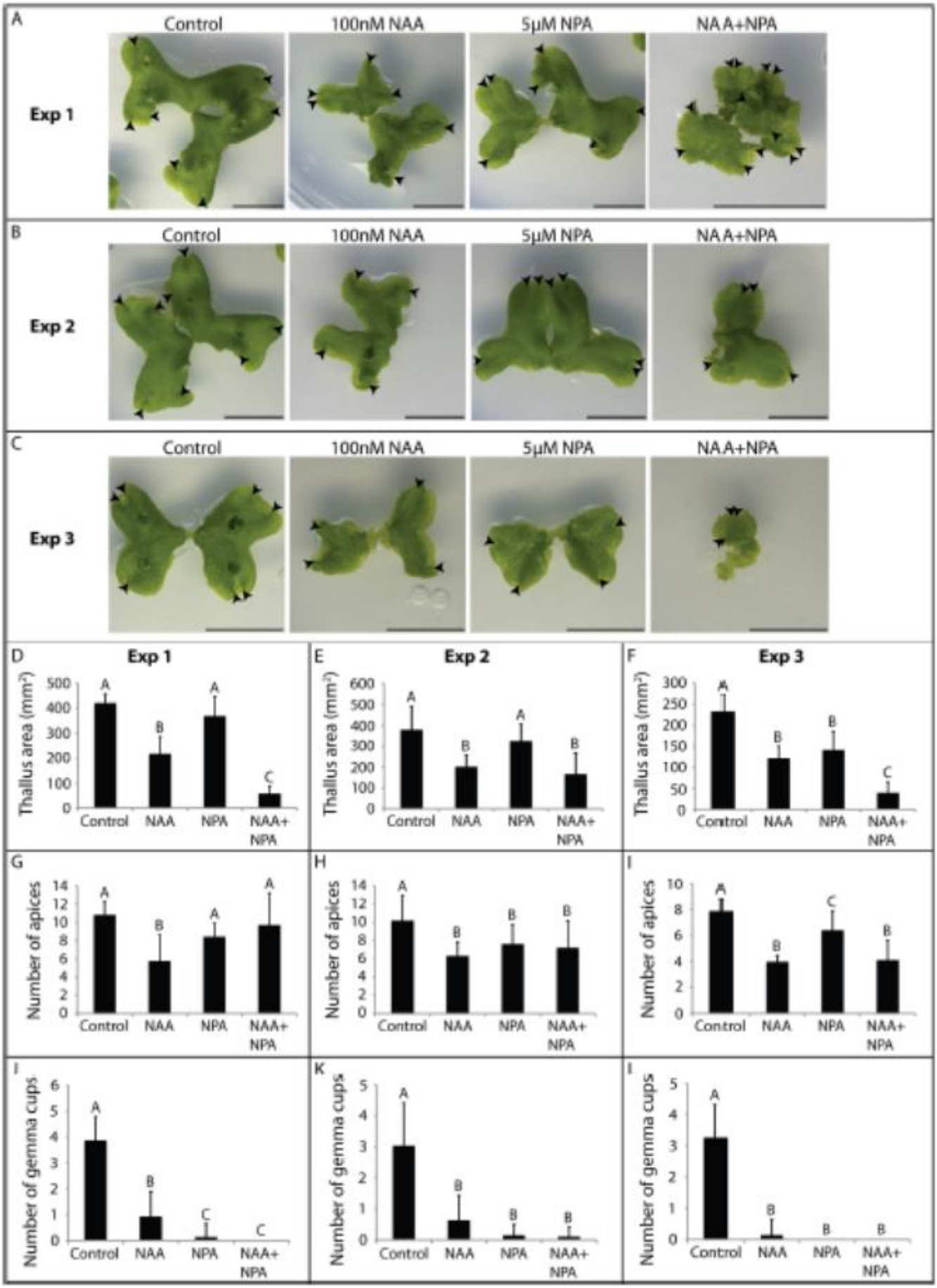
A
Control
100nM NAA
5µM NPA
NAA+NPA
Exp 1
B
Exp 2
C
Exp 3
D
Exp 1
E
Exp 2
F
Exp 3
Thallus area (mm²)
Control
NAA
NPA
NAA+ NPA
G
H
I
Number of apices
J
K
L
Number of gemma cups

Mppinz mutants at three weeks

I grew Tak-1 plants from gemmae on media containing the exogenous plant hormone for three weeks. Plants were photographed using a Keyence VHX-1000 digital light microscope at 10 X magnification. Images were processed using ImageJ, and area, width, and length measurements were made. Three independently grown experimental replicates were performed, with at least 30 plants grown for each line after those plants with gross developmental defects were removed.

By three weeks of tissue growth, *Mppinz* thalli were observed to have diverged significantly from the wild-type by growth across more planes resulting in a phenotype resembling a ball of tissue. Therefore only measures of thallus area and the number of gemma cups were taken, as these could be easily compared with the NAA and NPA data of three week old plants taken from Solly (2015). **Figure 3.15A** shows the phenotype of *Mppinz* mutant which has diverged significantly from the wild-type. Thallus area was measured using the same method as plants at earlier developmental stages and was significantly lower in both mutant lines compared to wild-type (**Figure 3.15B**).

The observation of gemma cups was atypical at this developmental stage, with observations of mutant stock lines grown for longer time periods and with additional sucrose to promote gemma cup formation still mostly lacking gemma cups.

The phenotype of the *Mppinz* mutant line resembles the phenotype of wild-type plants grown on both NAA and NPA following three weeks of growth. Both the mutant line and the pharmacological approach result in plants with significantly smaller thallus areas when compared to the wild-type in each experiment. This observation supports the implication that PINs in *M. polymorpha* transport auxin made in the notch to regulate growth across the thallus.

Figure 3.15: After three weeks of growth *Mppinz* mutants are smaller and have fewer gemma cups compared to wild-type.

(**A**) Light micrographs of a typical phenotype of each Tak-1 and both *Mppinz* mutants after six days of growth from gemmae. Scale bar represents 1mm. (**B-G**) Suitable thalli were selected and quantified. Measurements of width, length and area were taken, from which width: length ratios were calculated (see methods). Sample sizes for each line indicated in figure. (**B**,**D**,**F**) Boxplots showing the smaller thallus area (mm^2) of *Mppinz* mutants relative to the wild-type. (**C**,**E**,**G**) Boxplots quantifying the longer and thinner thallus shape of the loss-of-function mutants, shown as a lower width: length ratio.

* significant at $p < 0.05$; ** significant at $p < 0.01$; *** significant at $p < 0.001$; **** significant at $p < 0.0001$.

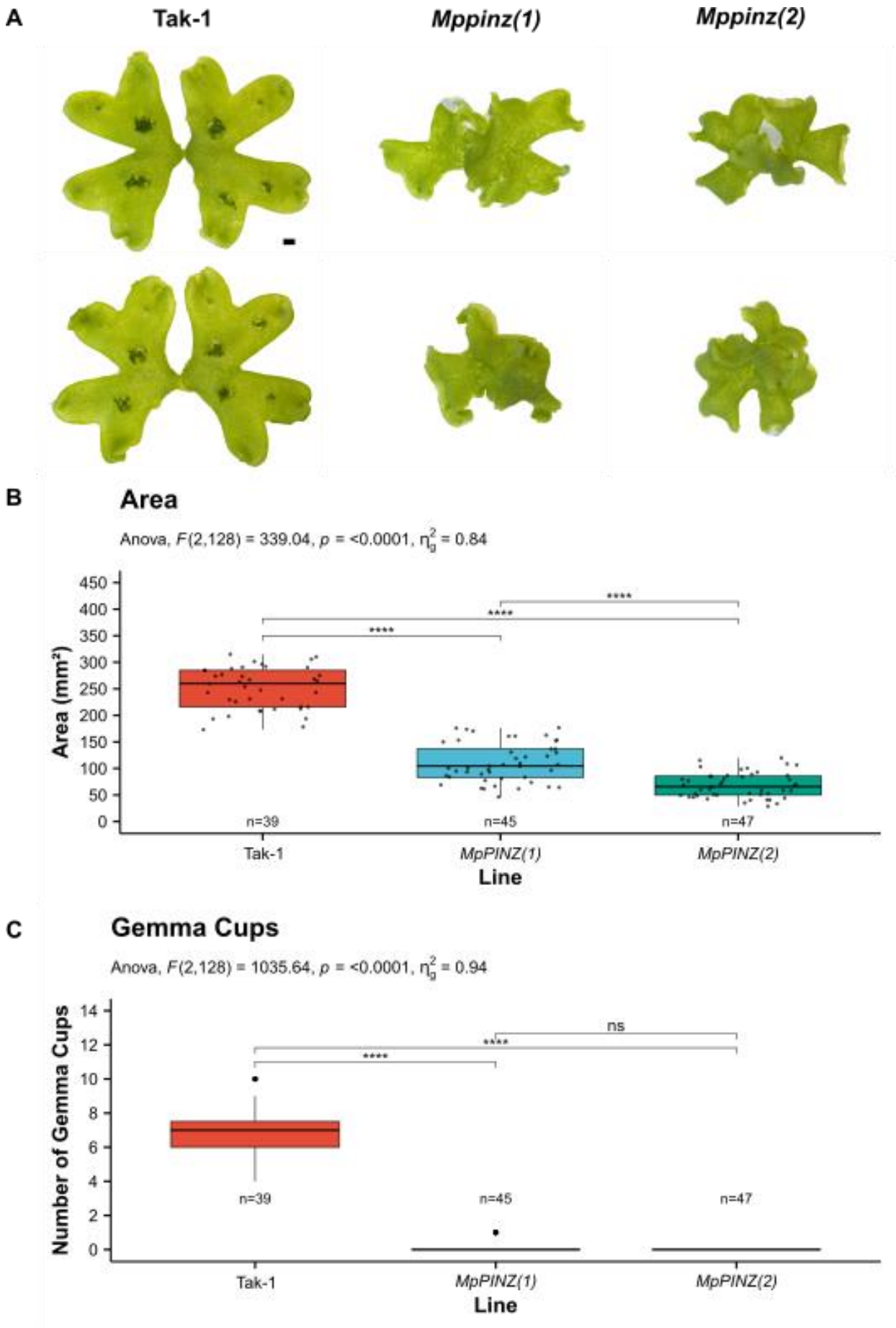
A
Tak-1
Mppinz(1)
Mppinz(2)
B
Area
Anova, F(2,128) = 339.04, p = <0.0001, η²g = 0.84
Area (mm²)
450
400
350
300
250
200
150
100
50
0
****
****
****
n=39
n=45
n=47
Tak-1
MpPINZ(1)
MpPINZ(2)
Line
C
Gemma Cups
Anova, F(2,128) = 1035.64, p = <0.0001, η²g = 0.94
Number of Gemma Cups
14
12
10
8
6
4
2
0
ns
****
****
n=39
n=45
n=47
Tak-1
MpPINZ(1)
MpPINZ(2)
Line

Chapter Discussion

Pharmacological and mutant approaches indicate roles for auxin and cytokinin in polarity determination when compared to a modelling approach

This chapter has used both pharmacological and transgenic approaches to manipulate *M. polymorpha* thalli growth to understand the role of plant hormones involved in shape determination during development. The loss-of-function mutants show that proper MpPINZ function is essential for proper shape determination during *M. polymorpha* development. The treatments involving the application of the auxin transport inhibitor NPA and synthetic auxin (NAA) also led to observation of such elongation growth, suggesting both polar MpPINZ protein function and localisation have key roles in auxin transport and thus shape determination.

When compared to model outputs generated previously, the growth experiments I have conducted support most the model output variant where APEX, around the notches, acts as the source of POLARISER and the regional thallus identity across the central thallus portion, MIDLINE, acts as the sink (**Figure 3.2**). This most clear with treatments resulting in a longer and thinner thallus shape resembling model variants with Kpar/Kper = 1.5, and treatments resembling a broader thallus shape where Kpar/Kper = 1.

Both experimental approaches have also identified shape parallels between treatments and lines. Thalli treated with NAA and NPA both have a longer and thinner thalli shape, resembling Mppinz mutants. This supports the hypothesis that auxin is accumulating in the notch but cannot be transported across the thallus resulting in elongation growth.

Growth experiments resulted in many developmental defects across treatments

A potential shortcoming of understanding tissue development through the addition of growth hormones to media is that only tissue in contact with the media is involved in the uptake of the exogenous hormones, potentially explaining the wide range of developmental perturbations observed across the pharmacological treatments (see Appendices). This plastic development was seen across all treatments, potentially suggesting some regional toxicity of hormone in the growth media. However, the similarities in phenotypes generated by pharmacological approaches resembles those by transgenic approaches, giving confidence to the experimental methods used for these growth experiments.

Mppinz mutants phenocopy wild-type thalli with perturbed auxin biology

The loss-of-function mutants show that proper MpPINZ protein function and localisation is essential for proper shape determination during *M. polymorpha* development. The treatments involving the application of the auxin transport inhibitor (NPA) and synthetic auxin (NAA) also led to observation of such elongation growth, suggesting both polar PIN protein function and localisation have key roles in auxin transport and thus shape determination. These results both support a model of auxin accumulation in the notch, by lack of transport or by exogenous application, as facilitating the transition to a longer and thinner thallus shape.

Auxin and cytokinin feedback determines thalli shape during development

The results clearly show a strong phenotypic effect of perturbed auxin and cytokinin biology. Such phenotypic effects were observed to be distinct, with mutant thalli with increased cytokinin levels across the tissue having the most divergent phenotype to thalli treated with a pharmacological auxin treatment. Auxin and cytokinin have been noted to often work in complementary patterns which result in divergent developmental programmes, for example in the balance between stem cell maintenance and cell differentiation (Schaller et al., 2015). I therefore suggest that auxin and cytokinin do work in contrast, potentially modulating the same developmental programme, MpPINZ proteins.

However, if shape in *M. polymorpha* was solely determined via MpPINZ proteins a clearer picture of shape determination should have been evident by the treatment of cytokinin mutants with NPA. The lack of clarity in experimental replicates indicates potentially other avenues of shape determination or polarity regulation beyond MpPINZ proteins. It has also been observed in a moss model system that NPA only partially disrupts transport (Bennett et al., 2014b). There is some evidence for NPA acting beyond the realm of PIN proteins (Peer et al., 2009). It would therefore be interesting to explore other transport pathways across the thalli, such as the ATP binding cassette (ABC) transporters, of which *M. polymorpha* has several auxin efflux orthologs (Bowman et al., 2017). However, a more recent investigation into NPA mode of action which suggests that NPA inhibits auxin transport by PIN proteins themselves and not a common intermediary with ABCs as was hypothesised (Abas et al., 2021).

These growth experiments at two developmental stages have provided steps towards a complete model for polarity-dependent shape determination in *M. polymorpha* described in the thesis discussion (Chapter 5). However, a suitable next step after growth experiments was to question if and where MpPINZ proteins, known to have polar localisations in the *A. thaliana* model system, are localised in *M. polymorpha*. The data from both growth experiments and a confocal approach can then be combined to better understand the role of polarity in *M. polymorpha* shape determination.

Chapter 4. Using Confocal Microscopy to Understand MpPINZ Protein Localisations in *M. polymorpha*

Introduction

Confocal microscopy enables the localisation of fluorescently labelled proteins to be identified. Localisations can then be compared across different lines, timepoints, and treatments to garner a greater understanding of the role of a given protein in the development of a plant. This chapter uses a confocal microscopy approach to better understand the localisations of MpPINZ proteins in *M. polymorpha*.

MpPINZ localisations in *M. polymorpha* are previously undescribed, and a detailed understanding of such localisations, in combination with the modelling approach and growth experiments can help elucidate the role for polarity in determining shape during the development of *M. polymorpha*. This chapter presents analysis of MpPINZGFP lines to start to understand where MpPINZ is localised across the thallus and to start to link PIN protein localisations in real *M. polymorpha* plants with the regions of interest identified by model variants (**Figure 3.2**). Confocal imaging and analysis focused on regions of the thallus where model variants had indicated to be regions of particular interest. These were across the top and bottom of the thallus, around the notches and also across the central portion of the thallus.

The aim of this chapter was to understand which of the MpPINZGFP lines are reflective of MpPINZ protein localisations in *M. polymorpha* and to start to understand localisations of such proteins. This was achieved by a combination of growth experiments to understand the phenotype of the MpPINZGFP lines relative to both wild-type thalli and *Mppinz* mutants, followed by a confocal approach to first identify which lines are of most interest and then a more detailed look into these lines.

Previous work in bryophytes using an immunolocalisation approach in the moss *Physcomitrella patens* indicates PINs as plasma membrane localised with a strong polar distribution (Bennett et al., 2014b; Viaene et al., 2014). The endpoint of confocal microscopy was to understand if the lines could be used to show where MpPINZ proteins localised in the early development of *M. polymorpha* and to assay support for hypotheses generated using a modelling approach about the orientation of polar proteins may be in shape determination. Future work will be needed to supplement the hypotheses that can be made from this preliminary data to understand the localisation of MpPINZ proteins and link this more closely to model variant outputs for a complete model of polarity-dependent shape determination in *M. polymorpha*.

The lines described in this chapter were generated and provided by Dr. Satoshi Naramoto and the materials and methods (Chapter 2) details these MpPINZGFP line generation. Throughout experiments, a positive control SNARE (MpSYP13B; Kanazawa et al., 2020) line was included as a membrane marker, and this line is also described in the materials and methods section.

Results

Growth experiments to assess the phenotype of MpPINZGFP lines

To understand the phenotype of *MpPINZGFP*-expressing lines and assay protein function (**Table 4.1**), all lines were grown and imaged after six days of growth. Plants were photographed in situ using a Keyence VHX-1000 digital light microscope at 50 X magnification. Both wild-type (Tak-1) and *Mppinz* mutant (*Mppinz(1)* and *Mppinz(2)*) lines were grown alongside the GFP-expressing lines in order to identify which phenotype they more closely resembled. A bright citrulline positive control, MpSYP13B, was also included.

Table 4.1: Details of GFP-expressing *M. polymorpha* PIN lines acquired from the lab of Dr. Satoshi Naramoto (see Chapter 2 for details of line generation). Tak1 43 1-b refers to the *Mppinz* mutant.

Abbreviation	Line Name	Sex
CIRCLE1	Tak1 43 1-b LineB #9 cup1	F
CIRCLE2	Tak1 43 1-b LineB #9 cup2	F
STAR1	Tak1 43 1-b lineD #14 cup1	M
STAR2	Tak1 43 1-b lineD #14 cup1	M
#17-A	Tak1 43 1-b #17 cupA	M
#17-B	Tak1 43 1-b #17 cupB	M
#22-B	Tak1 43 1-b #22 cupB	M

For MpPINZGFP lines to be suitable for use in explaining the localisation of MpPINZ proteins in *M. polymorpha*, a phenotype resembling the wild-type, Tak-1, was needed. Following six days of growth of approximately 50 plants of each line, most of the MpPINZGFP gemmae more closely resembled the Tak-1 gemmae when compared to the *Mppinz* mutants (**Figure 4.1**). As the mutants were produced in the *Mppinz* background, this was unexpected. At this point of development however, the STAR1 and STAR2 lines exhibited a longer and narrower shape more similar to the M*ppinz* mutants. The positive control for this series of experiments, MpSYP13B, closely resembled the wild-type.

For a comparison of the plants at a later developmental stage, I also imaged the plants following two weeks of growth and shown are a representative gemmae of each line (**Figure 4.2**). At this developmental stage there was a more obvious deviation from the wild-type phenotype in *Mppinz* mutants, but none of the MpPINZGFP lines resembled the additional lobe or such narrow thalli shape. Although not quantified, the MpPINZGFP lines all appeared to have a smaller thallus area when compared to the wild-type. The MpSYP13B line was most similar to the wild-type.

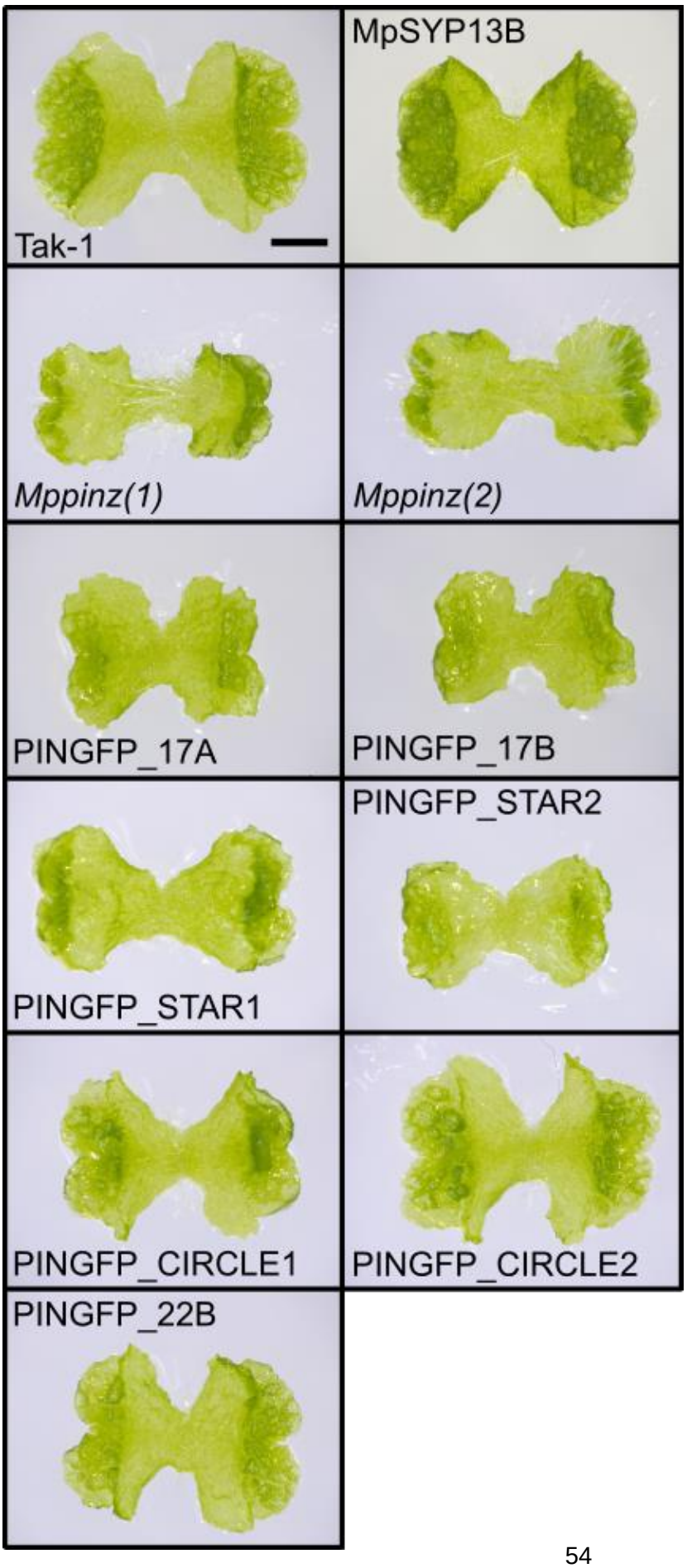

Figure 4.1: MpPINZGFP lines display phenotypes on a spectrum matching wild-type to Mppinz after 6 days

Light micrographs showing a representative gemmae from each MpPINZGFP line after six days of growth and imaged in situ.

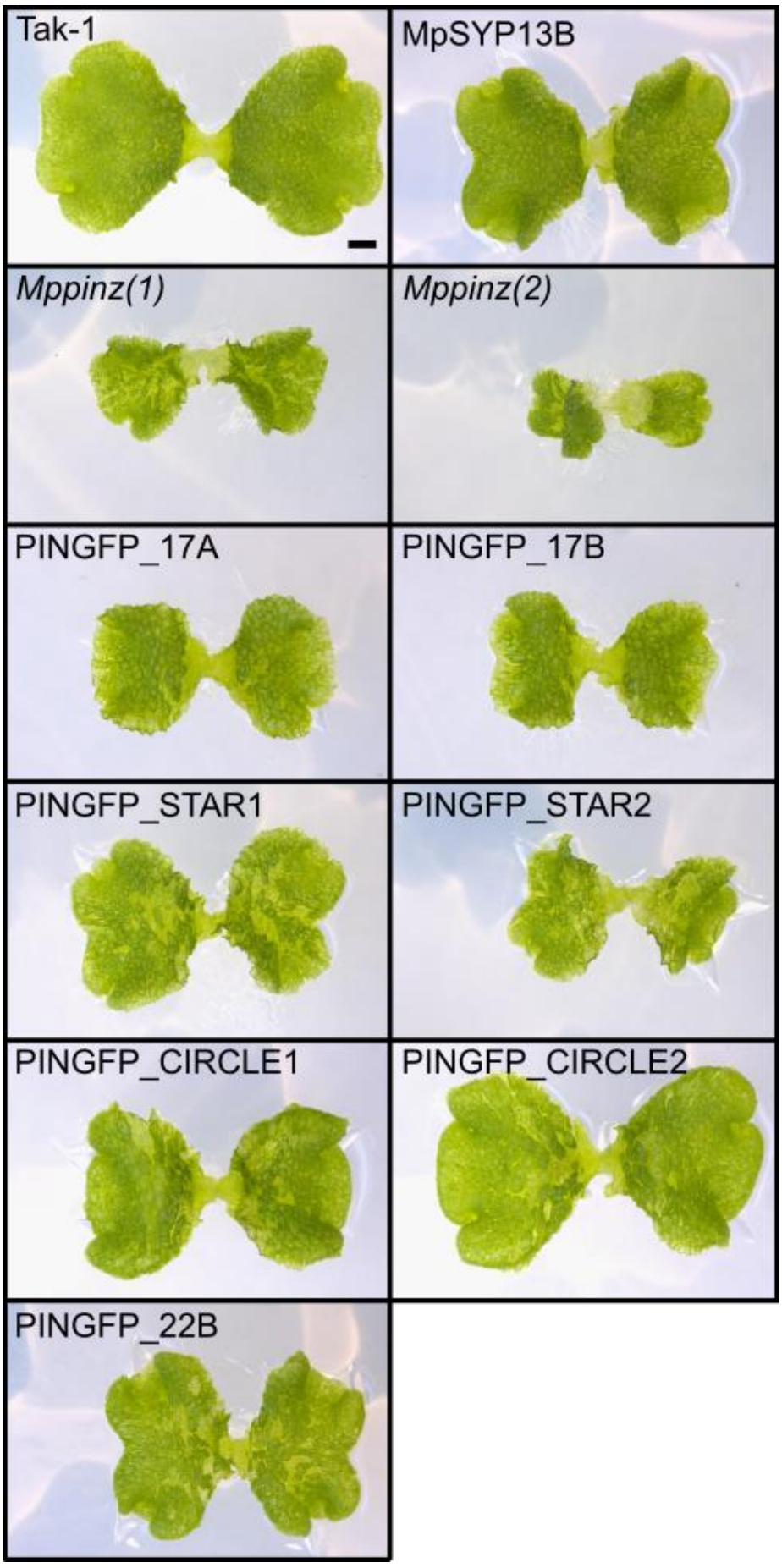

Figure 4.2: MpPINZGFP lines display phenotypes mostly diverged from wild-type after 12 days

Light micrographs showing a representative gemmae from each MpPINZGFP line after 12 days of growth and imaged in situ.

Screening potential MpPINZGFP lines by confocal imaging

To understand the quality of the GFP expression, all lines were imaged using a confocal laser scanning microscope. Gemmalings were removed from the gemma cup two hours prior to imaging and secured between a microscope slide and a coverslip.

Comparison of the images involved analysis of two channels on the confocal microscope, at different emission spectra. The first was to identify GFP expression in the samples and was at 500-550nm. A second channel at 620-680nm allowed me to pick up any autofluorescence in the samples. Collectively, this allowed the generation of composite images to visualise the MpPINZ localisations across the gemmae. There was a strong autofluorescence across all samples from chlorophyll fluorescence.

All MpPINZGFP lines were included in this confocal screen, in addition to the wild-type Tak-1 and also the positive control MpSYP13B, a SNARE protein YFP line. This line had a strong localisation under the confocal so could be used to ensure the experimental set-up was effective. **Figure 4.3** shows the collective confocal screen of a representative gemmae from all lines at both emission channels and also with a composite image generated. There was a high level of variation between the lines, with micrographs showing regional and intensity differences between the lines. An interesting observation that was made clear during the screen was the relationship between GFP localisations and cells lacking chloroplast, which are the cells that develop into rhizoids. These were helpful in identifying thalli between time points in other experiments conducted.

Upon comparison of the images, I decided that together with descriptions phenotypes acquired during growth experiments, lines #17-A, #17-B, and STAR2 were chosen for further analysis. These lines appeared to show GFP expression at the plasma membrane and had a phenotype which more closely resembled the wild-type across the lines grown. The MpSYP13B line proved to be a strong positive control for future experiments. This led to the exclusion of lines #22-B, CIRCLE1, CIRCLE2, and STAR1 from future experiments as no clear signal that differed from the autofluorescence generated by the thalli was observed.

Figure 4.3: Confocal screen of MpPINZGFP lines to assess lines to use in future experiments.

Confocal screen of green fluorescent protein (GFP)-tagged MpPINZ protein localisations across a representative gemmae in different GFP lines two hours post gemma cup removal to identify which lines show any localisation of MpPINZ protein and should be identified further. Both a wild-type line (Tak-1) and positive control MpSYP13B line are included. The two emission spectra channels from different detectors shown were chosen at these spectra to show GFP (500-550nm) and autofluorescence (620-680nm). Composite image included of both detectors of each line. Scale bar represents 100µM.

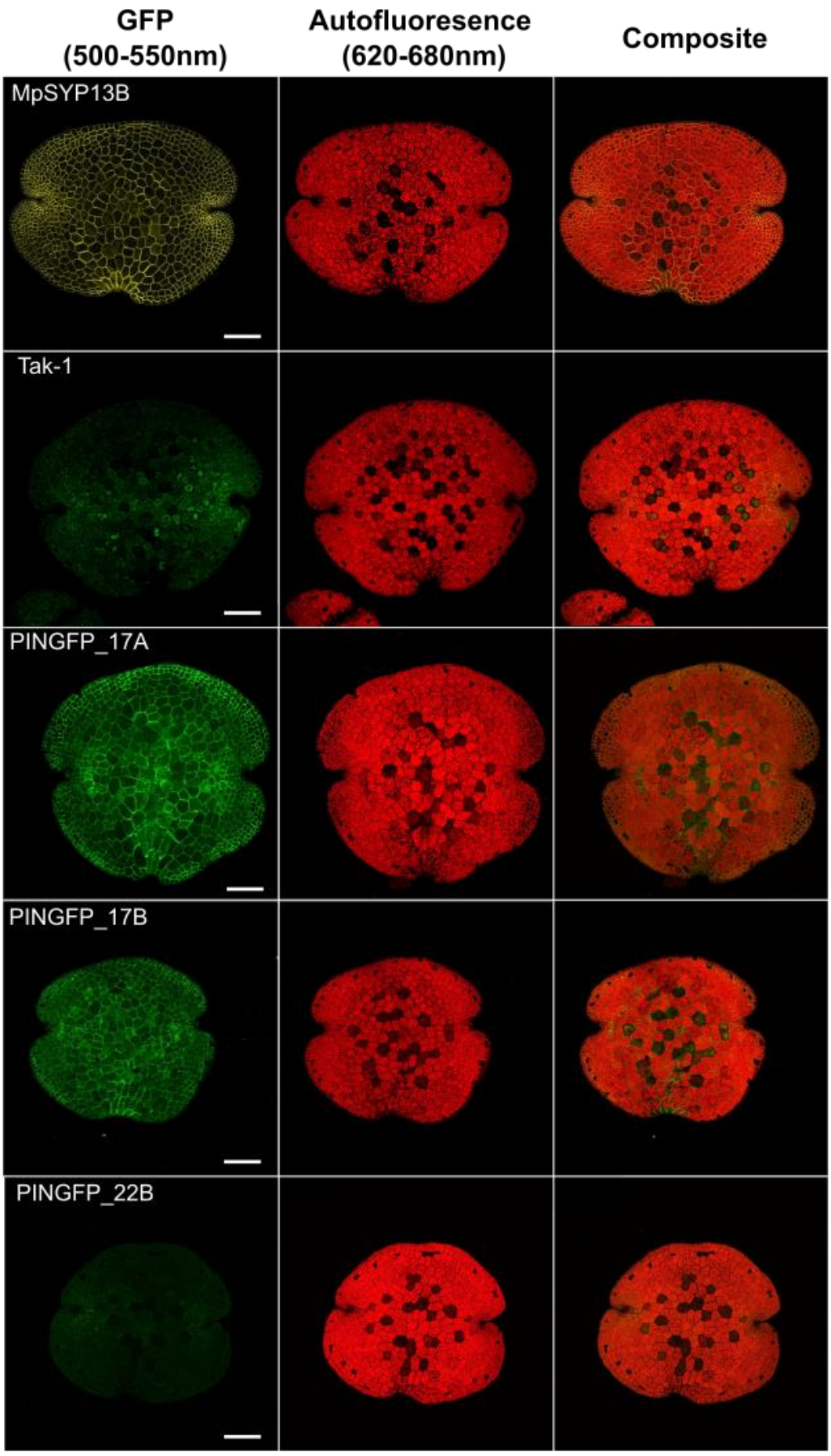
GFP
(500-550nm)
Autofluoresence
(620-680nm)
Composite
MpSYP13B
Tak-1
PINGFP_17A
PINGFP_17B
PINGFP_22B

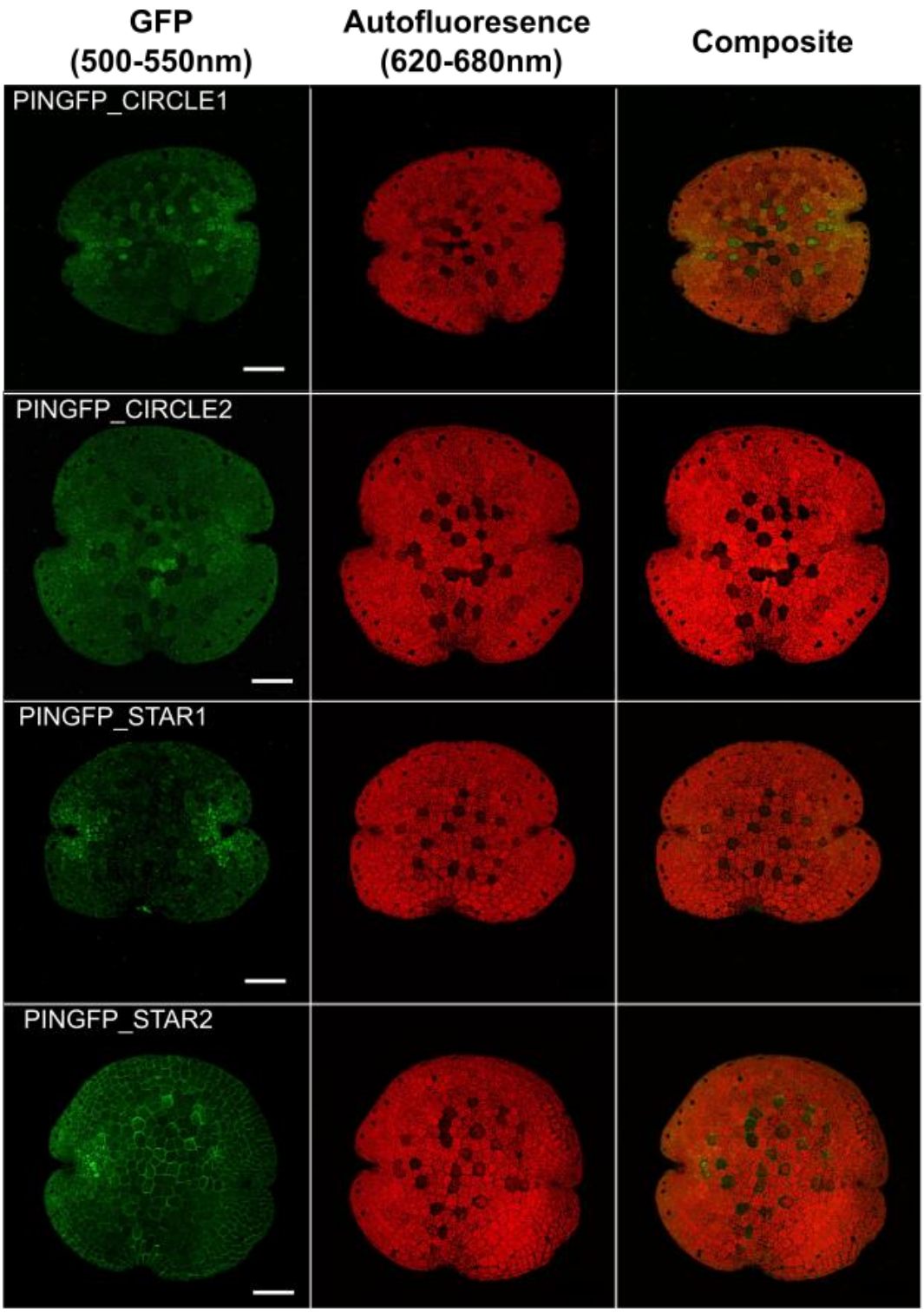
GFP
(500-550nm)
Autofluoresence
(620-680nm)
Composite
PINGFP_CIRCLE1
PINGFP_CIRCLE2
PINGFP_STAR1
PINGFP_STAR2

Growth of selected lines at two time points in early thalli development

In order to understand MpPINZ protein localisation in early development, and identify any changes to localisation through time, representative gemmae were imaged after both 2 and 24 hours (**Figure 4.4**). Gemmae at this stage, immediately following removal from the gemma cup, have just started synchronous growth by lateral expansion of the tissue (Solly et al., 2017).

The endpoint for this experiment was to explore the localisations in lines previsouly identified in the screen to show the MpPINZ localisations. I chose to include all three lines to see if there was any variation among the lines in question. The MpSYP13B line was again included as a positive control. The results are shown as a summary in **Figure 4.4**, as well as a detailed analysis of a representative gemmae at each of the lines at both time points (**Figures 4.5-4.12**). Each of these lines will each be described at the time points of both two hours and after a day of being removed from the gemma cup, before themes between lines and time points are reflected upon in the chapter discussion. All figures for each line will follow the body of text.

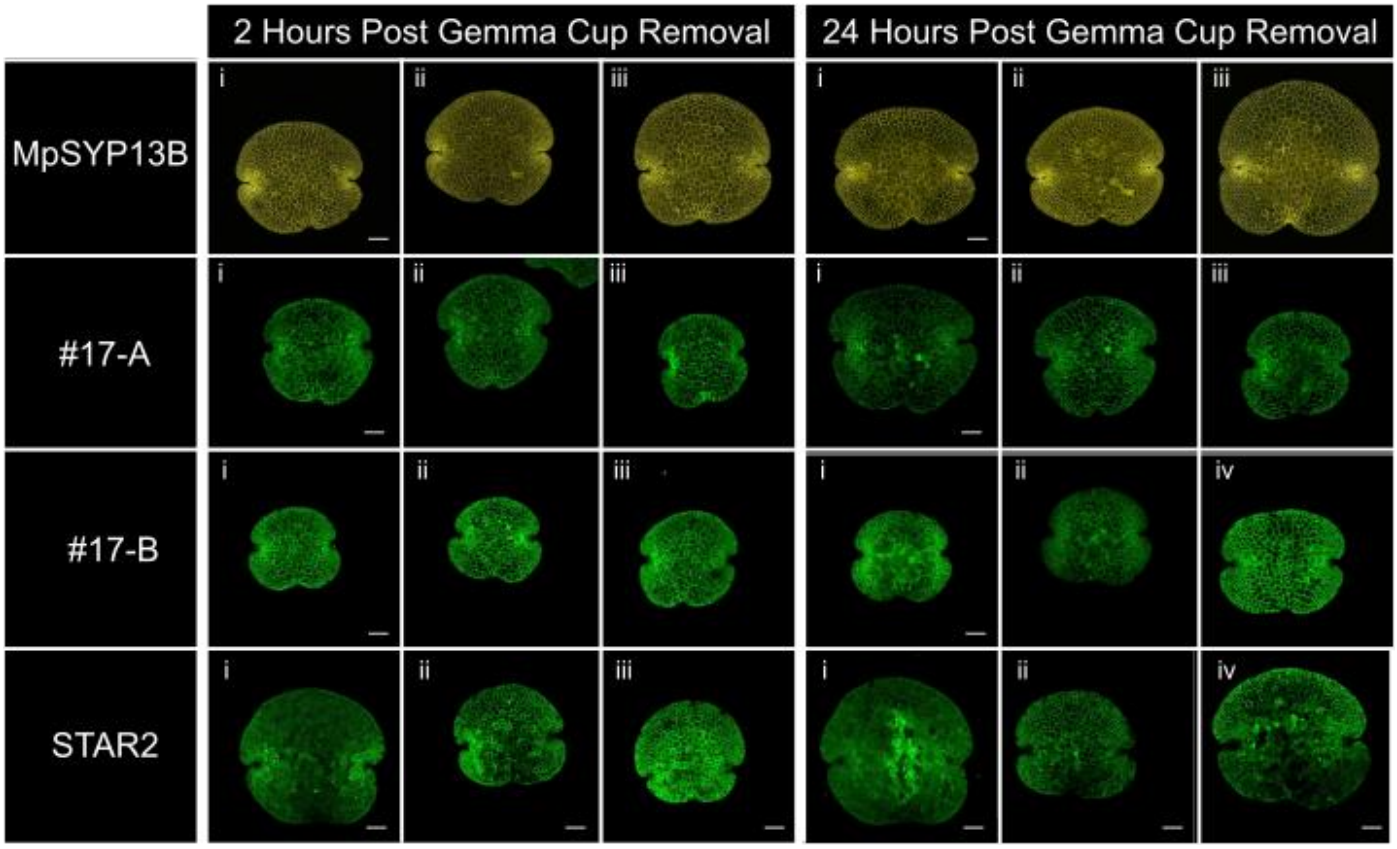

Figure 4.4: Overview of gemmae imaged for further MpPINZGFP localisation after both 2 hours and 24 hours following removal from gemma cup.

The MpPINZGFP lines of interest (17-A, 17-B, STAR2) were imaged after both 2 hours and 24 hours following removal from gemma cup to show changes in MpPINZ protein localisation in the early development of thallus. Images which share the same letter under both the 2 hour and 24 hour treatment are in the same gemmae. Where additional letters are used an additional gemma has been included. Scale bar represents 100 µM.

MpPINZ localisation after two hours of being removed from the gemma cup

Each figure shows the whole gemma of each line in addition to various magnified regions across the gemmae and includes a map figure of the gemmae to show where each magnfied region can be found on the gemma. The gemmae selected was representative out of the approximately 10 gemmae observed under the microscope, in addition to the expected phenotype from prior screening of the lines. The apical notches are slighlty indented, most obvious from analysis of the XY orthogonal view of the thalli in the panels **D** and **E** in the figures. These panels also show that the gemmae were not fixed completely flat between the glass slide and coverslip. **Figures 4.5-4.8** show the gemmae of each line after 2 hours following removal from gemma cup.

Figure 4.5 (page 56) shows the positive control MPSYP13B (gemmae ii in **Figure 4.4**). When the whole thallus is considered the localisations appear to be uniform. There seemed to be no significant difference in the localisation of the SNARE proteins across the middle of the gemma, but across the top and bottom there does seem to be some basal polarity in the cells. These polarities are indicated by arrows in the figure. The region around the notch did however appear to be brighter, suggesting an increased SNARE abundance around the apices. This may be described by the increased activity around the stem cells however. This line therefore acted well as a positive control for the MpPINZGFP lines across the body of the gemmae in the experiment. However, when the orthogonal views are considered there does appear to be bands of polar localisations, although these do not appear to be distinct across the gemmae as a whole, rather at the top and the bottom.

Confocal imaging of line 17A showed localisations of MpPINZ proteins across all thallus regions (**Figure 4.6**; page 57). This gemma corresponds to image ii of line 17A after 2 hours in **Figure 4.4**. The most striking result is across the bottom of the gemmae which showed a localisation most clear at the base of cells, towards the site of the attachment to the gemma cup in the gemmalings. Across the top of the gemma there also appeared to be bands of polarity, supported by the YZ orthogonal view. The orthogonal views also indicate localisations around the notch. Despite the observation of localisations across the middle of the thallus, the MpPINZ protein localisations did not appear to be so distinct in this region, with some cells lacking clear localisations altogether.

Figure 4.7 (page 58) shows a closer look at the line 17B (gemmae ii in **Figure 4.4**). When the whole thallus is considered the GFP seemed evident across the entirety of the thallus, again with the notch particularly saturated. Strong bands of signal were detected across the base of cells at the bottom of the thallus and again at the top of the thallus. As with line 17B the localisations did not appear to be so distinct across the middle of the thallus, with some cells lacking clear localisations altogether. From the orthogonal views, the most evident bands of signal were across the base of the thallus in the XZ view.

Confocal imaging of the MpPINZGFP line STAR2 in **Figure 4.8** (page 59) showed localisations of MpPINZ proteins across the whole thallus (gemmae iii in **Figure 4.4**). Distinct bands of MpPINZ protein are not so easily observed in comparison to the other GFP lines imaged at this time point in development. The magnified images of thallus regions made the basal localisation of protein in cells across the middle of the thallus most evident, conflicting the results observed in other lines. However, orthogonal views show bands at the top and bottom of the thallus.

Overall analysis across the three lines following two hours removal from the gemma cup showed consistent localisations around the edges of cells particularly across the base of cells towards the bottom of the thallus and at the side of cells along the top of the thallus. The same thalli were then left to grow and observed in the same experimental set-up the following day.

MpPINZ localisation after 24 hours of being removed from the gemma cup

Similarly to those figures following two hours of gemma cup removal, **Figures 4.9-4.12** show the analysis of a representative gemmae of each line after 24 hours following removal from the gemma cup of stock lines.

Figure 4.9 (page 60) shows the positive control MPSYP13B (gemmae ii in **Figure 4.4**). Across the thallus, the localisations appear to be uniform but in a similar fashion to the same gemmae after two hours, more activity around the apical notch. There seemed to be no consistent significant difference in the localisation of the SNARE proteins across the middle of the gemma, but across the top and bottom there was some basal polarities in the cells which is supported by observation using orthogonal views.

Figure 4.10 (page 61) shows analysis of line 17A (gemmae ii in **Figure 4.4**). The overall change in polarities when the whole thallus is considered does not appear to be significant across the time points for this line. Similar to the previous time point there were still localisations of GFP across the whole thallus, notably across the bottom of the thallus. However, as shown in the magnified view across the middle of the thallus the polarities appear to be more basally located in cells. The orthogonal views did not show such a clear image of bands across the thalli.

The line 17B gemma was unfortunately damaged in the time between both images being taken, but **Figure 4.11** (page 62) shows the images taken following 24 hours (gemmae ii in **Figure 4.4**). It is easiest to see damage to the thallus across the middle of the gemma. Despite this, localisations across the bottom of the thallus were much reduced when compared to the same time the day before. In other thalli from the same line such changes were not observed. The orthogonal views appear to show no polarities across the thallus.

Figure 4.12 (page 63) shows the MpPINZGFP line STAR2 (gemmae ii in **Figure 4.4**) which also appeared to be damaged, particularly across the middle and bottom of the thallus. The polarities across the top of the thalli remained distinct, but not quite so easily observed in orthogonal views.

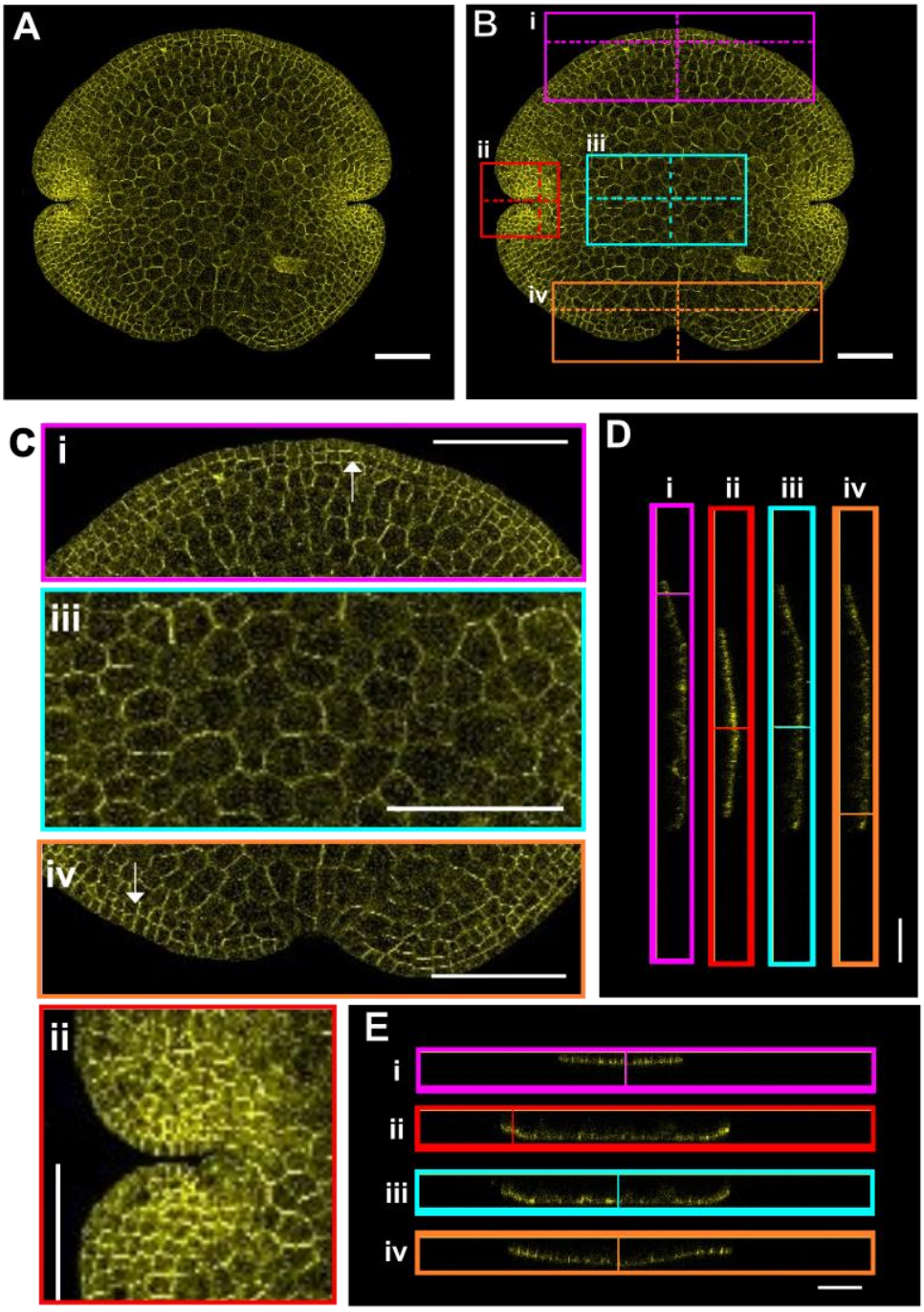

Figure 4.5: MpSYP13B line imaged after 2 hours following removal from the apical notch.

(**A**) A view of the whole gemmae. (**B**) A map for other panels, showing which areas of the gemma have been enlarged. The dashed lines represent the planes for the orthogonal views in panels **D** and **E**. (**C**) Enlarged images of different regions of the thallus. Arrows indicate the localisations of interest identified across the gemma. (**i**) The top of the thallus enlarged by 200 % relative to the original image. (**ii**) One of the apical notches of the gemma enlarged at 300 % relative to the original image. (**iii**) A view across the middle of the gemma enlarged at 300 % relative to the original image. (**iv**) The bottom of the thallus enlarged at 200 % relative to the original image. (**D**) The YZ orthogonal view across the thallus. The horizontal dashed lines in **B** corresponds to the position of the horizontal dashed lines in each part of panel **D**. (**E**) The XZ orthogonal view across the thallus. The vertical dashed lines in **B** corresponds to the position of the vertical dashed lines in each part of panel **D**. All scale bars represent 100 µM.

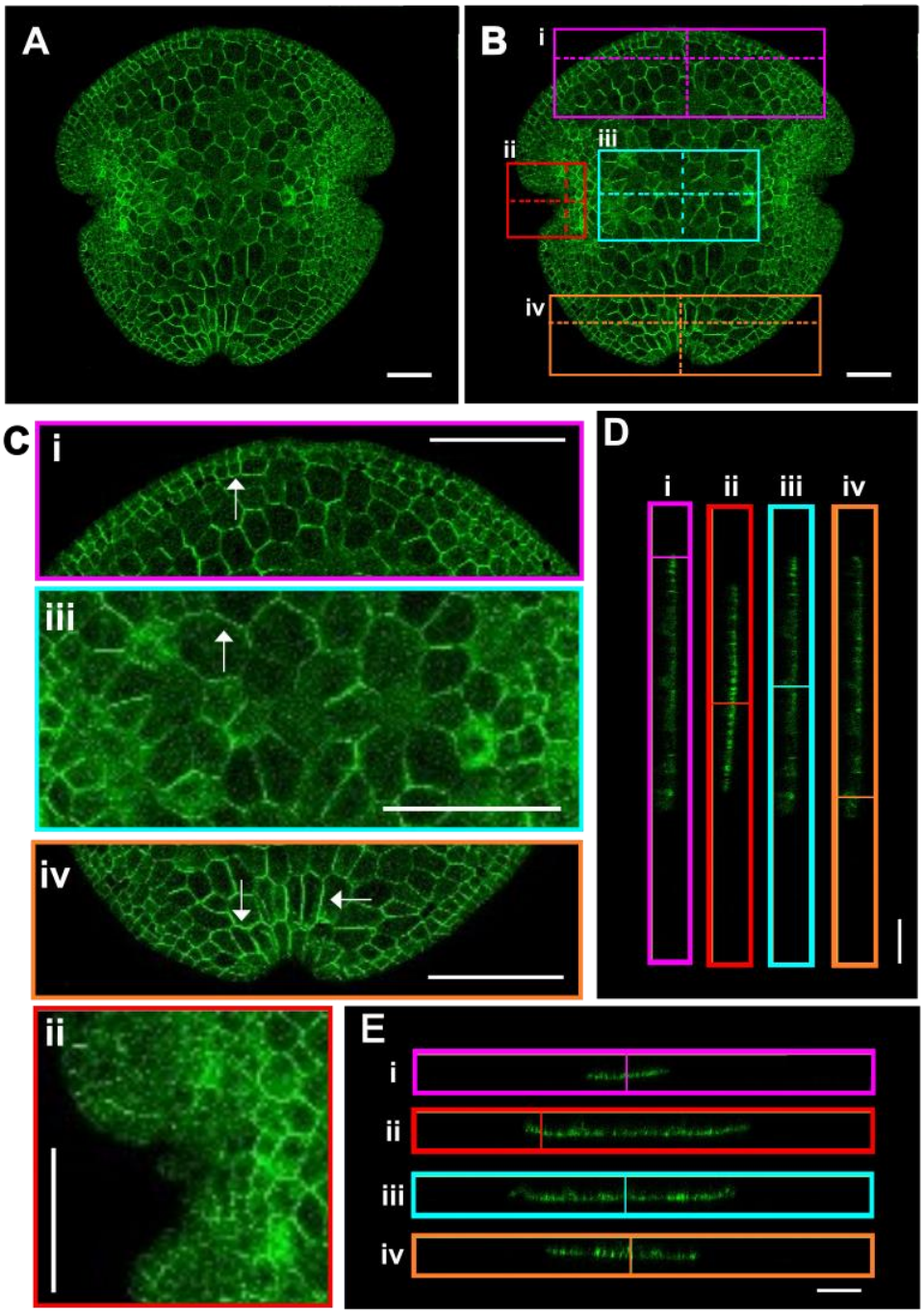

Figure 4.6: Line 17A imaged after 2 hours following removal from the apical notch.

(**A**) A view of the whole gemmae. (**B**) A map for other panels, showing which areas of the gemma have been enlarged. The dashed lines represent the planes for the orthogonal views in panels **D** and **E**. (**C**) Enlarged images of different regions of the thallus. Arrows indicate the localisations of interest identified across the gemma. (**i**) The top of the thallus enlarged by 200 % relative to the original image. (**ii**) One of the apical notches of the gemma enlarged at 300 % relative to the original image. (**iii**) A view across the middle of the gemma enlarged at 300 % relative to the original image. (**iv**) The bottom of the thallus enlarged at 200 % relative to the original image. (**D**) The YZ orthogonal view across the thallus. The horizontal dashed lines in **B** corresponds to the position of the horizontal dashed lines in each part of panel **D**. (**E**) The XZ orthogonal view across the thallus. The vertical dashed lines in **B** corresponds to the position of the vertical dashed lines in each part of panel **D**. All scale bars represent 100 µM.

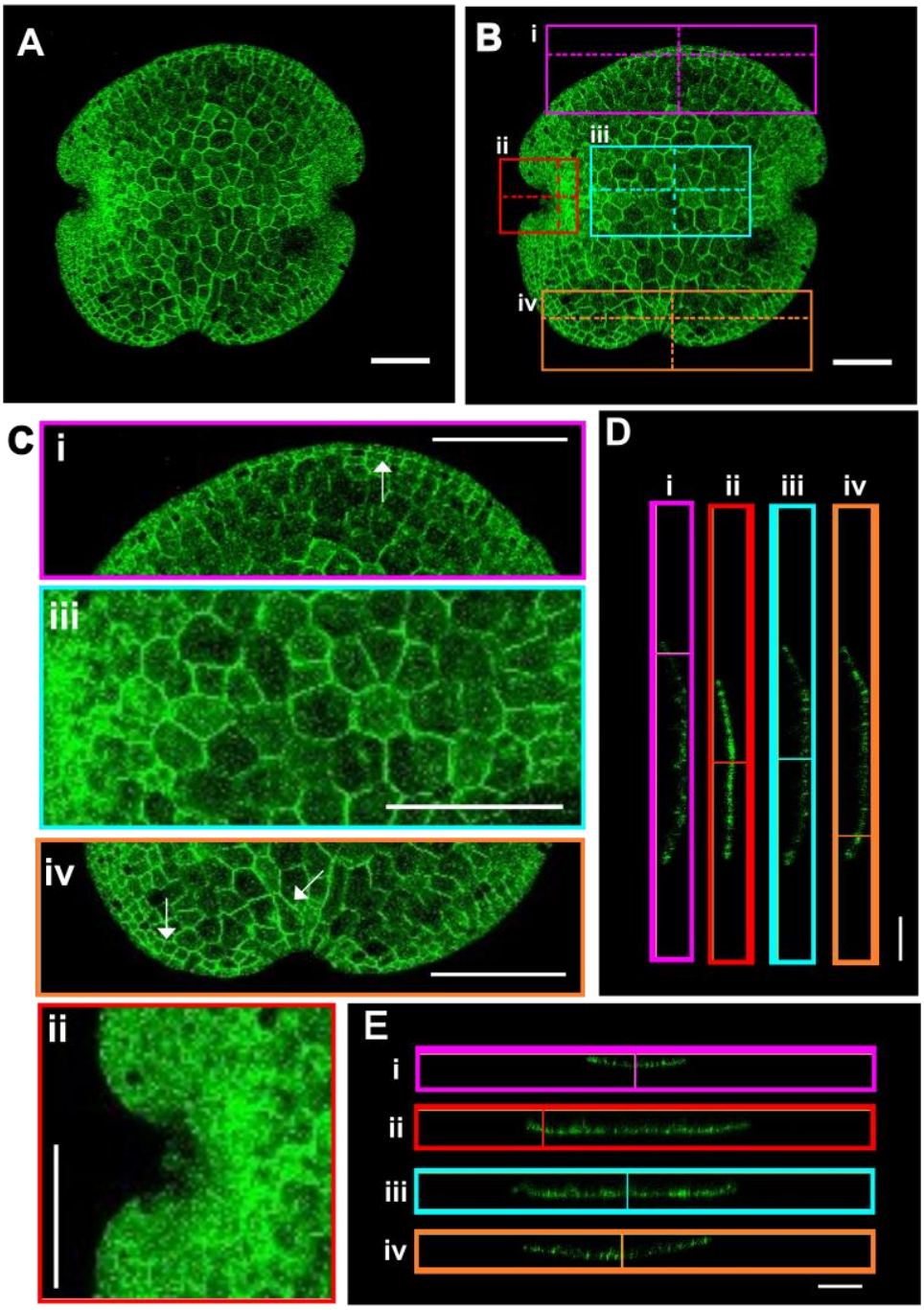

Figure 4.7: Line 17B imaged after 2 hours following removal from the apical notch.

(**A**) A view of the whole gemmae. (**B**) A map for other panels, showing which areas of the gemma have been enlarged. The dashed lines represent the planes for the orthogonal views in panels **D** and **E**. (**C**) Enlarged images of different regions of the thallus. Arrows indicate the localisations of interest identified across the gemma. (**i**) The top of the thallus enlarged by 200 % relative to the original image. (**ii**) One of the apical notches of the gemma enlarged at 300 % relative to the original image. (**iii**) A view across the middle of the gemma enlarged at 300 % relative to the original image. (**iv**) The bottom of the thallus enlarged at 200 % relative to the original image. (**D**) The YZ orthogonal view across the thallus. The horizontal dashed lines in **B** corresponds to the position of the horizontal dashed lines in each part of panel **D**. (**E**) The XZ orthogonal view across the thallus. The vertical dashed lines in **B** corresponds to the position of the vertical dashed lines in each part of panel **D**. All scale bars represent 100 µM.

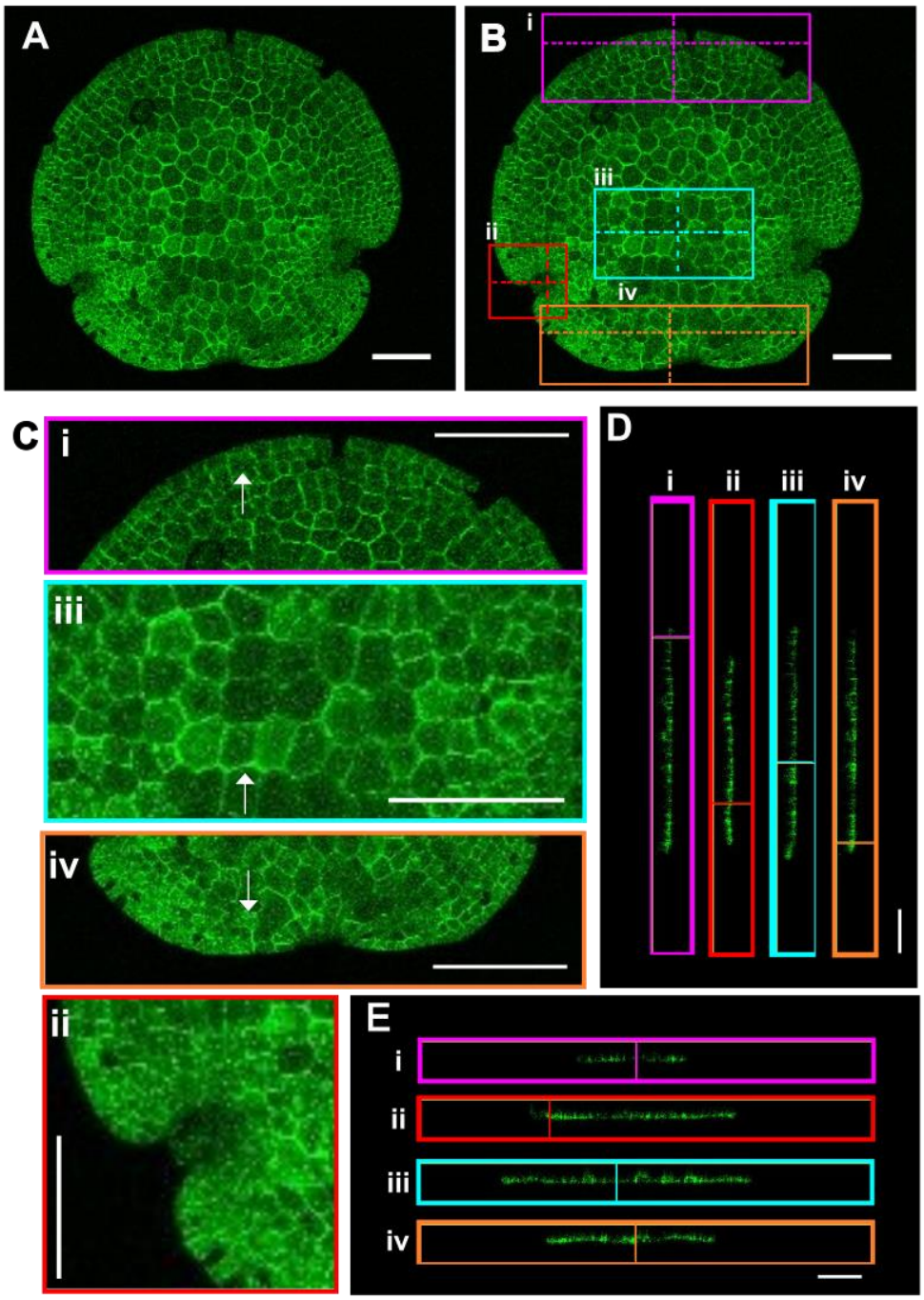

Figure 4.8: Line STAR2 imaged after 2 hours following removal from the apical notch.

(**A**) A view of the whole gemmae. (**B**) A map for other panels, showing which areas of the gemma have been enlarged. The dashed lines represent the planes for the orthogonal views in panels **D** and **E**. (**C**) Enlarged images of different regions of the thallus. Arrows indicate the localisations of interest identified across the gemma. (**i**) The top of the thallus enlarged by 200 % relative to the original image. (**ii**) One of the apical notches of the gemma enlarged at 300 % relative to the original image. (**iii**) A view across the middle of the gemma enlarged at 300 % relative to the original image. (**iv**) The bottom of the thallus enlarged at 200 % relative to the original image. (**D**) The YZ orthogonal view across the thallus. The horizontal dashed lines in **B** corresponds to the position of the horizontal dashed lines in each part of panel **D**. (**E**) The XZ orthogonal view across the thallus. The vertical dashed lines in **B** corresponds to the position of the vertical dashed lines in each part of panel **D**. All scale bars represent 100 µM.

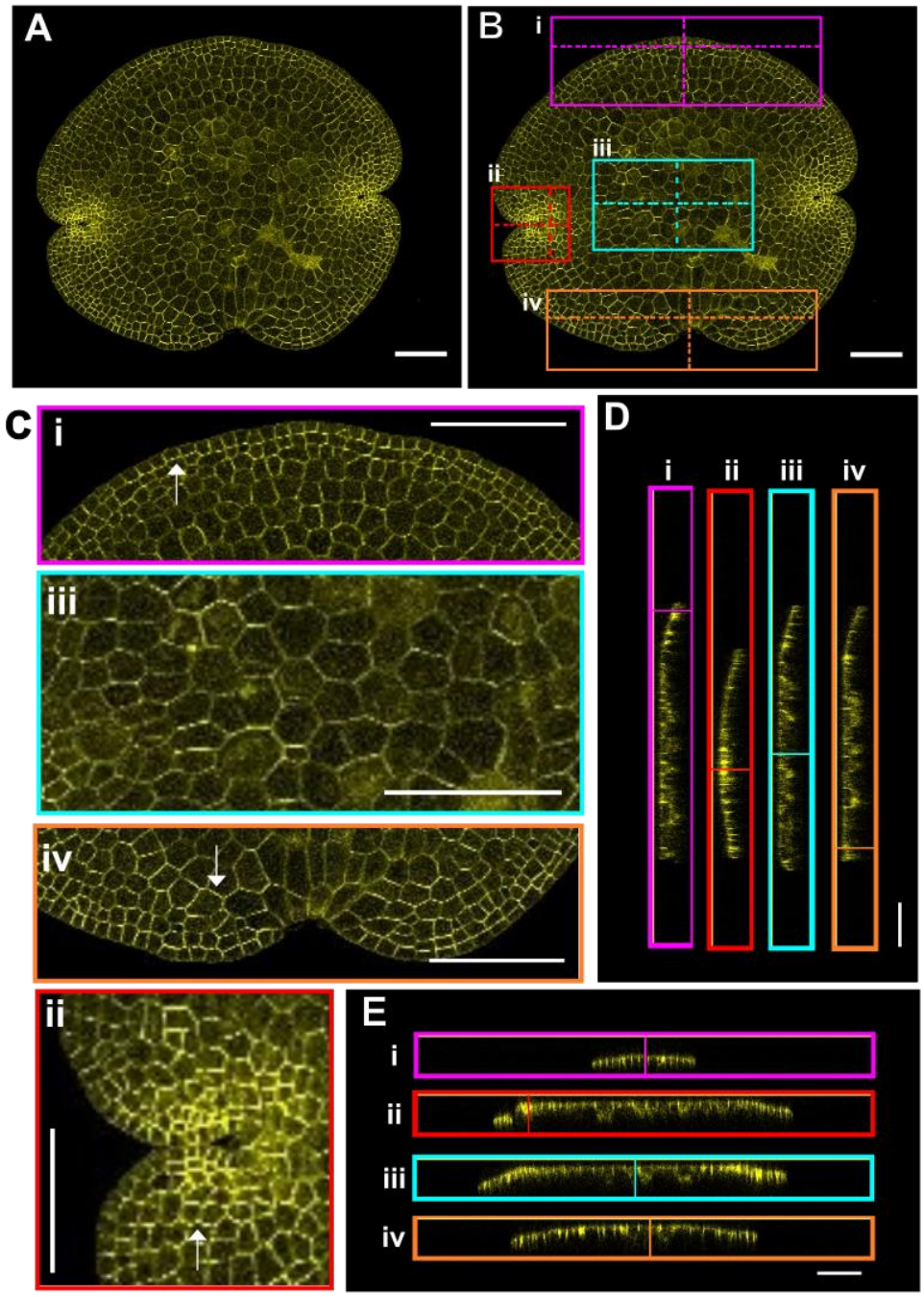

Figure 4.9: MpSYP13B line imaged after 24 hours following removal from the apical notch.

(**A**) A view of the whole gemmae. (**B**) A map for other panels, showing which areas of the gemma have been enlarged. The dashed lines represent the planes for the orthogonal views in panels **D** and **E**. (**C**) Enlarged images of different regions of the thallus. Arrows indicate the localisations of interest identified across the gemma. (**i**) The top of the thallus enlarged by 200 % relative to the original image. (**ii**) One of the apical notches of the gemma enlarged at 300 % relative to the original image. (**iii**) A view across the middle of the gemma enlarged at 300 % relative to the original image. (**iv**) The bottom of the thallus enlarged at 200 % relative to the original image. (**D**) The YZ orthogonal view across the thallus. The horizontal dashed lines in **B** corresponds to the position of the horizontal dashed lines in each part of panel **D**. (**E**) The XZ orthogonal view across the thallus. The vertical dashed lines in **B** corresponds to the position of the vertical dashed lines in each part of panel **D**. All scale bars represent 100 µM.

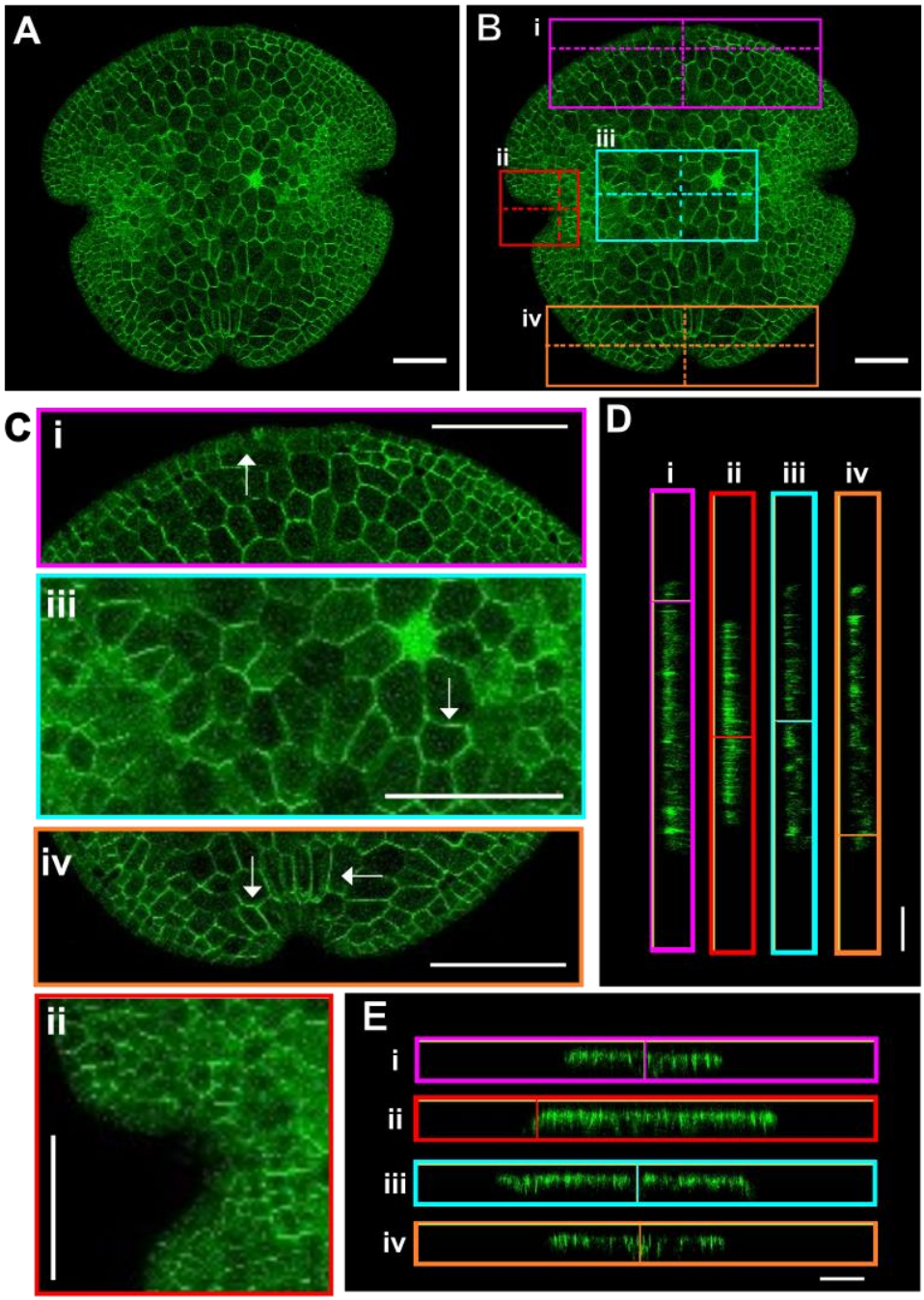

Figure 4.10: Line 17A imaged after 24 hours following removal from the apical notch.

(**A**) A view of the whole gemmae. (**B**) A map for other panels, showing which areas of the gemma have been enlarged. The dashed lines represent the planes for the orthogonal views in panels **D** and **E**. (**C**) Enlarged images of different regions of the thallus. Arrows indicate the localisations of interest identified across the gemma. (**i**) The top of the thallus enlarged by 200 % relative to the original image. (**ii**) One of the apical notches of the gemma enlarged at 300 % relative to the original image. (**iii**) A view across the middle of the gemma enlarged at 300 % relative to the original image. (**iv**) The bottom of the thallus enlarged at 200 % relative to the original image. (**D**) The YZ orthogonal view across the thallus. The horizontal dashed lines in **B** corresponds to the position of the horizontal dashed lines in each part of panel **D**. (**E**) The XZ orthogonal view across the thallus. The vertical dashed lines in **B** corresponds to the position of the vertical dashed lines in each part of panel **D**. All scale bars represent 100 µM.

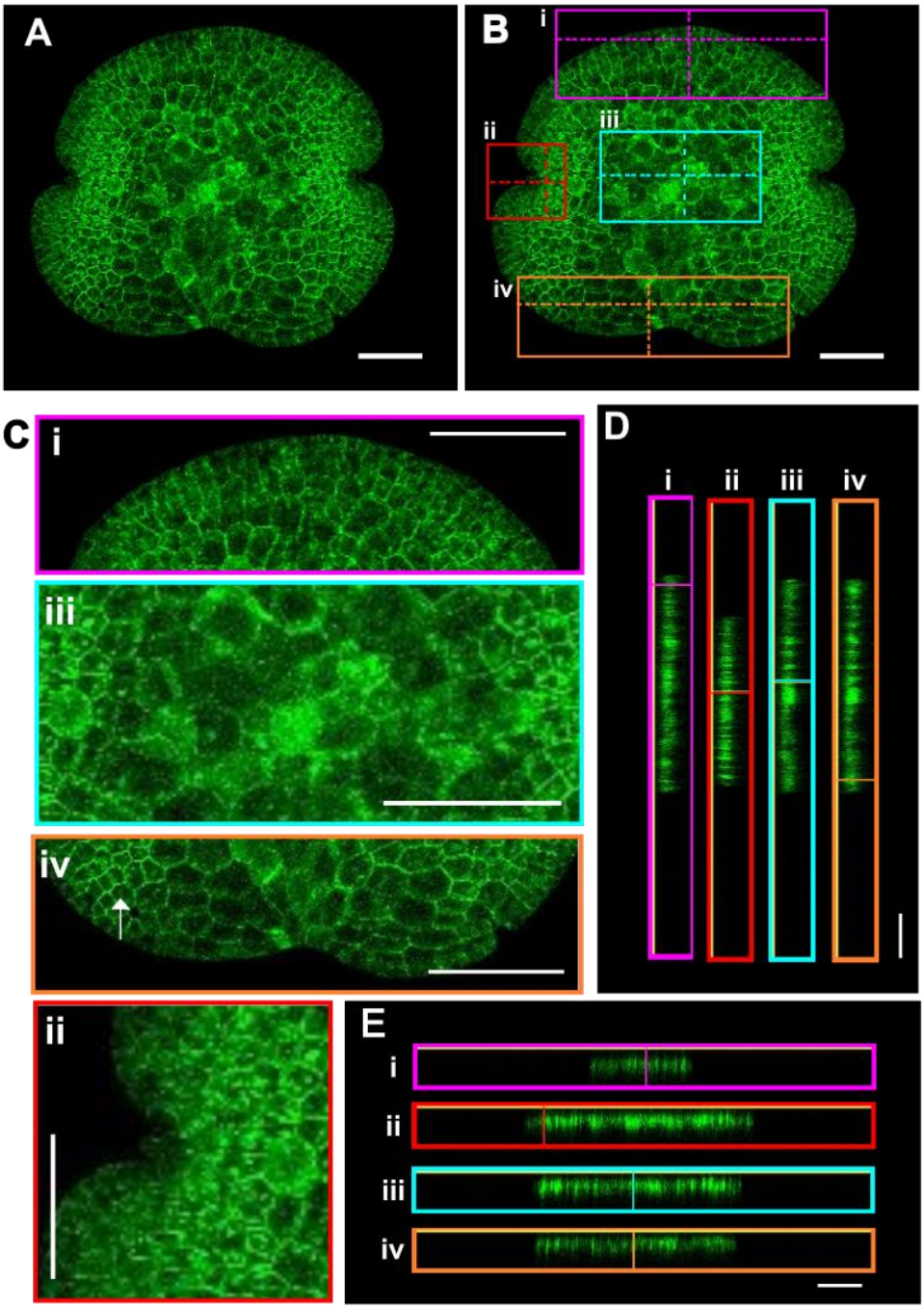

Figure 4.11: Line 17B imaged after 24 hours following removal from the apical notch.

(**A**) A view of the whole gemmae. (**B**) A map for other panels, showing which areas of the gemma have been enlarged. The dashed lines represent the planes for the orthogonal views in panels **D** and **E**. (**C**) Enlarged images of different regions of the thallus. Arrows indicate the localisations of interest identified across the gemma. (**i**) The top of the thallus enlarged by 200 % relative to the original image. (**ii**) One of the apical notches of the gemma enlarged at 300 % relative to the original image. (**iii**) A view across the middle of the gemma enlarged at 300 % relative to the original image. (**iv**) The bottom of the thallus enlarged at 200 % relative to the original image. (**D**) The YZ orthogonal view across the thallus. The horizontal dashed lines in **B** corresponds to the position of the horizontal dashed lines in each part of panel **D**. (**E**) The XZ orthogonal view across the thallus. The vertical dashed lines in **B** corresponds to the position of the vertical dashed lines in each part of panel **D**. All scale bars represent 100 µM.

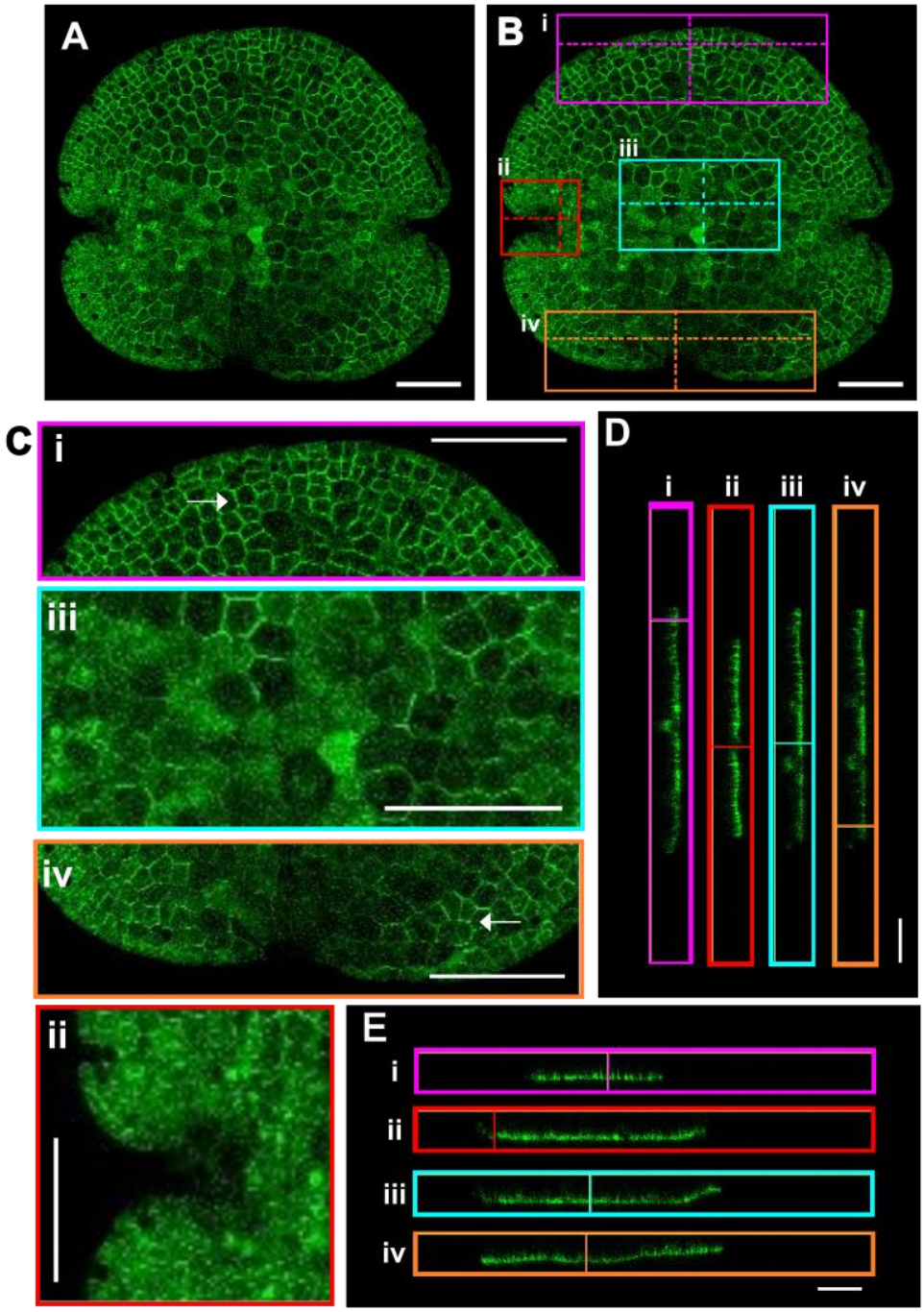

Figure 4.12: Line STAR2 imaged after 2 hours following removal from the apical notch.

(**A**) A view of the whole gemmae. (**B**) A map for other panels, showing which areas of the gemma have been enlarged. The dashed lines represent the planes for the orthogonal views in panels **D** and **E**. (**C**) Enlarged images of different regions of the thallus. Arrows indicate the localisations of interest identified across the gemma. (**i**) The top of the thallus enlarged by 200 % relative to the original image. (**ii**) One of the apical notches of the gemma enlarged at 300 % relative to the original image. (**iii**) A view across the middle of the gemma enlarged at 300 % relative to the original image. (**iv**) The bottom of the thallus enlarged at 200 % relative to the original image. (**D**) The YZ orthogonal view across the thallus. The horizontal dashed lines in **B** corresponds to the position of the horizontal dashed lines in each part of panel **D**. (**E**) The XZ orthogonal view across the thallus. The vertical dashed lines in **B** corresponds to the position of the vertical dashed lines in each part of panel **D**. All scale bars represent 100 µM.

Are MpPINZ proteins localised to the plasma membrane?

To understand whether MpPINZ is localised to the plasma membrane, gemmalings were subject to a mannitol treatment to plasmolyse the cells, with the rationale that plasmolysis should lead signal to draw away from the edge of the cell if targeting was to the plasma membrane. Around 30 Tak-1 gemmalings were removed from the gemma cup and immediately placed in differing mannitol solutions. Gemma were then secured between a microscope slide and coverslip prior to imaging following two hours in solution (**Figure 4.13**). Plasmolysis was observed by cell contents bunching together and was most obvious at a mannitol concentration of 1M. I therefore used a 1 M solution for confocal imaging of select MpPINZGFP lines.

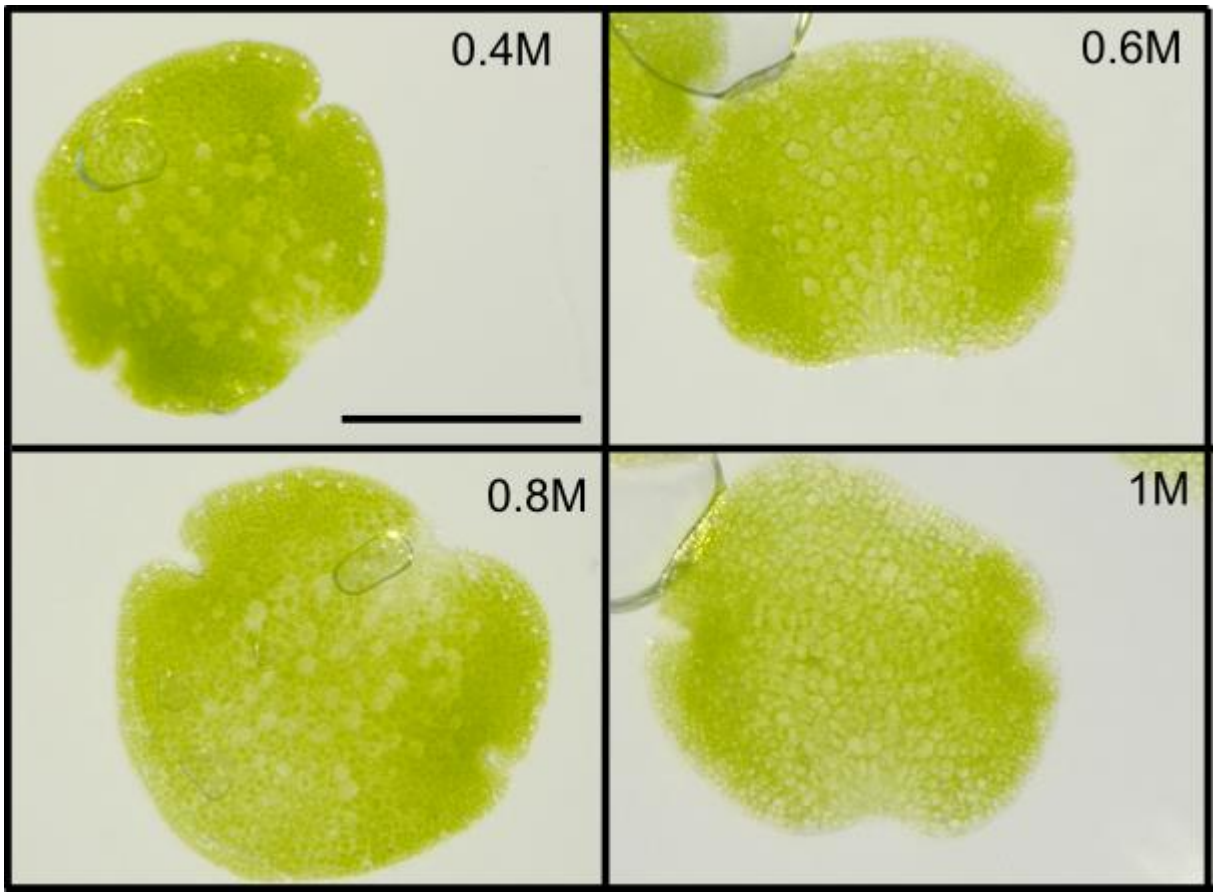

Figure 4.13: Mannitol treatment leads to plasmolysis of cells across the gemma in two hours

Light micrographs taken using a Keyence VHX-1000 digital light microscope at 50 X magnification. Four different mannitol concentrations were used to determine mannitol concentration in order to observe plasmolysis before confocal microscopy. Scale bar represents 0.5 mm.

Confocal imaging on thalli treated with a mannitol solution

Gemmae from lines #17A, #17B and the positive control MpSYP13B were placed into a 1M solution of mannitol and then imaged using the confocal microscope.

Figure 4.14A shows micrographs of gemmae treated with mannitol following 24 hours of incubation and untreated controls for each line. These micrographs were captured at a wavelength of 500-550nm, and a 620-680nm band was also collected to highlight background autofluorescence from the gemmae (**Figure 4.14B**). Composite images show lack of chloroplast in cells which will become rhizoid-bearing.

The plasmolysis of cells across the gemmae is not clearly depicted, so I have included **Figure 4.15** which shows an enlarged view across the top central region of the composite gemma images. Here, it was clearer that the cell contents were more concentrated than in untreated cells, and gaps between the cells appeared, suggesting the cells were plasmolysed. Despite this, some MpPINZGFP signal is still observable around the outline of the cell contents. Taken with the observations of the MpPINZGFP lines in early screens, these data suggest that the MpPINZ localisation bound to the plasma membrane in *M. polymorpha*.

Figure 4.14: Confocal imaging of gemmalings subject to mannitol application

(**A**) Images of the whole gemmae of plants treated with mannitol solution. The figure shows a control gemma for each line as well as a gemma treated with mannitol solution. (**B**) Composite images of the same thalli as shown in (**A**). Red represents autofluorescence from each gemma. Scale bars represent 1 mm.

A

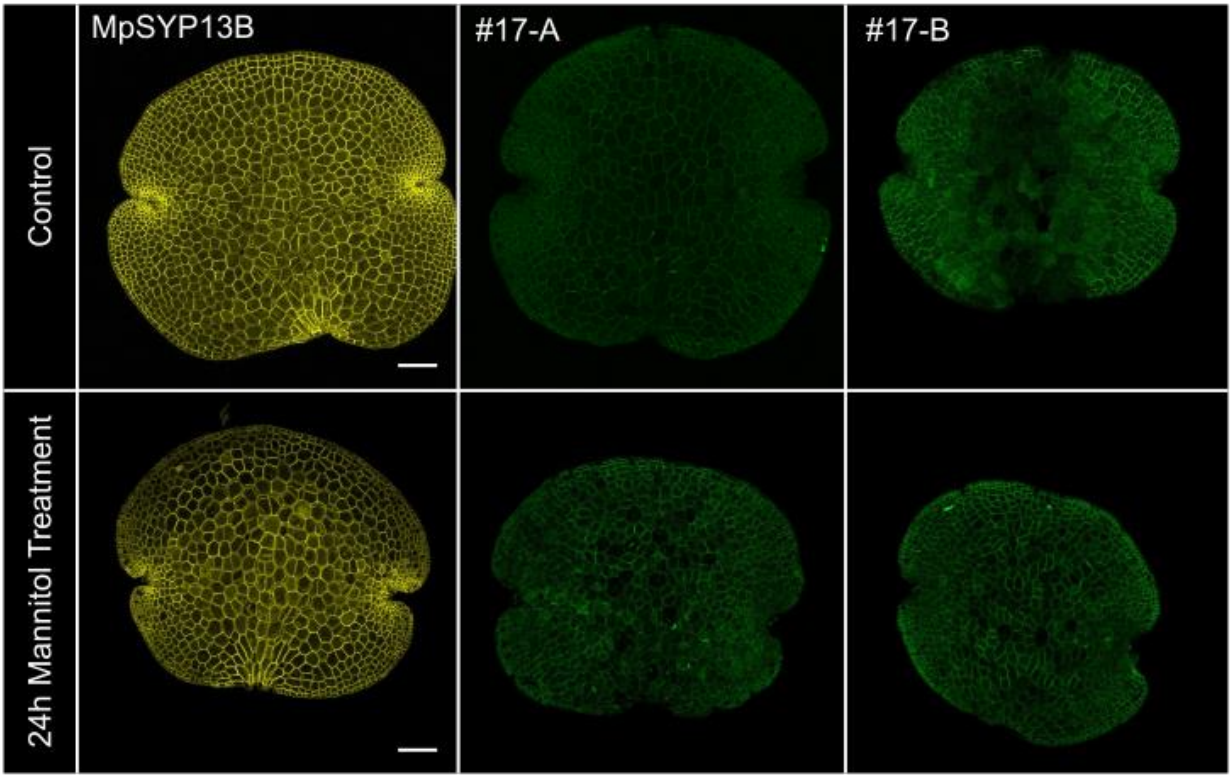
MpSYP13B
#17-A
#17-B
Control
24h Mannitol Treatment

B

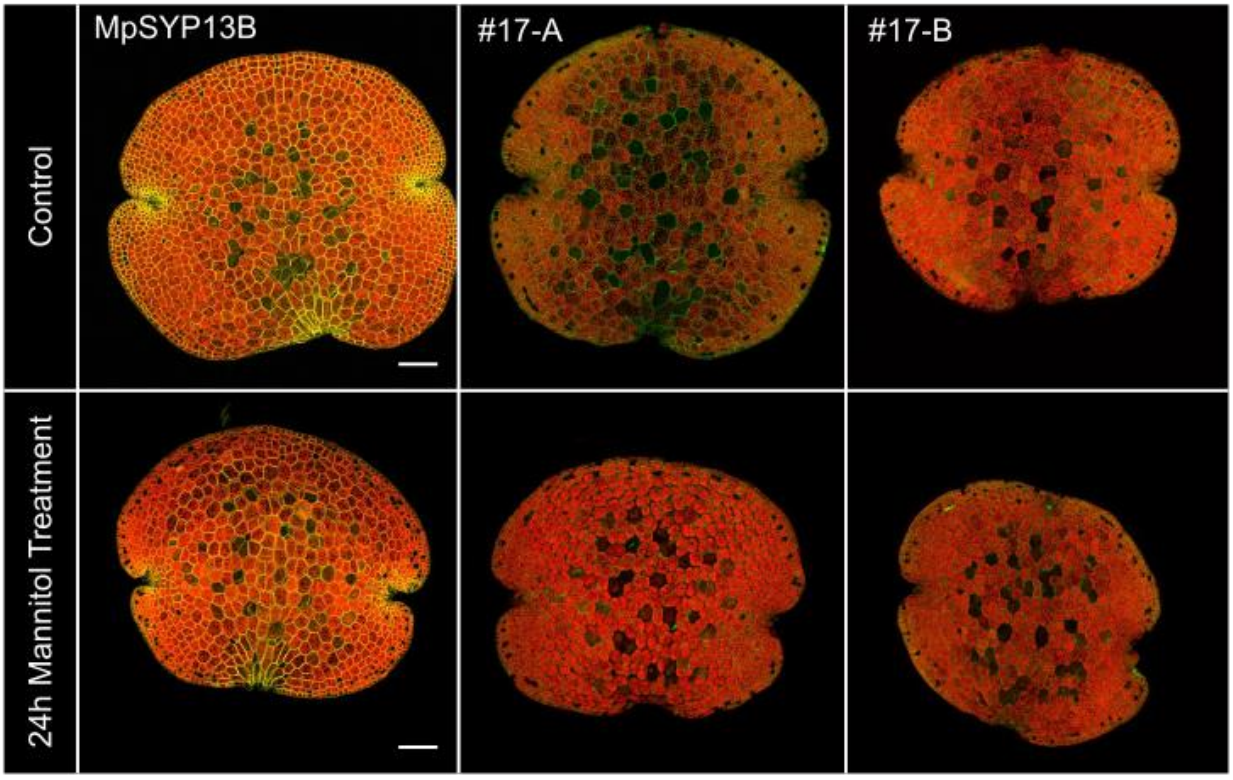
MpSYP13B
#17-A
#17-B
Control
24h Mannitol Treatment

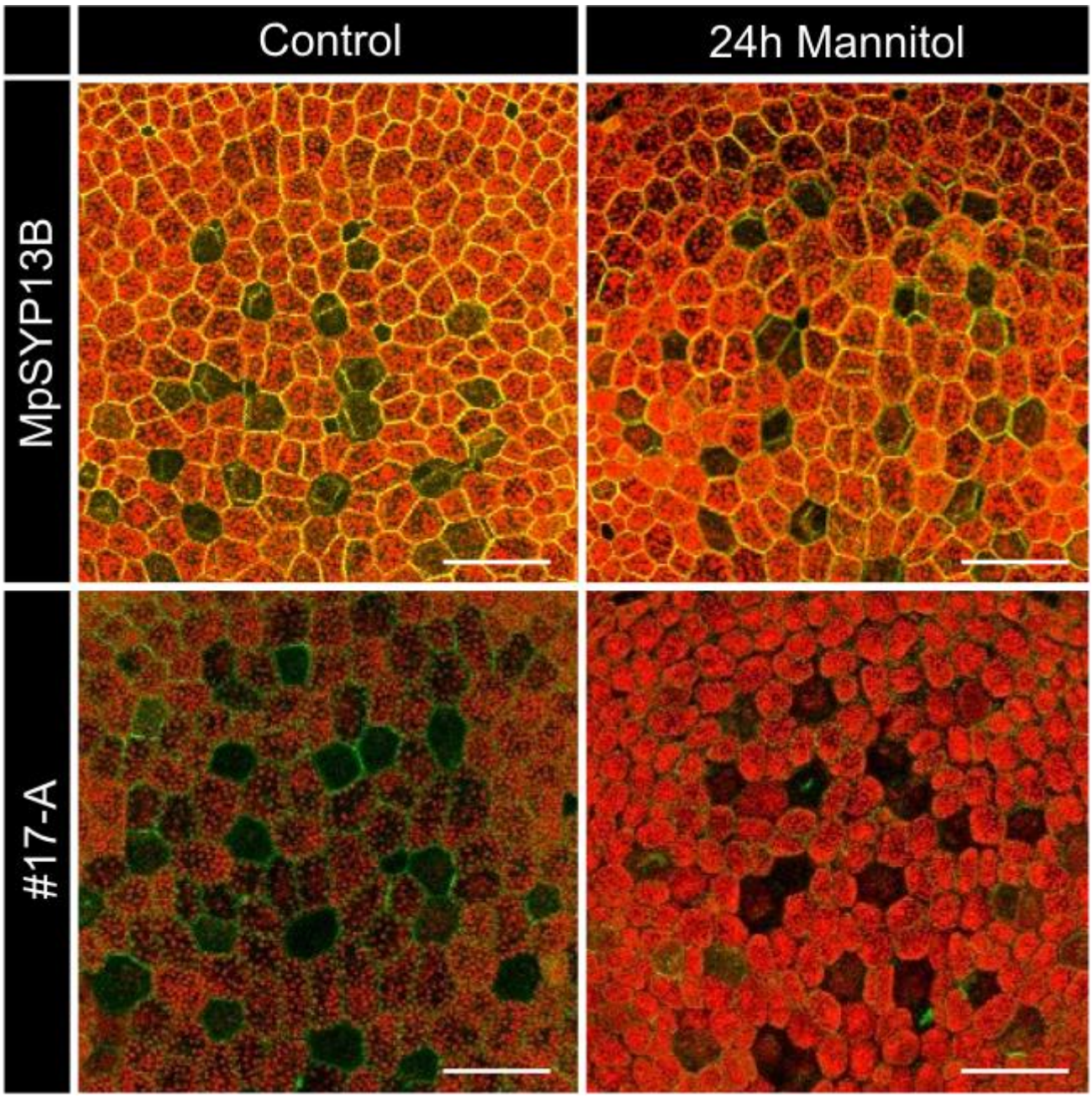

Figure 4.15: Enlarged view of composite images showing gemmae subject to mannitol treatment for 24h.

Digitally magnified view of gemmae from the positive control SNARE line and #17A. Control gemmae and those treated for 24 hours (24h) in mannitol solution are not the same gemmae. Scale bars represent 100 µm.

Chapter Discussion

The endpoint of confocal microscopy was to understand if the MpPINZGFP lines acquired showed signal, and where within cells and across thalli such signal was observed.

MpPINZ proteins show polarity in *M. polymorpha*

Identification of protein localisations was most successful in MpPINZGFP lines 17A, 17B and STAR2 and these lines were used in further work, alongside the MpSYP13B positive control. Differences were observed both between lines and between the time points in experiments. Although further confocal work is needed for verification, preliminary suggestions of links to the model describing the role of polarity across the thallus on shape variation in *M. polymorpha* are made.

Similarities and differences in MpPINZ localisation observed between MpPINZGFP lines

Similarities between lines were most clear at the earlier time point, with MpPINZGFP lines consistently showing significant localisation of MpPINZ towards the bottom of cells along the edge of the bottom of the gemma. There were also significant similarities between the bands of MpPINZ localisations forming across the top edge of the gemma. Here, protein localisations appeared lateral to each cell, suggesting more auxin export along the edges between cells. This is contrast to the MpSYB13B line in which localisation was relatively more consistent around the entirety of the cells along the top edge of the thallus. Between the lines a difference was however the localisations observed across the middle of the thallus, with no consistent observation for localisations of proteins, apart from around that of rhizoid precursor cells which are described below.

Similarities and differences in MpPINZ localisations across 24 hours of thallus development

Damaged thalli made conclusions from the later time point data set harder to draw. However, the observations made at the earlier time point were generally still valid following 24 hours of development outside of the gemma cup. The MpSYP13B line acted well as a positive control over this time period, with a similar distribution observed at earlier and later time points. The lateral localisation of the MpPINZs, especially evident in line 17A following 24 hours, was still observed suggesting that this distribution is stable under normal growth conditions.

MpPINZ protein localisations are less distinct around cells which will develop rhizoids

An interesting observation from the screen of the GFP lines is the omission of chloroplast in the cells which develop rhizoids which are akin in form and function to those found in vascular plants (Shimamura, 2016). The GFP localisation was also observed to be less distinct around these cells. A notable MpPINZ localisation of surrounding cells could have been expected with auxin known to promote rhizoid development by regulation of key transcription factor activity in *P. patens*, and the same genes critical for rhizoid development in *M. polymorpha* (Jang et al., 2011; Proust et al., 2016). This could also have implications on further research into the localisations of MpPINZ proteins across the thallus, with polarity across the thallus potentially interrupted by rhizoid precursor cells. However, this supports recent work into rhizoid cell patterning independently of auxin in *M. polymorpha* which shows a lateral inhibition model regulated by the action of microRNAs on a key transcription factor determines rhizoid distribution across the thallus (Thamm et al., 2020).

MpPINZ proteins are localised to the plasma membrane in *M. polymorpha*

My results show that the canonical PIN in *M. polymorpha* (MpPINZ), of which the GFP lines are generated to show localisation of, is localised to the plasma membrane. Studies in the *A. thaliana* model system have shown such distribution is in order to perform the bulk export of auxin from cells (Wisniewska et al., 2006). This contrasts to the non-canonical PIN proteins, of which *M. polymorpha* has three, which are known in *A. thaliana* to be involved in cellular homeostasis and internal auxin transport (Mravec et al., 2009). Treatment with mannitol appeared to show the plasmolysis of cells, confirming the localisation of the canonical MpPINZ to the plasma membrane.

M. polymorpha PIN protein localisations reflect some model variant polarities

Linking MpPINZ localisations to model variants described earlier in this thesis (**Figure 3.2**) can offer progress towards a more complete understanding of the role of polarity in shape determination in *M. polymorpha*. From this work, combining observations from early development, MpPINZ localisations appeared laterally across the top of the thallus suggesting side-to-side gemma polarity. Such polarity was observed in model variants were APEX was the source and MIDLINE the sink. However, this model variant also pointed towards similar lateral polarities across the bottom of the thallus, which were not observed. Rather, the polarities seemed to be basal across the bottom of the thallus as indicated by the MpPINZ localisations. This more closely resembles the model variant where APEX acts as the source, but the EDGE fixed identity factor acted as the sink for POLARISER.

To clarify the MpPINZ distribution across the thallus, more confocal work could enhance the resolution of polarities. Specifically, greater resolution using a more powerful lens could help resolve more precisely the localisation of MpPINZ across the thallus. Potential quantification of results would be significant in more accurately linking observed localisations to model variants.

Chapter 5. Thesis Discussion

This thesis explored roles for polarity in the determination of shape in the liverwort model system *Marchantia polymorpha*. By combining results from the growth experiments and confocal work, I present evidence for which model variant is best supported to explain the shape changes observed and therefore be a good indicator for the role of polarities involved in shape determination.

A model for shape determination in *M. polymorpha*

The results of modelling and growth experiments together suggest that thallus shape can be generated by modifying polarity gradients, with real plants resembling model variants with differing modelled movement of a morphogen acting as a polarity determinant across the thallus. The link to PINs and polar auxin transport is such that PIN proteins could facilitate such gradient formation, as PIN proteins can localise to result in auxin flow in a particular direction (Gälweiler et al., 1998; Wisniewska et al., 2006). Such PIN-dependent auxin gradients which have been shown to represent a fundamental common module accessed during the development of all plant organs (Benková et al., 2003).

My growth experiments suggested that there is some feedback between auxin and cytokinin. A key theme for plants with auxin transport defects, both through pharmacological treatment and those with genetically perturbed transport show similar phenotypes, is that auxin accumulates within the cells around the notch.

Model suitability

The suitability of a computational model in relation to the reality of the biology in a system is a crucial area for discussion in any work involving *in silico* research. With regards to the polarity model described in this thesis, whether the model shows the maximum variation is important to consider. Comparing the model variants to the real plants grown suggests that there may be some more elongation possible in the model. For example the JES32#10 mutants treated with NPA produced much narrower thalli shapes compared to the model. Other model variants were described by the modelling approach that are not included in this thesis. For example model variants where the EDGE is the source of morphogen production and there is no sink. However, as previous work has already described the apical notch as the site of auxin production (Eklund et al., 2015), these modelling variants were not considered as biologically plausible.

Towards a complete model for shape determination in *M. polymorpha*

The growth experiments in this thesis most closely matched the model output where APEX, around the notches, acts as the source of POLARISER and the regional thallus identity across the central thallus portion, MIDLINE, acts as the sink (**Figure 3.2**). The polarities in this model variant were approximately parallel to the edge and notch to notch axis in respective canvas regions. This signal was observed across the top of the gemma in confocal work, giving further support for this model output explain the role of polarity in *M. polymorpha* shape determination. The basal signal across the bottom of the thallus may be explained by the stalk attachment in the gemma cup. Confocal work across a slightly later stage of development, towards the end of the first plastochron, could help explain the signal observed in cells along the bottom of the thallus. Here, the observation of side-to-side signal would further support the model variant where MIDLINE acts as the sink.

Such divergent model has been shown to explain petal shape in *A. thaliana*, with growth rates increasing in a perpendicular fashion to the local polarities at the distal end of the petal (Sauret-Güeto et al., 2013). The authors also connected auxin dynamics with clear polarities observed by MpPINZGFP reporter lines. Such divergent model contrasts with evidence for a convergent model which can explain PIN expression in *A. thaliana* leaf primordia (Scarpella et al., 2006). If such conclusions could be verified in *M. polymorpha,* genetic modulation could start to be understood in an early diverging land plant species. This importance of polarity gradients in determining plant tissue shape is conserved within land plant evolution, with the potential for specific modulators to be identified.

Future work may involve the use of auxin sensitive assays to better visualise the local and global auxin levels across the thallus tissue, making use of recent advances such as DII-Venus or more recent fluorescently labelled auxins (Bieleszová et al., 2019; Brunoud et al., 2012). Technical limitations have led to little understanding of auxin distribution of auxin throughout tissues at the single cell level and such visualisation could open doors for future modelling approaches (see Pařízková et al., 2017 for review).

At the cellular level, the mechanical stress of formation of lobes in *A. thaliana* has been postulated as one way in which cells can lower mechanical stress whilst maintaining isotropic growth (Sapala et al., 2018). This was shown in a study of puzzle-shaped epidermal cells and shows the possibility for modelling approaches without the use of chemical signals. Such modelling requires mechanical forces to transmit this information, however little is known about how mechanical forces are sensed. The role of enzyme trafficking interpreting mechanical signals through stress at the cellular level which can then pattern plant development has been demonstrated (Hamant et al., 2008). Regardless of future model direction, the importance of mechanical stress must remain central to the model.

Future work could also include a more precise quantifiable approach. For example, measures of thallus area and shape quantification could be achieved using 3D growth analysis. This would be especially useful for mutant or treated plants at later stages of development where polarity reversals result in the folding of thalli shapes. This has been demonstrated recently in an approach that uses micro-computed tomography (Micro-CT) to capture morphology in three dimensions (Furuya et al., 2019).

Enhancing the knowledge of the role of the phytohormones discussed in this thesis could also be an avenue for future study. The effect of strigolactone treatment could be observed on plant shape, as the hormone is believed to inhibit PINs similarly to the action of NPA in the *A. thaliana* model system (Shinohara et al., 2013). This could be used to validate the cytokinin mutants treated with NPA results observed if a similar effect on polarity is achieve. A useful next step for pharmacological treatments would be to implicate the results from the growth experiments into the confocal approach using MpPINZGFP and MpSYP13B lines. Observation of MpPINZ localisation changes with pharmacological treatment, such as exogenous auxin or auxin transport inhibition allows changes in polarity to be observed. Such prospect offers an exciting future course for research to understand how shape is determined in the *M. polymorpha* model system.

References

Abas, L., Kolb, M., Stadlmann, J., Janacek, D. P., Lukic, K., Schwechheimer, Claus Stadlmann, J., Sazanov, L. A., Mach, L., Friml, J., & Hammes, U. Z. (2021). Naphthylphthalamic acid associates with and inhibits PIN auxin transporters. Proceedings of the National Academy of Sciences of the United States of America, *118*, e2020857118. https://doi.org/10.1073/pnas.2102232118

Adamowski, M., & Friml, J. (2015). PIN-dependent auxin transport: Action, regulation, and evolution. Plant Cell, *27*, 20–32. https://doi.org/10.1105/tpc.114.134874

Aki, S. S., Mikami, T., Naramoto, S., Nishihama, R., Ishizaki, K., Kojima, M., Takebayashi, Y., Sakakibara, H., Kyozuka, J., Kohchi, T., & Umeda, M. (2019). Cytokinin signaling is essential for organ formation in *Marchantia polymorpha*. Plant & Cell Physiology, *60*, 1842–1854. https://doi.org/10.1093/pcp/pcz100

Bassel, G. W., Stamm, P., Mosca, G., Barbier, P., Reuille, D., Gibbs, D. J., & Winter, R. (2014). Mechanical constraints imposed by 3D cellular geometry and arrangement modulate growth patterns in the *Arabidopsis* embryo. Proceedings of the National Academy of Sciences of the United States of America, *111*, 8685–8690. https://doi.org/10.1073/pnas.1404616111

Benková, E., Michniewicz, M., Sauer, M., Teichmann, T., Seifertová, D., Jürgens, G., & Friml, J. (2003). Local, efflux-dependent auxin gradients as a common module for plant organ formation. Cell, *115*, 591–602. https://doi.org/10.1016/S0092-8674(03)00924-3

Bennett, T., Brockington, S. F., Rothfels, C., Graham, S. W., Stevenson, D., Kutchan, T., Rolf, M., Thomas, P., Wong, G. K. S., Leyser, O., et al. (2014a). Paralogous radiations of PIN proteins with multiple origins of noncanonical PIN structure. Molecular Biology and Evolution, *31*, 2042–2060. https://doi.org/10.1093/molbev/msu147

Bennett, T., Liu, M. M., Aoyama, T., Bierfreund, N. M., Braun, M., Coudert, Y., Dennis, R. J., O'Connor, D., Wang, X. Y., White, C. D., et al. (2014b). Plasma membrane-targeted PIN proteins drive shoot development in a moss. Current Biology, *24*, 2776–2785. https://doi.org/10.1016/j.cub.2014.09.054

Bieleszová, K., Pařízková, B., Kubeš, M., Husičková, A., Kubala, M., Ma, Q., Sedlářová, M., Robert, S., Doležal, K., Strnad, M., et al. (2019). New fluorescently labeled auxins exhibit promising anti-auxin activity. New Biotechnology, *48*, 44–52. https://doi.org/10.1016/j.nbt.2018.06.003

Bowman, J. L., Kohchi, T., Yamato, K. T., Jenkins, J., Shu, S., Ishizaki, K., Yamaoka, S., Nishihama, R., Nakamura, Y., Berger, F., et al. (2017). Insights into land plant evolution garnered from the *Marchantia polymorpha* genome. Cell, *171*, 287-304.e15. https://doi.org/10.1016/j.cell .2017.09.030

Brunoud, G., Wells, D. M., Oliva, M., Larrieu, A., Mirabet, V., Burrow, A. H., Beeckman, T., Kepinski, S., Traas, J., Bennett, M. J., & Vernoux, T. (2012). A novel sensor to map auxin response and distribution at high spatio-temporal resolution. Nature, *482*, 103–106. https://doi.org/10.1038 /nature10791

Coen, E., Rolland-Lagan, A. G., Matthews, M., Bangham, J. A., & Prusinkiewicz, P. (2004). The genetics of geometry. Proceedings of the National Academy of Sciences of the United States of America, *101*, 4728–4735. https://doi.org/10.1073/pnas.0306308101

Eklund, D. M., Ishizaki, K., Flores-Sandoval, E., Kikuchi, S., Takebayashi, Y., Tsukamoto, S., Hirakawa, Y., Nonomura, M., Kato, H., Kouno, M., et al. (2015). Auxin produced by the indole-3-pyruvic acid pathway regulates development and gemmae dormancy in the liverwort *Marchantia polymorpha*. Plant Cell, *27*, 1650–1669. https://doi.org/10.1105/tpc.15.00065

Flores-Sandoval, E., Eklund, D. M., & Bowman, J. L. (2015). A simple auxin transcriptional response system regulates multiple morphogenetic processes in the liverwort *Marchantia polymorpha*. PLoS Genetics, *11*, 1–26. https://doi.org/10.1371/journal.pgen.1005207

Furuya, T., Kimori, Y., & Tsukaya, H. (2019). A method for evaluating three-dimensional morphological features: a case study using *Marchantia polymorpha*. Frontiers in Plant Science, *10*, 1214. https://doi.org/10.3389/fpls.2019.01214

Gälweiler, L., Guan, C., Müller, A., Wisman, E., Mendgen, K., Yephremov, A., & Palme, K. (1998). Regulation of polar auxin transport by AtPIN1 in *Arabidopsis* vascular tissue. Science, *282*, 2226–2230. https://doi.org/10.1126/science.282.5397.2226

Gray, W. M., Kepinski, S., Rouse, D., Leyser, O., & Estelle, M. (2001). Auxin regulates SCFTIR1 - dependent degradation of AUX / IAA proteins. Nature, *414*, 271–276. https://doi.org/10.1038 /35104500

Hamant, O., Heisler, M. G., Jönsson, H., Krupinski, P., Uyttewaal, M., Bokov, P., Corson, F., Sahlin, P., Boudaoud, A., Meyerowitz, E. M., et al. (2008). Developmental patterning by mechanical signals in *Arabidopsis*. Science, *322*, 1650–1655. https://doi.org/10.1126/science.1165594

Harrison, C. J. (2017). Development and genetics in the evolution of land plant body plans. Philosophical Transactions of the Royal Society B: Biological Sciences, *372*, 20–25. https://doi.org/10.1098/rstb.2015.0490

Heisler, M. G., Ohno, C., Das, P., Sieber, P., Reddy, G. V., Long, J. A., & Meyerowitz, E. M. (2005). Patterns of auxin transport and gene expression during primordium development revealed by live imaging of the *Arabidopsis* inflorescence meristem. Current Biology, *15*, 1899–1911. https://doi.org/10.1016/j.cub.2005.09.052

Ishizaki, K., Chiyoda, S., Yamato, K. T., & Kohchi, T. (2008). *Agrobacterium*-mediated transformation of the haploid liverwort *Marchantia polymorpha* L., an emerging model for plant biology. Plant and Cell Physiology, *49*, 1084–1091. https://doi.org/10.1093/pcp/pcn085

Ishizaki, K., Nishihama, R., Yamato, K. T., & Kohchi, T. (2016). Molecular genetic tools and techniques for *Marchantia polymorpha* research. Plant and Cell Physiology, *57*, 262–270. https://doi.org/10.1093/pcp/pcv097

Ishizaki, K., Nonomura, M., Kato, H., Yamato, K. T., & Kohchi, T. (2012). Visualization of auxin-mediated transcriptional activation using a common auxin-responsive reporter system in the liverwort *Marchantia polymorpha*. Journal of Plant Research, *125*, 643–651. https://doi.org/10.1007/s10265-012-0477-7

Jang, G., Yi, K., Pires, N. D., Menand, B., & Dolan, L. (2011). RSL genes are sufficient for rhizoid system development in early diverging land plants. Development, *138*, 2273–2281. https://doi.org/10.1242/dev.060582

Kanazawa, T., Morinaka, H., Ebine, K., Shimada, T. L., Ishida, S., Minamino, N., Yamaguchi, K., Shigenobu, S., Kohchi, T., Nakano, A., & Ueda, T. (2020). The liverwort oil body is formed by redirection of the secretory pathway. Nature Communications, *11*, 1–11. https://doi.org/10.1038/s41467-020-19978-1

Kania, U., Fendrych, M., & Friml, J. (2014). Polar delivery in plants ; commonalities and differences to animal epithelial cells. Open Biology, *4*, 140017. https://doi.org/10.1098/rsob.140017

Kennaway, R., Coen, E., Green, A., & Bangham, A. (2011). Generation of diverse biological forms through combinatorial interactions between tissue polarity and growth. PLoS Computational Biology, *7*. https://doi.org/10.1371/journal.pcbi.1002071

Kieber, J. J., & Schaller, G. E. (2014). Cytokinins. The Arabidopsis Book, *12*, e0168. https://doi.org/10.1199/tab.0168

Kuchen, E. E., Fox, S., Barbier de Reuille, P., Kennaway, R., Bensmihen, S., Avondo, J., Calder, G. M., Southam, P., Robinson, S., Bangham, A., & Coen, E. (2012). Generation of leaf shape through early patterns of growth and tissue polarity. Science, *335*, 1092–1096. https://doi.org/10.2307/j.ctv9zcj2n.53

Kumar, S., Stecher, G., Li, M., Knyaz, C., and Tamura, K. (2018) MEGA X: Molecular Evolutionary Genetics Analysis across computing platforms. Molecular Biology and Evolution, *35*, 1547-1549. https://doi.org/10.1093/molbev/msy096

Leyser, O. (2018). Founders Review: Auxin Signaling. Plant Physiology, *176*, 465–479. https://doi.org/10.1104/pp.17.00765

Mansfield, C., Newman, J. L., Olsson, T. S. G., Hartley, M., Chan, J., & Coen, E. (2018). Ectopic BASL reveals tissue cell polarity throughout leaf development in *Arabidopsis thaliana*. Current Biology, *28*, 2638-2646.e4. https://doi.org/10.1016/j.cub.2018.06.019

Marhavý, P., Duclercq, J., Weller, B., Feraru, E., Bielach, A., Offringa, R., Friml, J., Schwechheimer, C., Murphy, A., & Benková, E. (2014). Cytokinin controls polarity of PIN1-dependent Auxin transport during lateral root organogenesis. Current Biology, *24*, 1031–1037. https://doi.org/10.1016/j.cub.2014.04.002

Morris, J. L., Puttick, M. N., Clark, J. W., Edwards, D., Kenrick, P., Pressel, S., Wellman, C. H., Yang, Z., Schneider, H., & Donoghue, P. C. J. (2018). The timescale of early land plant evolution. Proceedings of the National Academy of Sciences of the United States of America, *115*, E2274–E2283. https://doi.org/10.1073/pnas.1719588115

Mravec, J., Skůpa, P., Bailly, A., Hoyerová, K., Křeček, P., Bielach, A., Petrášek, J., Zhang, J., Gaykova, V., Stierhof, Y. D., et al. (2009). Subcellular homeostasis of phytohormone auxin is mediated by the ER-localized PIN5 transporter. Nature, *459*, 1136–1140. https://doi.org/10.1038/nature08066

Niklas, K. J., & Kerchner, V. (1984). Mechanical and photosynthetic constraints on the evolution of plant shape. Paleobiology, *10*, 79–101. https://doi.org/10.1017/S0094837300008034

Okada, K., Ueda, J., Komaki, M. K., Bell, C. J., & Shimura, Y. (1991). Requirement of the auxin polar transport system in early stages of *Arabidopsis* floral bud formation. Plant Cell, *3*, 677–684. https://doi.org/10.1105/tpc.3.7.677

Pařízková, B., Pernisová, M., & Novák, O. (2017). What has been seen cannot be unseen—detecting auxin in vivo. International Journal of Molecular Sciences, *18*, 1–26. https://doi.org/10.3390/ijms18122736

Peer, W. A., Hosein, F. N., Bandyopadhyay, A., Makam, S. N., Otegui, M. S., Lee, G. J., Blakeslee, J. J., Cheng, Y., Titapiwatanakun, B., Yakubov, B., et al. (2009). Mutation of the membrane-associated M1 protease APM1 results in distinct embryonic and seedling developmental defects in *Arabidopsis*. Plant Cell, *21*, 1693–1721. https://doi.org/10.1105/tpc.108.059634

Pires, N. D., & Dolan, L. (2012). Morphological evolution in land plants: New designs with old genes. Philosophical Transactions of the Royal Society B: Biological Sciences, *367*, 508–518. https://doi.org/10.1098/rstb.2011.0252

Proust, H., Honkanen, S., Jones, V. A. S., Morieri, G., Prescott, H., Kelly, S., Ishizaki, K., Kohchi, T., & Dolan, L. (2016). RSL class I genes controlled the development of epidermal structures in the common ancestor of land plants. Current Biology, *26*, 93–99. https://doi.org/10.1016/j.cub.2015.11.042

Roeder, A. H. K., Tarr, P. T., Tobin, C., Zhang, X., Chickarmane, V., Cunha, A., & Meyerowitz, E. M. (2011). Computational morphodynamics of plants: Integrating development over space and time. Nature Reviews Molecular Cell Biology, *12*, 265–273. https://doi.org/10.1038/nrm3079

RStudio Team (2020). RStudio: Integrated Development for R. RStudio, PBC, Boston, MA. http://www.rstudio.com/.

Sabatini, S., Beis, D., Wolkenfelt, H., Murfett, J., Guilfoyle, T., Malamy, J., Benfey, P., Leyser, O., Bechtold, N., Weisbeek, P., & Scheres, B. (1999). An auxin-dependent distal organizer of pattern and polarity in the *Arabidopsis* root. Cell, *99*, 463–472. https://doi.org/10.1016/S0092-8674(00)81535-4

Santner, A., Calderon-Villalobos, L. I. A., & Estelle, M. (2009). Plant hormones are versatile chemical regulators of plant growth. Nature Chemical Biology, *5*, 301–307. https://doi.org/10.1038/nchembio.165

Sapala, A., Runions, A., Routier-Kierzkowska, A. L., Gupta, M. Das, Hong, L., Hofhuis, H., Verger, S., Mosca, G., Li, C. B., Hay, A., et al. (2018). Why plants make puzzle cells, and how their shape emerges. eLife, *7*, e32794. https://doi.org/10.7554/eLife.32794

Sauret-Güeto, S., Schiessl, K., Bangham, A., Sablowski, R., & Coen, E. (2013). JAGGED controls *Arabidopsis* petal growth and shape by interacting with a divergent polarity field. PLoS Biology, *11*, e1001550. https://doi.org/10.1371/journal.pbio.1001550

Scarpella, E., Marcos, D., Friml, J., & Berleth, T. (2006). Control of leaf vascular patterning by polar auxin transport. Genes and Development, *20*, 1015–1027. https://doi.org/10.1101/gad.1402406

Schaller, G. E., Bishopp, A., & Kieber, J. J. (2015). The yin-yang of hormones: Cytokinin and auxin interactions in plant development. Plant Cell, *27*, 44–63. https://doi.org/10.1105/tpc.114.133595

Schneider, C., Rasband, W., & Eliceiri, K. (2012). ImageJ. Nature Methods, *9*, 671–675. https://doi.org/10.1007/978-1-84882-087-6_9

Shimamura, M. (2016). *Marchantia polymorpha*: Taxonomy, phylogeny and morphology of a model system. Plant and Cell Physiology, *57*, 230–256. https://doi.org/10.1093/pcp/pcv192

Shinohara, N., Taylor, C., & Leyser, O. (2013). Strigolactone can promote or inhibit shoot branching by triggering rapid depletion of the auxin efflux protein PIN1 from the plasma membrane. PLoS Biology, *11*, e1001474. https://doi.org/10.1371/journal.pbio.1001474

Solly, J. (2015). Regulation of thallus shape in the liverwort *Marchantia polymorpha*. PhD Thesis, Clare College, Cambridge.

Solly, J., Cunniffe, N. J., & Harrison, C. J. (2017). Regional growth rate differences specified by apical notch activities regulate liverwort thallus shape. Current Biology, *27*, 16–26. https://doi.org/10.1016/j.cub.2016.10.056

Solly, J., and Harrison, C. J. (2016) Auxin and cytokinin regulate (PIN-mediated) polarity and thallus length to breadth ratios in a liverwort. Unpublished manuscript.

Su, Y. H., Liu, Y. B., & Zhang, X. S. (2011). Auxin-cytokinin interaction regulates meristem development. Molecular Plant, *4*, 616–625. https://doi.org/10.1093/mp/ssr007

Teale, W., & Palme, K. (2018). Naphthylphthalamic acid and the mechanism of polar auxin transport. Journal of Experimental Botany, *69*, 303–312. https://doi.org/10.1093/jxb/erx323

Thamm, A., Saunders, T. E., & Dolan, L. (2020). MpFEW RHIZOIDS1 miRNA-mediated lateral inhibition controls rhizoid cell patterning in *Marchantia polymorpha*. Current Biology, *30*, 1905-1915.e4. https://doi.org/10.1016/j.cub.2020.03.032

Viaene, T., Landberg, K., Thelander, M., Medvecka, E., Pederson, E., Feraru, E., Cooper, E. D., Karimi, M., Delwiche, C. F., Ljung, K., et al. (2014). Directional auxin transport mechanisms in early diverging land plants. Current Biology, *24*, 2786–2791. https://doi.org/10.1016/j.cub.2014.09.056

Whitewoods, C. D., Gonçalves, B., Cheng, J., Cui, M., & Kennaway, R. (2019). Evolution of carnivorous traps from planar leaves through simple shifts in gene expression. Science, *5433*, 1–10. https://doi.org/10.1126/science.aay5433

Wickham, H., Averick, M., Bryan, J., Chang, W., McGowan, L., François, R., Grolemund, G., Hayes, A., Henry, L., Hester, J., et al. (2019). Welcome to the Tidyverse. Journal of Open Source Software, *4*, 1686. https://doi.org/10.21105/joss.01686

Wisniewska, J., Xu, J., Seifartová, D., Brewer, P. B., Růžička, K., Blilou, L., Rouquié, D., Benková, E., Scheres, B., & Friml, J. (2006). Polar PIN localization directs auxin flow in plants. Science, *312*, 883. https://doi.org/10.1126/science.1121356

Yoshida, S., van der Schuren, A., van Dop, M., van Galen, L., Saiga, S., Adibi, M., Möller, B., ten Hove, C. A., Marhavy, P., Smith, R., et al. (2019). A SOSEKI-based coordinate system interprets global polarity cues in *Arabidopsis*. Nature Plants, *5*, 160–166. https://doi.org/10.1038/s41477-019-0363-6

Zhang, Y., Rodriguez, L., Li, L., Zhang, X., & Friml, J. (2020). Functional innovations of PIN auxin transporters mark crucial evolutionary transitions during rise of flowering plants. Science Advances, *6*, 1–15. https://doi.org/10.1126/sciadv.abc8895

Appendices

Suitability criteria for growth experiments

Data is shown for the sample sizes of each of the growth experiments conducted in Chapter 1 of my thesis. The Type I gemmae is following the protocol to determine suitable thalli, outlined by Jeremy Solly in his PhD thesis. I have included some images for reference of Type I gemmae and also those which were excluded from quantification (Figure A1).

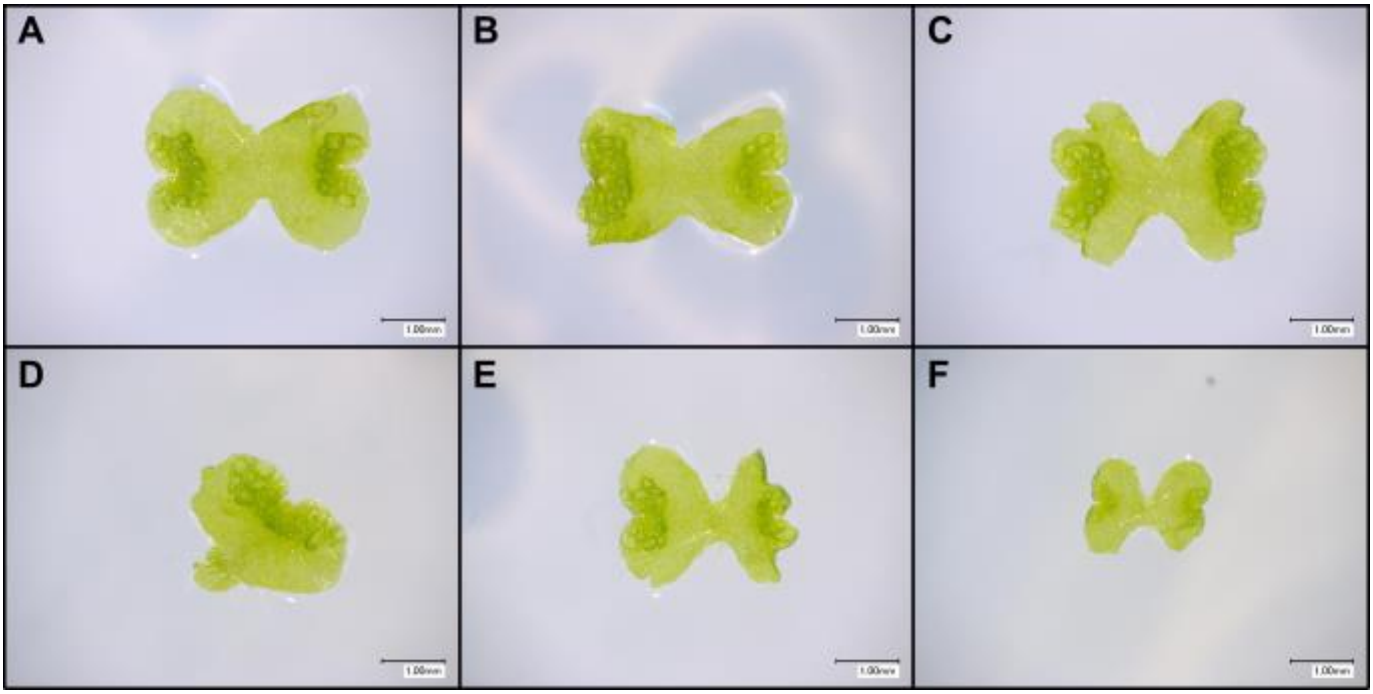

Figure A1: Gemmae with gross developmental defects were not included in growth experiment shape quantification. Thalli were imaged using a Keyence VHX-1000 digital light microscope at 50 X magnification. These thalli are all Tak-1, taken from a replicate of the *Mppinz* phenotype analysis growth experiment (Chapter 3, **Figure 3.7**) . (**A-C**) Examples of Type I thalli included in shape quantification experiments. (**D-F**) Thalli excluded from shape analysis, with either only half the thalli growing (**D**), clear growth asymmetry (**E**), or gemmae not yet at the same developmental stage at the end of plastochron 1 (**F**). Scale bars in all images represents 1 mm.

Suitability criteria for growth experiments during early development

Exogenous auxin (NAA) treatment

Table A1: Relating to data shown in Chapter 3, Figure 3.3.

Replicate	Treatment	No. Type I	No. Other	Total gemmae	% Type I
1	0nM	50	30	80	62.50
	400nM	55	20	75	73.33
	500nM	61	17	78	78.21
2	0nM	41	37	78	52.56
	400nM	60	21	81	74.07
	500nM	65	10	75	86.67
3	0nM	45	30	75	60.00
	400nM	48	25	73	65.75
	500nM	48	22	70	68.57

Auxin biosynthesis inhibitor (L-Kyn) treatment

Table A2: Relating to data shown in Chapter 3, Figure 3.4.

Replicate	Treatment	No. Type I	No. Other	Total gemmae	% Type I
1	0nM	46	33	79	58.23
	30µM	42	32	74	56.76
	60µM	30	35	65	46.15
2	0nM	42	33	75	56.00
	30µM	30	44	74	40.54
	60µM	30	48	78	38.46
3	0nM	48	27	75	64.00
	30µM	39	36	75	52.00
	60µM	45	29	74	60.81

Auxin transport inhibitor (NPA) treatment

Table A3: Relating to data shown in Chapter 3, Figure 3.5.

Replicate	Treatment	No. Type I	No. Other	Total gemmae	% Type I
1	0nM	18	12	30	60.00
	5µM	17	13	30	56.67
	10µM	17	13	30	56.67
2	0nM	11	19	30	36.67
	5µM	23	7	30	76.67
	10µM	10	20	30	33.33
3	0nM	26	4	30	86.67
	5µM	27	3	30	90.00
	10µM	22	8	30	73.33

Mppinz mutant line analysis

Table A4: Relating to data shown in Chapter 3, Figure 3.7.

Replicate	Line	No. Type I	No. Other	Total gemmae	% Type I
1	Tak-1	68	4	72	94.44
	Mppinz(1)	56	12	68	82.35
	Mppinz(2)	45	26	71	63.38
2	Tak-1	61	11	72	84.72
	Mppinz(1)	54	17	71	76.06
	Mppinz(2)	50	23	73	68.49
3	Tak-1	44	30	74	59.46
	Mppinz(1)	45	27	72	62.50
	Mppinz(2)	30	37	67	44.78

Cytokinin mutant lines analysis

Table A5: Relating to data shown in Chapter 3, Figure 3.8.

Replicate	Line	No. Type I	No. Other	Total gemmae	% Type I
1	Tak-1	51	14	65	78.46
	JES32#10	39	35	74	52.70
	JES43#18	48	20	68	70.59
2	Tak-1	49	14	63	77.78
	JES32#10	36	20	56	64.29
	JES43#18	60	8	68	88.24
3	Tak-1	71	2	73	97.26
	JES32#10	50	23	73	68.49
	JES43#18	72	4	76	94.74

Cytokinin mutant lines treated with auxin transport inhibitor (NPA)

Table A6: Relating to data shown in Chapter 3, Figure 3.9.

Replicate	Line	Treatment	No. Type I	No. Other	Total gemmae	% Type I
1	Tak-1	0nM	39	8	47	82.98
		5µM	34	13	47	72.34
		10µM	33	16	49	67.35
	JES32#10	0nM	27	21	48	56.25
		5µM	30	17	47	63.83
		10µM	34	17	51	66.67
	JES43#18	0nM	38	12	50	76.00
		5µM	42	10	52	80.77
		10µM	33	14	47	70.21
2	Tak-1	0nM	47	5	52	90.38
		5µM	46	5	51	90.20
		10µM	44	11	55	80.00
	JES32#10	0nM	34	16	50	68.00
		5µM	30	17	47	63.83
		10µM	34	13	47	72.34
	JES43#18	0nM	41	8	49	83.67
		5µM	44	5	49	89.80
		10µM	42	10	52	80.77
3	Tak-1	0nM	38	10	48	79.17
		5µM	42	8	50	84.00
		10µM	34	15	49	69.39
	JES32#10	0nM	30	27	57	52.63
		5µM	34	17	51	66.67
		10µM	36	13	49	73.47
	JES43#18	0nM	37	12	49	75.51
		5µM	39	9	48	81.25
		10µM	35	13	48	72.92

Suitability criteria for growth experiments at later developmental stages

Mppinz mutant line analysis following two weeks of growth

Table A7: Relating to data shown in Chapter 3, Figure 3.11.

Replicate	Line	No. Type I	No. Other	Total gemmae	% Type I
1	Tak-1	39	9	48	81.25
	Mppinz(1)	34	14	48	70.83
	Mppinz(2)	31	17	48	64.58

Auxin transport inhibitor (NPA) treatment following two weeks of growth

Table A8: Relating to data shown in Chapter 3, Figure 3.12.

Replicate	Treatment	No. Type I	No. Other	Total gemmae	% Type I
1	0nM	16	14	30	53.33
	5µM	11	19	30	36.67
	10µM	4	26	30	13.33
2	0nM	5	25	30	16.67
	5µM	17	13	30	56.67
	10µM	7	23	30	23.33
3	0nM	29	1	30	96.67
	5µM	25	5	30	83.33
	10µM	11	19	30	36.67

Mppinz mutant line analysis following three weeks of growth

Table A9: Relating to data shown in Chapter 3, Figure 3.15.

Replicate	Line	No. Type I	No. Other	Total gemmae	% Type I
1	Tak-1	39	9	48	81.25
	Mppinz(1)	45	2	47	95.74
	Mppinz(2)	47	1	48	97.92